

**Analysis of intracellular transport and functionality
of human kidney anion exchanger 1 (kAE1) in yeast
and mammalian cells**

Dissertation

zur Erlangung des akademischen Grades des
Doktors der Naturwissenschaften
der Naturwissenschaftlich-Technischen Fakultät
der Universität des Saarlandes

von

Master of Science

S M A Hasib

Saarbrücken

2020

Tag des Kolloquiums:	12. Februar 2021
Dekan:	Prof. Dr. Jörn Erik Walter
Berichtersteller:	Prof. Dr. Manfred J. Schmitt Prof. Dr. Ekkehard Neuhaus
Vorsitz:	Prof. Dr. Bruce Morgan
Akademischer Mitarbeiter:	Dr. Frank Hannemann

“Life is like riding a bicycle. To keep your balance, you must keep moving.”

- Albert Einstein

Publications

Parts of this thesis have been published in a scientific journal:

- ◆ **Sarder, H. A. M.**, Li, X., Funaya, C., Cordat, E., Schmitt, M. J., & Becker, B. (2020). *Saccharomyces cerevisiae*: First Steps to a Suitable Model System To Study the Function and Intracellular Transport of Human Kidney Anion Exchanger 1. *mSphere*, 5(1), 16. <https://doi.org/10.1128/mSphere.00802-19>

Conference Participation

Parts of this thesis were presented at the following conference:

- ◆ **CSMB-61**, 2018 (Banff, Canada): Dissecting intracellular trafficking and mis-traffic of human kidney AE1 in yeast and mammalian cells (**Poster**).

Table of Contents

List of abbreviations	8
Abstract.....	10
1. Introduction	12
1.1 Nephron: the functional unit of the kidney	12
1.2 The intercalated cells	14
1.3 The SLC4A1 bicarbonate transporter	16
1.3.1 Bicarbonate transport mechanisms in human	16
1.3.2 SLC4A1 isoforms: eAE1 and kAE1	18
1.3.3 Structure of eAE1 and kAE1	19
1.3.4 Intracellular trafficking of eAE1 and kAE1	21
1.4 Distal renal tubular acidosis (dRTA).....	23
1.4.1 dRTA associated with kAE1 mutants	24
1.4.2 Controversy on the intracellular localization of kAE1 in dominant dRTA	27
1.5 Alternative model systems for investigating kAE1 physiology	28
1.6 Aims of this study.....	31
2. Materials and Methods	32
2.1 Organisms	32
2.1.1 Bacterial strains	32
2.1.2 Yeast strains	32
2.1.3 Mammalian cell lines.....	33
2.2 Growth media and culture condition	33
2.2.1 Bacteria.....	33
2.2.2 Yeast.....	34
2.2.3 Mammalian cells	35
2.3 Cryopreservation	36
2.3.1 Cryopreservation of bacteria and yeast.....	36
2.3.2 Cryopreservation of mammalian cells	36
2.4 Plasmids.....	37
2.5 Polymerase chain reaction (PCR).....	38
2.6 Site-directed mutagenesis	40
2.7 TOPO TA cloning	41
2.8 Restriction digestion.....	42
2.9 Agarose gel electrophoresis	43

2.10	Transformation of microorganisms	44
2.10.1	Electroporation of <i>E. coli</i>	44
2.10.2	Transformation of <i>S. cerevisiae</i>	46
2.11	Lentiviral transduction of mammalian cells.....	48
2.11.1	Construction of the response plasmid.....	49
2.11.2	Generation of stable mIMCD3 cell lines.....	50
2.12	Plasmid isolation from microorganisms	51
2.12.1	Plasmid isolation from <i>E. coli</i>	51
2.12.2	Extraction of plasmid from yeast.....	52
2.13	Determination of DNA concentration	52
2.14	Protein biochemical methods.....	52
2.14.1	Lysis of yeast cells.....	52
2.14.2	Lysis of mammalian cells.....	53
2.14.3	SDS-PAGE.....	54
2.14.4	Silver staining.....	56
2.14.5	Western blot analysis	57
2.14.6	Determination of protein half-lives.....	59
2.14.7	Cell surface biotinylation	60
2.14.8	Enzymatic deglycosylation.....	60
2.15	Boric acid tolerance assay.....	61
2.16	Indirect immunofluorescence.....	62
2.17	Microscopy techniques	63
2.17.1	Fluorescence microscopy	63
2.17.2	Confocal laser scanning microscopy.....	63
2.17.3	Spinning disc confocal microscopy.....	64
2.18	pH measurement of the kAE1 expressing yeast cells.....	64
2.19	Anion exchange chromatography.....	66
2.20	MTS assay.....	68
2.20.1	Cell counting by hemocytometer.....	68
2.20.2	MTS assay for investigating mIMCD3 cell proliferation.....	68
2.21	Data analysis and statistics.....	69
3.	Results	70
3.1	Construction of different kAE1 derivatives for <i>S. cerevisiae</i>	71
3.1.1	Expression profiles of the different kAE1 variants.....	72
3.1.2	Improvement of protein extraction	74
3.2	Intracellular localization of the kAE1 derivatives in <i>S. cerevisiae</i>	76
3.2.1	Localization of untagged ykAE1	76

3.2.2	Localization of tagged ykAE1 variants.....	77
3.3	Colocalization of kAE1 with the yeast plasma membrane protein Pma1p.....	79
3.3.1	Construction of N-terminally and intramolecularly tagged ykAE1 variants	79
3.3.2	Colocalization analysis	80
3.4	Approaches for improving the kAE1 plasma membrane localization.....	84
3.5	Biochemical detection of plasma membrane located kAE1.....	90
3.6	Glycosylation analysis of ykAE1 variants with glycosidase enzymes	91
3.7	Functional analysis of full-length ykAE1 variants in yeast	93
3.7.1	Analyzing functional homology between kAE1 and Bor1p.....	93
3.7.2	Correlation of intracellular pH and kAE1 expression.....	96
3.7.3	Dose-dependent correlation of cytosolic pH and kAE1 expression.....	98
3.7.4	Determination of intracellular chloride transport in dependency of kAE1 expression	101
3.8	Expression and localization analysis of kAE1 mutants in <i>S. cerevisiae</i>	102
3.9	Characterization of novel dRTA mutants in mammalian cells	104
3.9.1	Half-life of the three novel kAE1 mutants.....	105
3.9.2	Impact on p62 level in mIMCD3 cells.....	108
3.9.3	Effect on mIMCD3 cells viability	110
4.	Discussion	113
5.	Outlook.....	130
6.	Summary	131
7.	References	132
	Appendix.....	151
	Acknowledgements	158
	Declaration of originality.....	160
	Curriculum vitae.....	161

List of abbreviations

Amp	Ampicillin
ATP	Adenosine triphosphate
APS	Ammonium peroxodisulfate
BiP	Binding immunoglobulin protein
bp/kb	Base pair/kilobase pair
BSA	Bovine serum albumin
cDNA	Complementary DNA
CLSM	Confocal laser scanning microscopy
C-terminus	Carboxyl terminus
d/o	Drop-out
Da/kDa	Dalton/Kilodalton
DMSO	Dimethyl sulfoxide
DNA	Deoxyribonucleic acid
dsDNA	Double-stranded DNA
dNTP	Deoxynucleotide triphosphate
DTT	Dithiothreitol
EDTA	Ethylenediaminetetraacetic acid
ER	Endoplasmic reticulum
ERAD	“Endoplasmic-reticulum-associated protein degradation”
FITC	Fluorescein isothiocyanate
GFP	Green fluorescent protein
GLB	Gel loading buffer
GTE	Glucose-Tris-EDTA
HRP	Horseradish peroxidase
LB	Lysogeny broth
LiAc	Lithium acetate
mRNA	Messenger RNA
N-terminus	Amino terminus
OD	Optical density

ORF	Open reading frame
PBS	Phosphate buffer saline
PEG	Polyethylene glycol
PM	Plasma membrane
PVDF	Polyvinylidene difluoride
RNA	Ribonucleic acid
RNase	Ribonuclease
rpm	Revolutions per minute
RT	Room temperature
SDS	Sodium dodecyl sulfate
SS	Signal sequence
Taq	<i>Thermus aquaticus</i>
TBE	Tris-Borate-EDTA
TBS	Tris-buffered saline
TE	Tris-EDTA
TEMED	N,N,N',N'-Tetramethylethan-1,2-diamin
TGN	Trans-Golgi-network
Tris	Tris(hydroxymethyl)aminomethane
UAS	Upstream activation sequence
UV	Ultraviolet
v/v	Volume per volume
w/v	Weight per volume
YPD	Yeast extract peptone dextrose
YNB	Yeast nitrogen base

Abstract

Anion exchanger proteins facilitate chloride-bicarbonate movement across the plasma membrane and play an important role in maintaining acid-base homeostasis in the human body. Kidney anion exchanger 1 (kAE1) is one of the major bicarbonate transporters among this group and helps to reabsorb bicarbonate for chloride in distal nephrons. Defects of this protein result in functional impairment of the anion exchange process that eventually leads to the development of a clinical condition known as distal renal tubular acidosis (dRTA). Although the genetic basis of kAE1 mutants leading to disease is largely known, the precise molecular processes of dRTA pathophysiology are still inadequately understood. Here, the potential of baker's yeast was evaluated to address various cellular aspects of kAE1 physiology. For the first time, unmodified and tagged full-length versions of kAE1 were successfully expressed in yeast. Moreover, partial localization of the anion exchanger at the plasma membrane was validated by accomplishing several light and confocal microscopy techniques and biochemical assays. Subsequently, biological activity of the protein was demonstrated by performing intracellular pH measurements and chloride uptake assays. Additionally, a set of novel dRTA mutants was characterized in mIMCD3 cells, resembling the closest cellular model to α -intercalated cells. In sum, this study highlights novel possibilities to investigate kAE1-related physiology and pathology in more detail.

Anionenaustauscherproteine erleichtern die Bewegung von Chlorid-Bicarbonat durch die Plasmamembran und spielen eine wichtige Rolle bei der Aufrechterhaltung der Säure-Base-Homöostase im menschlichen Körper. Der Anionenaustauscher 1 (kAE1) der Niere ist einer der wichtigsten Bicarbonat-Transporter, der die Resorption von Bicarbonat für Chlorid im distalen Nephron unterstützt. Defekte dieses Proteins führen zu einer Beeinträchtigung des Anionen-Austauschprozesses und zur Entwicklung der distalen renalen tubulären Azidose (dRTA). Obwohl der genetische Hintergrund der krankmachenden kAE1-Mutanten weitgehend bekannt ist, sind die molekularen Prozesse der dRTA-Pathophysiologie nur unzureichend verstanden. In dieser Studie wurde die Bäckerhefe zur Untersuchung zellulärer Aspekte der kAE1-Physiologie eingesetzt. Erstmals wurden eine unmodifizierte und getaggte kAE1-Volllängenversion erfolgreich in Hefe exprimiert. Darüber hinaus wurde die partielle Lokalisierung des Anionenaustauschers in der Plasmamembran durch Mikroskopietechniken und biochemische Assays validiert. Anschließend wurde die biologische Proteinaktivität durch

intrazelluläre pH-Messungen und Chlorid-Aufnahmestudien nachgewiesen. Zusätzlich wurde eine Reihe von neuen dRTA-Mutanten in mIMCD3-Zellen charakterisiert, die als zelluläres Modell den α -interkalierten Zellen am nächsten kommen. Damit eröffnet die vorliegende Dissertation neue Möglichkeiten, die kAE1-Physiologie und -Pathologie genauer untersuchen zu können.

1. Introduction

1.1 Nephron: the functional unit of the kidney

Every day various metabolic waste products from consumed food and the surrounding environment are generated in the human body which need to be excreted. In this respect, the human body depends on two main organs for detoxification and secretion of unwanted metabolites, toxins and chemicals: the liver and the kidney. The latter, naturally found pairwise in vertebrates, represents the central organ of the urinary system and plays a fundamental role in filtering blood plasma to remove waste products. Hence, they excrete the metabolic waste along with toxins through the urine and reabsorb solutes, essential molecules such as glucose, amino acids, and water eventually returning them into the bloodstream. Moreover, kidneys also participate in controlling the blood volume, pH, osmolarity and ionic composition by regulating the water-electrolyte and acid-base balance (Kriz & Kaissling, 2013).

The kidney possesses a complex structure consisting of its functional unit known as nephron. A single kidney of a healthy adult is composed of about one million nephrons, which contribute to the urine formation through a series of sophisticated processes involved in filtering, reabsorption, secretion and excretion of molecules to and from the blood. Each nephron comprises a renal corpuscle and a renal tubule (Figure 1.1). The renal corpuscle is formed of a tuft of capillaries known as glomerulus and the surrounding double-walled epithelial cup, the so-called glomerular capsule or Bowman's capsule. Blood from the afferent arteriole enters into the renal corpuscle, and the blood plasma is then filtered by traversing through the fenestrated glomerular endothelial cells (GEnC). Thereafter, the filtered fluid passes through the renal tubule which contains three different sections: the proximal convoluted tubule, the nephron loop (also known as the loop of Henle) and the distal convoluted tubule. Next, the collecting duct, linked to the distal convoluted tubule by the connecting tubule, is accumulating luminal fluid from the distal convoluted tubule of several nephrons and releases into the minor calyx (Kriz *et al.*, 1988). Each section of the nephron is composed of diverse groups of cells and, thereby, the functions of each segment is determined by its cell types, tight junction properties and expressed ion-channels or solute carriers. Interestingly, the conversion from one section to the next takes place gradually because the expression of several essential proteins is overlapping between one-another. For example, the sodium-chloride cotransporter and the epithelium

sodium channel (ENaC) can be found in the transitional section of the distal convoluted tubule as well as in the collecting duct (Lashhab *et al.*, 2019; Tortora & Derrickson, 2014).

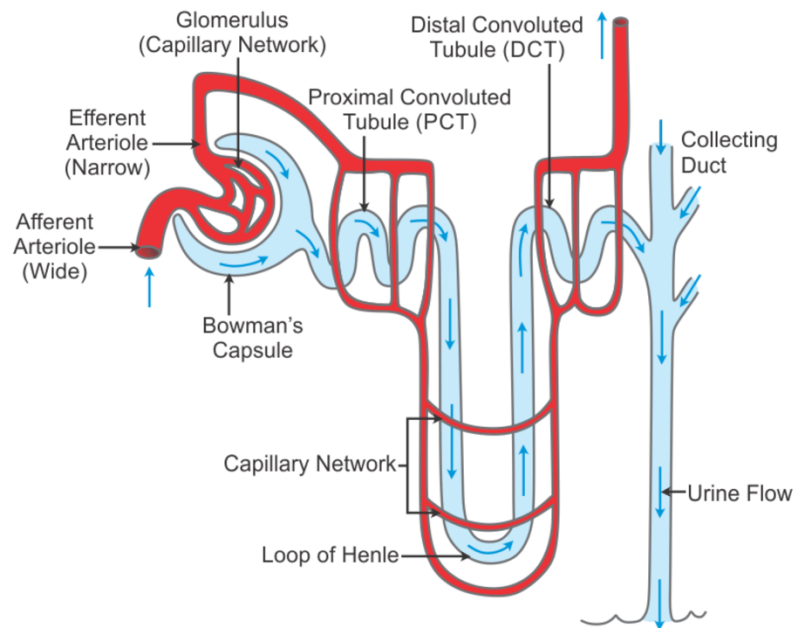


Figure 1.1: Schematic outline of nephron anatomy.

The diagram is showing a nephron (blue) associated with a blood vessel (red). Blood from the afferent arteriole flows into the glomerulus for filtration. The filterable blood components pass through the capillary network of the glomerulus and move into the Bowman's capsule. Then, the filtrate travels across the renal tubule consisting of the proximal convoluted tubule, loop of Henle, and distal convoluted tubule, where most of the electrolytes, macromolecules, and water reabsorption happens. Eventually, the tubular fluid arrives into the collecting duct system in which the final reabsorption of ions occurs, and the urine is formed (adopted from Tortora & Derrickson, 2014).

The filtered fluid in the proximal tubule has a similar composition as the blood plasma, except that it contains a lower amount of proteins. While passing through the nephron, the filtrate composition is constantly modified by reabsorption and excretion of its substances. In the proximal tubule, a significant portion of ions, solutes and water is reabsorbed, whereas the reabsorption of calcium, magnesium, sodium and chloride occurs in both, the nephron loop and distal convoluted tubule. Furthermore, the collecting duct controls the final absorption of protons, sodium, bicarbonate, chloride, potassium and water, thereby fine-tuning the urine composition and acidification. This absorption of water and electrolytes in the collecting duct

is mediated through both transcellular and paracellular pathways by the participation of at least three types of cells: the principal cells, α -, and β -intercalated cells (Koeppen *et al.*, 2013).

1.2 The intercalated cells

Kloth and colleagues reported that the electron microscopy of the embryonic collecting duct epithelium reveals a heterogeneous structure composed of different cell types where the light cells refer to the principal cells and the dark cells refer to the intercalated cells (Kloth *et al.*, 1993). In mouse, rat, and rabbit, one-third of the cortical collecting duct's cells were found to be intercalated cells (Kim *et al.*, 1999; LeFurgey & Tisher, 1979). These cells are characterized by their high enrichment of mitochondria, a dark cytoplasm and apically located microprojections (Schuster, 1993). Depending on the cell morphology and localization of the key surface proteins, three types of intercalated cells have been identified, α -type-A intercalated cells, β -type-B intercalated cells and non- α /non- β (or non-A/non-B) intercalated cells (Roy *et al.*, 2015).

The α -intercalated cells (also known as acid-secreting cells) have a columnar shape with the micro-projections at the apical pole and tubulovesicular structure beneath the apical surface. These cells express V-H⁺-ATPase and H⁺/K⁺-ATPase, two major proton pumps, at their apical membrane, while the kidney anion exchanger 1 (kAE1), a spliced variant of erythroid anion exchanger 1 (eAE1), is expressed at the basolateral membrane (Figure 1.2, left). The α -intercalated cells contribute to the acid-base homeostasis and urine acidification in distal nephrons by extruding protons (H⁺) through the two proton pumps and absorbing bicarbonate ions (HCO₃⁻) generated by the hydrolysis of endogenous carbon dioxide via kAE1.

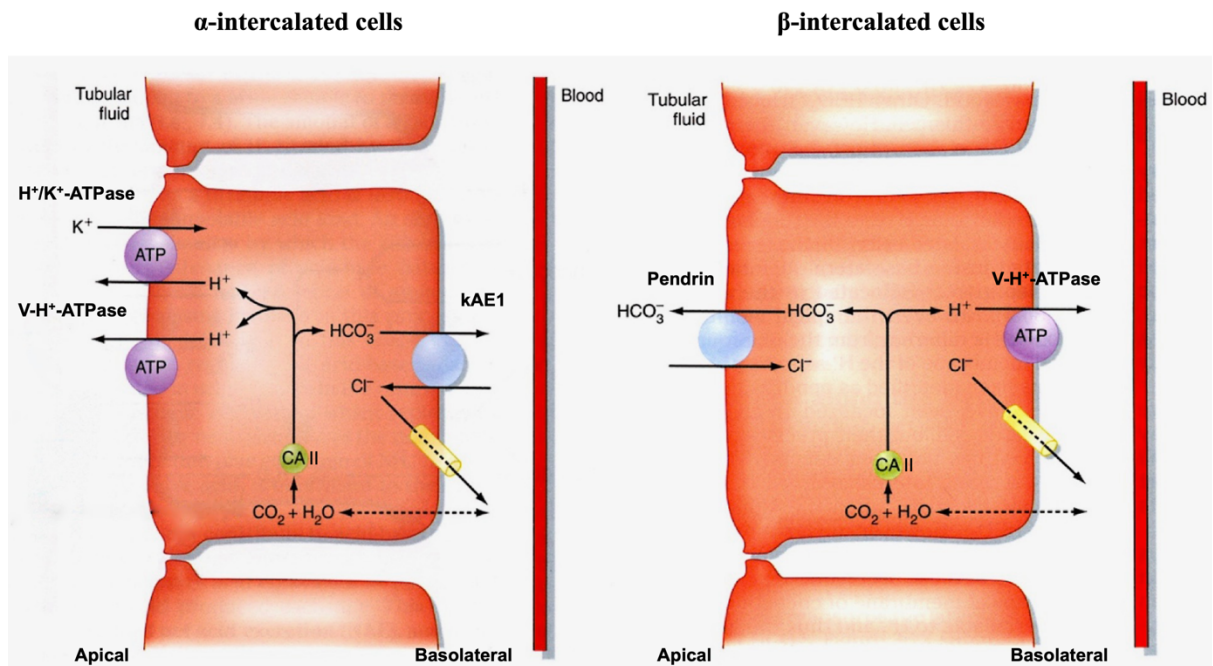


Figure 1.2: Model illustrating transepithelial transport of bicarbonate and protons in α - and β -intercalated cells.

In the collecting duct of the kidney, α -intercalated cells (left) excrete H^+ through apically located $V-H^+-ATPase$ and $H^+/K^+-ATPase$, and exchange HCO_3^- for Cl^- across the basolateral membrane through $kAE1$ to the interstitium in an electroneutral manner. This leads to the acidification of urine and distribution of HCO_3^- into the blood. Conversely, β -intercalated cells (right) secrete HCO_3^- into the tubular fluid using $pendrin$ and reabsorb H^+ into the blood via the basolaterally expressed $V-H^+-ATPase$. This results in the maintenance of the blood pH during alkalemia. Both cells also express a chloride channel at the basolateral membrane that regulates Cl^- homeostasis in the distal nephron (modified from Koeppen, 2009).

In contrast, β -intercalated cells are not only displaying a squamous-like structure but also have a smooth apical side and an organelle-free zone under the apical membrane. Moreover, they possess an opposite polarity compared to α -intercalated cells manifesting in a basolateral location of the $V-H^+-ATPase$ and expression of a different bicarbonate exchanger named $pendrin$ (SLC26A4) at the apical membrane (Figure 1.2, right). In case of alkalosis, β -intercalated cells contribute to the excretion of excess HCO_3^- and reabsorption of H^+ maintaining the acid-base balance. In addition, these cells are involved in chloride (Cl^-) reabsorption leading to ion homeostasis. Finally, non- α -/non- β -intercalated cells are identified by the expression of both, $pendrin$ and $V-H^+-ATPase$, at the apical membrane with a large number of cytoplasmic vesicles. The function of this type of intercalated cells is still not well

understood. However, the location of pendrin and V-H⁺-ATPase at the same pole suggests that these cells might participate in ion homeostasis rather than in acid-base balance, or they represent an intermediate cell-type that underwent interconversion (Almomani *et al.*, 2014; Lashhab *et al.*, 2019; Teng-umnuay *et al.*, 1996a). It has been reported that immortalized β -intercalated cells can convert into α -intercalated cells by basolateral deposition of the extracellular matrix protein hensin. In support of these findings, hensin knock-out mice exhibit a significantly higher number of β -intercalated cells with a simultaneously reduced number of α -intercalated cells in the collecting duct and a progression of metabolic acidosis (Gao *et al.*, 2010).

1.3 The SLC4A1 bicarbonate transporter

1.3.1 Bicarbonate transport mechanisms in human

Carbon dioxide (CO₂) represents a conjugate acid that is continuously generated as a metabolic byproduct in the human body. To maintain acid-base equilibrium, it needs to be eliminated from the body. CO₂ is released through the lungs and kidneys as part of a CO₂/HCO₃⁻ buffer system by the following reaction: $\text{CO}_2 + \text{H}_2\text{O} \leftrightarrow \text{H}_2\text{CO}_3 \leftrightarrow \text{H}^+ + \text{HCO}_3^-$. Unlike gaseous CO₂ that can permeate across the plasma membrane (PM), HCO₃⁻ is negatively charged and cannot penetrate membranes freely. However, HCO₃⁻ transport is facilitated by bicarbonate transporters which are integral membrane proteins ubiquitously expressed in various cell-types (Cordat & Casey, 2009). Fourteen gene products have been identified facilitating bicarbonate transport in the human body (Figure 1.3). According to the Human Genome Organization, these bicarbonate transport proteins are classified as solute carriers or “SLC” and belong to two evolutionarily distinct superfamilies, SLC4 and SLC26 (Wain, 2004).

The SLC4 gene family contains ten members, where the majority of them (nine proteins) are bicarbonate transporters. This gene family is further categorized into three subfamilies: (1) electroneutral Na⁺-independent Cl⁻/HCO₃⁻ exchangers SLC4A1–3 (AE1–3), (2) electrogenic Na⁺-coupled HCO₃⁻ cotransporters SLC4A4 and 5 (NBCe1 and NBCe2), and (3) electroneutral Na⁺-coupled HCO₃⁻ cotransporters SLC4A7, 8, 10 (NBCn1, NDCBE and NBCn2) and SLC4A9. SLC4A11 clusters separately within the SLC4 superfamily as it is

known to transport borate ions (Park *et al.*, 2005) and water (Vilas *et al.*, 2013) or exchange Na^+/H^+ (Jalimarada *et al.*, 2013).

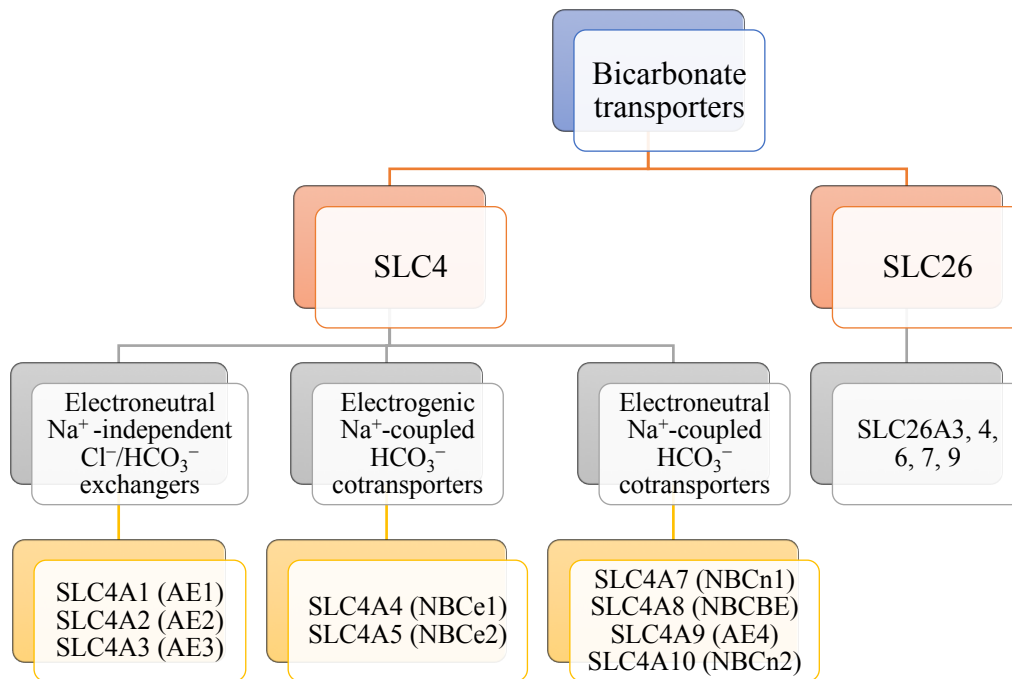


Figure 1.3: Bicarbonate transporters in mammals.

Bicarbonate transporters cluster into the two superfamilies SLC4 and SLC26 comprising fourteen gene products in total. SLC4 can be further subdivided into three sub-families, the electroneutral Na^+ -independent transporters, the electrogenic Na^+ -coupled cotransporters and the electroneutral Na^+ -coupled cotransporters. In the SLC26 superfamily, SLC26A3, 4, 6, 7, and 9 are involved in transporting HCO_3^- (modified from Alka & Casey, 2014).

In contrast, the SLC26 family members act as Na^+ -independent anion exchangers or anion channels that transport a wide range of substrates including Cl^- , Γ , HCO_3^- , SO_4^{2-} , formate, glycolate and oxalate. The SLC26 family consists of eleven members, where *SLC26A10* is considered to be a pseudogene (Alper & Sharma, 2013). Among these eleven members, only five (SLC26A3, 4, 6, 7, and 9) are transporting HCO_3^- (Ohana *et al.*, 2009; Shcheynikov *et al.*, 2008).

1.3.2 SLC4A1 isoforms: eAE1 and kAE1

The *SLC4A1* gene encodes two anion exchanger 1 (AE1) isoforms in humans, one of them is the erythroid anion exchanger 1 (eAE1, also named as Band 3), which is also the most studied bicarbonate transport protein of the SLC4 superfamily (Cordat & Reithmeier, 2014). The gene is located on chromosome 17 (17q21–q22) with a length of approximately 20 kb and composes of 20 exons split by 19 introns (Tanner *et al.*, 1988). In 1971, Fairbanks and colleagues identified eAE1 by analyzing red blood cell (RBC) ghost membrane proteins by gel electrophoresis; the third major band within the top of the gel corresponded to eAE1 resulting in the initial name “Band 3” (Fairbanks *et al.*, 1971). The glycoprotein eAE1 consists of 911 amino acids and is highly abundant in the plasma membrane of RBCs. Initial findings suggested that eAE1 is expressed with a copy number of approximately 1×10^6 per cell, where it comprehends approximately 50% of all membrane proteins in RBCs (Yenchitsomanus *et al.*, 2005).

eAE1 mediates chloride/bicarbonate ($\text{Cl}^-/\text{HCO}_3^-$) anion exchange across the plasma membrane of RBCs. This activity is essential for efficient respiration, which requires the adequate delivery of oxygen (O_2) to tissues coupled with the removal of CO_2 . In tissues, the metabolic product CO_2 diffuses into RBCs, interacts with water, and is then converted into HCO_3^- and H^+ by the carbonic anhydrase II (CA II). This allows the Bohr effect to take place: an increase in the proton concentration results in a pH drop, leading to a conformational change of hemoglobin from its “relaxed form” to the so-called “taut form” which has a low-affinity for O_2 (Benner *et al.*, 2018). Thus, O_2 is released from hemoglobin and diffuses into tissues. This system does not only allow for the unloading of oxygen, but also results in the conversion of CO_2 to the more soluble HCO_3^- ions. HCO_3^- is the form in which ~90% of CO_2 is transported to the lung. The eAE1 protein is responsible for the efflux of HCO_3^- into the plasma in exchange for Cl^- , thereby inhibiting HCO_3^- accumulation in RBCs. In the lungs, however, the exchange activity of eAE1 reverses. Plasma HCO_3^- which moves into the RBCs through eAE1 is converted to CO_2 by the catalytic activity of CA II. Then, the produced CO_2 diffuses out of the RBCs and is breathed out by the lung. The high quantity of eAE1 protein in RBCs demonstrates the importance of this transport system, allowing the mediation of respiration (Cordat & Reithmeier, 2014; Reithmeier, 2001).

The kidney anion exchanger 1 (kAE1) represents the second isoform encoded by *SLC4A1* and is highly enriched at the basolateral membrane of the α -intercalated cells in the connecting tubule and the collecting duct. The kAE1 protein was initially described by Drenckhahn and colleagues in 1985 (Drenckhahn *et al.*, 1985). It resembles a truncated version of eAE1 lacking the first 65 N-terminal amino acids (aa), and plays a central role in the maintenance of renal acid-base balance. In the process of urine acidification, kAE1 mediates a Na^+ -independent electroneutral exchange of HCO_3^- for Cl^- , which permits the exit of HCO_3^- from the α -intercalated cells. The α -intercalated cells are involved in active H^+ secretion into the tubular lumen through the activity of apically located V- H^+ -ATPase. When CO_2 diffuses into α -intercalated cells, it is hydrolyzed by the catalytic activity of cytosolic CA II into carbonic acid (H_2CO_3) which subsequently dissociates into H^+ and HCO_3^- . H^+ is pumped out by the V- H^+ -ATPase into the tubular lumen, and HCO_3^- is absorbed into the interstitial fluid by the basolateral kAE1 protein. Thus, the function of kAE1 causes a net H^+ secretion into urine by absorbing HCO_3^- to the body (Alper *et al.*, 1989; Alper *et al.*, 2002).

1.3.3 Structure of eAE1 and kAE1

Apart from kAE1 lacking the first 65 N-terminal aa compared to eAE1, both AE1 variants share the same structural features. AE1 is divided into two distinct domains, the N-terminal cytosolic domain (1–360 aa) and the integral membrane domain (361–911 aa). Moreover, the protein consists of 14 transmembrane segments (TMs), six helical segments, and an N-glycosylation site at Asn⁶⁴² in the long disordered fourth extracellular loop that connects TM7 and TM8 (Figure 1.4). An important feature of AE1 is the division into separate structural and functional domains at the N- and C-terminus, respectively (Reithmeier *et al.*, 2016; Sahr *et al.*, 1994).

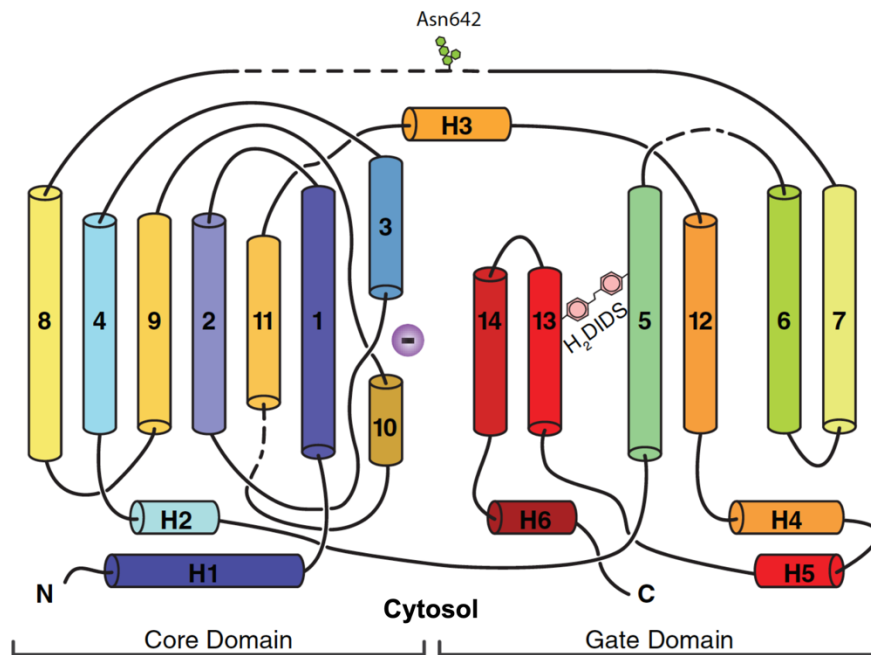


Figure 1.4: Membrane topology of monomeric AE1.

The topology model illustrates the membrane domain of AE1 (mdAE1) encompassing 14 transmembrane segments (TMs). The long cytosolic N-terminus is not depicted in this scheme, α helices are colored as blue to red from N-terminus to the C-terminal end and shown in proportion to their length. TMs are noted by numbers (1–14), and amphipathic helices on the protein surface are labeled as H1–6. mdAE1 comprises two domains: a core domain (left) consisting of TM1–4 and TM8–11, and a gate domain (right) containing TM5–7 and TM12–14. The anion binding site of AE1 is located in the core domain indicated by a “purple sphere” between TM3 and TM10. The protein is incorporated with a single N-glycosylation site located at Asn⁶⁴², in the fourth long exofacial loop connecting TM7 and 8. The binding site of the irreversible anion inhibitor H₂DIDS is shown that crosslinks between TM5 and 13 (adopted from Abbas *et al.*, 2018).

Many attempts have been made to determine the 3D structure of the membrane domain of AE1 (mdAE1) by using techniques such as cysteine scanning mutagenesis and N-glycan insertion. In 2015, Arakawa and colleagues were able to identify the crystal structure of the open 4,4-diisothiocyanatodihydro-stilbene-2,2-disulfonic acid (H₂DIDS) bound conformation of mdAE1 (Arakawa *et al.*, 2015). C-terminal mdAE1 is responsible for mediating the transport of anions across the lipid bilayer and is fully functional in the absence of the cytosolic N-terminus domain. mdAE1 can be further divided into the core (TM1–4 and 8–11) and gate (TM5–7 and 12–14) domains. The relative rocking movement of these two domains is responsible for the anion transport by changing the accessibility of the substrate-binding site of AE1 to either side

of the membrane. This permits translocation of substrates across the membrane, as well as the efficient transport mechanism allowing the transport of 1×10^5 anions per second per protein (Arakawa *et al.*, 2015; Reithmeier *et al.*, 2016).

Under physiological conditions, AE1 tends to dimerize at the plasma membrane, although dimerization is not required for its *in vivo* function. In addition, eAE1 can form tetramers via its N-terminal interactions with the cytoskeletal proteins ankyrin and EPB42. However, kAE1 does not tetramerize due to its lack of interaction with ankyrin in α -intercalated cells (Ding *et al.*, 1994). The crystal structure of mdAE1 reveals that the transmembrane domains 5, 6, and 7 of the gate domains are located at the dimer interface (1092\AA^2) and are involved in the dimerization through an interaction of TM5 and the Leu⁵⁷² residue at the end of TM6. So far, nothing is known about the interface during substrate transport, but it is likely that the dimer interface stays unchanged while the core domain shifts. However, a conformational transition during anion translocation can not be fully excluded (Arakawa *et al.*, 2015; Reithmeier *et al.*, 2016).

1.3.4 Intracellular trafficking of eAE1 and kAE1

Both eAE1 and kAE1 are imported into the endoplasmic reticulum (ER) and transported to the plasma membrane or the basolateral membrane, respectively. In the case of eAE1, the interaction with glycophorin A, a red blood cell membrane protein that acts as a chaperone, has facilitated its targeting to the red blood cell surface (Young & Tanner, 2003). It has been suggested that both proteins interact within the ER and are transported to the surface of the erythrocytes together. Previous studies in SLC4A1 knock-out mice (*Slc4a1*^{-/-}) indicated that there is a complete depletion of glycoporphin A in red blood cells of the mice (Hassoun *et al.*, 1998). Consequently, impaired activity of eAE1 could be detected at the erythrocyte surface in glycoporphin A-deficient patients (Bruce *et al.*, 2004). Glycophorin A most likely stabilizes the structural feature of eAE1 because its absence results in a flexible conformation of eAE1 with reduced transport activity. Moreover, it might be involved in blocking the movement of the core and gate domains of eAE1 within the ER and Golgi. eAE1 was identified as being inactive until it dissociates from glycoporphin A and is inserted into the plasma membrane. Thus, the coupling of eAE1 with glycoporphin A prevents fast HCO_3^- transport across the ER and Golgi membrane,

which is likely to stop eAE1 from interfering with the internal pH control of these organelles (Reithmeier *et al.*, 2016).

Interestingly, glycoporphin A is not expressed in α -intercalated cells (Tanphaichitr *et al.*, 1998). It has been reported that in α -intercalated cells, kAE1 directly interacts with the mu1A subunit of the adaptor protein complex 1 (AP-1 mu1A) via its C-terminus (Sawasdee *et al.*, 2010). The C-terminus of kAE1 contains the tyrosine-based sorting motif Y⁹⁰⁴DEV⁹⁰⁷, and a class-II PDZ-binding domain A⁹⁰⁸MPV⁹¹¹, which are known to be responsible for its targeting to basolateral membranes (Devonald *et al.*, 2003; Toye *et al.*, 2004). kAE1 binds to AP-1 mu1A through its tyrosine sorting motif identified by a yeast two-hybrid screen (Sawasdee *et al.*, 2010). In human embryonic kidney 293 cells (HEK293), the knock-down of AP-1 mu1A using short interfering RNA (siRNA) resulted in impaired kAE1 targeting to the basolateral membrane (Junking *et al.*, 2014). Furthermore, other interacting partners of kAE1 have been identified that are involved in its cell surface trafficking, such as glyceraldehyde 3-phosphate dehydrogenase (GAPDH), transmembrane protein 139 (TMEM139) and peroxiredoxin 6 (PRDX6). GAPDH protein was suggested to be involved in kAE1 trafficking to the basolateral membrane through interaction with the C-terminal D⁹⁰²EYDE⁹⁰⁶ motif of kAE1. In madin-darby canine kidney cells (MDCK), the knock-down of GAPDH results in intracellular retention of kAE1, postulating a role in the cell surface targeting of kAE1 (Su *et al.*, 2011). In case of TMEM139 protein, Nuiplot and colleagues found that TMEM139 overexpression in HEK293 cells results in an increased kAE1 protein level at the basolateral membrane. In addition, they also detected a kAE1-TMEM139 complex in the membrane fraction. It was thus proposed that TMEM139 acts as a chaperone that facilitates intracellular kAE1 trafficking (Nuiplot *et al.*, 2015). In addition, PRDX6, a protein with peroxidase and antioxidant activity, has been found to colocalize with kAE1 at the plasma membrane. This interaction is supposed to mediate kAE1 expression during cellular stress. Specifically, it was found that under conditions of metabolic acidosis PRDX6-deficient mice showed acutely reduced kAE1 expression level, suggesting PRDX6 stabilizes kAE1 at the basolateral membrane (Sorrell *et al.*, 2016).

1.4 Distal renal tubular acidosis (dRTA)

Mutations in the *SLC4A1* gene cause an impairment in trafficking or activity of kAE1 that ultimately leads to a renal disorder named distal renal tubular acidosis (dRTA). Primary dRTA, also known as type 1 RTA or complete dRTA, is characterized as a defect of urine acidification. Under such pathophysiological conditions, the α -intercalated cells are incapable of discharging the excessive amounts of H^+ produced in metabolic reactions. This general reduction in net acid excretion by the kidney results in the production of more alkaline urine with a pH that can not drop below 5.5 and does, eventually, manifest in systemic acidemia (Alper, 2002; Batlle *et al.*, 2001). Moreover, dRTA patients typically display a low plasma potassium concentration (hypokalemia), as well as a high plasma chloride (hyperchloremia) and CO_2 concentration which is often accompanied by a high amount of calcium in the urine (hypercalciuria). Prolonged disease conditions lead to calcium deposition in the kidney (nephrocalcinosis), kidney stone formation (nephrolithiasis) and eventually result in kidney failure (Buckalew, 1989; Yenchitsomanus *et al.*, 2005). Children suffering from dRTA show impairment of growth along with vomiting and dehydration (Sharma *et al.*, 2007). In a few patients, incomplete dRTA has been observed, which can be defined as the inability to acidify urine after an acute acid load (typically with ammonium chloride). Consequently, following a low acid diet, the bicarbonate concentration in the blood of these patients can be at normal levels without the display of metabolic acidosis. Thus, the risk for dRTA symptoms such as nephrocalcinosis and nephrolithiasis only increases in the case of severely high intakes of acid-containing food (Batlle & Haque, 2012; Soriano, 2002).

In addition to the variants related to kAE1, dRTA can also be developed due to the mutations in the genes coding for the $V-H^+$ -ATPase and CA II. $V-H^+$ -ATPase is a multi-subunit protein complex consisting of two functional domains: the cytoplasmic V_1 domain and the membrane-spanning V_0 domain. The V_1 domain encompasses a hexamer of three A subunits and three B subunits together with six other subunits (C-H), and catalyzes for ATP hydrolysis. The V_0 domain is composed of six different subunits (a, c, c', c'', d, and e) and responsible for proton translocation. In mammals, the a subunit is found in four isoforms (a1, a2, a3, and a4) and the B subunit exists in two isoforms (B1 and B2) (Stevens & Forgac, 1997; Toei *et al.*, 2010). Hereditary dRTA associated with defects in the $V-H^+$ -ATPase is caused by either mutation of the a4 or B1 isoform. Mutations of the a4 isoform often result in sensorineural deafness together

with other dRTA symptoms. In a4 knock-out mice, a severe dRTA phenotype develops, including nephrocalcinosis, hypocitraturia, deafness and defects in the olfactory sensation (Hennings *et al.*, 2012; Norgett *et al.*, 2012). In contrast, mutant variants of the B1 isoform do not result in such phenotypes, and it has been postulated that the B2 isoform of the V-H⁺-ATPase may compensate for a defective B1 isoform (Finberg *et al.*, 2005). Patients with mutant CA II variants develop dRTA, which is associated with the recessive mutations in the encoding gene *Car-2*, and display increased bone density (osteopetrosis), hearing defects, mental retardation along with a growth deficiency (Vainsel *et al.*, 1972). A previous study with a null mutation in the *Car-2^b* allele shows that these mice develop dRTA along with the down-regulation of multiple proteins in intercalated cells such as kAE1, pendrin and SLC26A7 which are involved in acid-base homeostasis (Lewis *et al.*, 1988; Sun *et al.*, 2008).

1.4.1 dRTA associated with kAE1 mutants

Mutant variants of kAE1 cause an impairment of HCO₃⁻ reabsorption across the basolateral membrane of α -intercalated cells, resulting in the intracellular accumulation of HCO₃⁻ ions. To maintain the intracellular acid-base and electrochemical balance, cells retain H⁺ or acid intracellularly albeit discharging it across the apical membrane into the tubular lumen. The accumulation of H⁺ and HCO₃⁻ ions subsequently reduces the intracellular dissociation of H₂CO₃. The impairment in H⁺ secretion into the urine due to the kAE1 defect will eventually lead to dRTA. Clinically, two types of mutations have been identified in the kAE1 encoding gene, triggering either autosomal dominant or autosomal recessive dRTA (Bruce *et al.*, 2000; Bruce *et al.*, 1997; Jarolim *et al.*, 1998; Tanphaichitr *et al.*, 1998). Dominant dRTA has only been found in a heterozygous background, suggesting that homozygous mutations might be lethal in an embryonic or postnatal stage. Moreover, dominant dRTA mutations in AE1 neither show any abnormal RBCs phenotype nor lead to hemolytic anemia. Conversely, patients with recessive dRTA have been reported to carry a homozygous or a compound heterozygous form involving two different mutations in the *SLC4A1* gene. Typically, recessive dRTA is often associated with hemolytic anemia, and patients additionally exhibit a different morphology of RBCs compared to a healthy person (Khositseth *et al.*, 2012; Yenchitsomanus *et al.*, 2005).

To characterize both dominant and recessive dRTA mutants, many studies have been performed in kidney cells such as MDCK cells and HEK293 cells. Dominant dRTA mutants expressed in

MDCK cells result in either intracellular retention (R589H, S613F) or mistargeting of kAE1 to the apical membrane (R901X, G609R). Besides, none of these dominant mutants displays an impaired anion exchange activity. On the contrary, recessive mutants expressed in MDCK cells exhibit different kAE1 trafficking defects such as a retention of the protein in the Golgi (G701D), or its proteasome-dependent degradation as misfolded protein (S773P) (Cordat *et al.*, 2006; Toye, 2005; Toye *et al.*, 2004). It has been reported that both dominant and recessive dRTA mutants can form heterodimers with wild-type kAE1 (Kittanakom *et al.*, 2004; Quilty *et al.*, 2002). Based on the different trafficking behavior of mutant kAE1 heterodimers in MDCK cells, phenotypic explanations of dominant and recessive dRTA have been proposed. In case of dominant dRTA conditions, when the mutants are co-expressed with wild-type protein, thereby mimicking the situation in dRTA patients, the heterodimers are retained in the ER (R589H) or mistargeted to the apical membrane (R901X) of polarized MDCK cells. Thus, dominant dRTA heterodimers exhibit a “dominant-negative effect” on kAE1 trafficking. Alternatively, homodimers of recessive mutants (G701D) could not exit from the secretory pathway and were retained in Golgi compartments. However, when wild-type kAE1 was co-expressed with recessive dRTA mutants (G701D or S773P), the heterodimers were able to reach the basolateral membrane. Here, the wild-type kAE1 shows a “dominant-positive effect” with respect to the recessive kAE1 mutant (Cordat *et al.*, 2006; Yenchitsomanus *et al.*, 2005). The before mentioned kAE1 G701D mutation (also called as “Band 3 Bangkok I”) is located in the hydrophilic loop that connects TM8 and 9 on the cytosolic side of the protein and results in a missense substitution of glycine by the aspartic acid in the AE1 peptide sequence (Reithmeier *et al.*, 2016). It was the first identified *SLC4A1* mutation associated with autosomal recessive dRTA (Tanphaichitr *et al.*, 1998). In *Xenopus* oocytes, the kAE1 G701D variant displayed a lack of cell surface expression and anion ion exchange activity, however, co-expression with glycophorin A could rescue its plasma membrane localization and chloride influx activity. This explains the normal cell surface expression and anion exchange activity of the kAE1 mutant in patients’ RBCs, which naturally contain glycophorin A. In recent years, nephrologist Dr. Rosa Verga-Poussou (Georges Pompidou Hospital in Paris) identified three new kAE1 mutants from patients with complete dRTA (Figure 1.5). Among them, one patient was carrying the homozygous kAE1 R295H mutation, and the other two patients were carrying heterozygous kAE1 Y413H and S525F mutations. The recessive kAE1 R295H mutation was the first dRTA-causing mutation detected in the cytosolic N-terminus of the protein, caused by a

missense mutation. On the contrary, the two dominant dRTA mutations were located within the transmembrane domains TM1 (Y413H) and TM5 (S525F) (Reithmeier *et al.*, 2016).

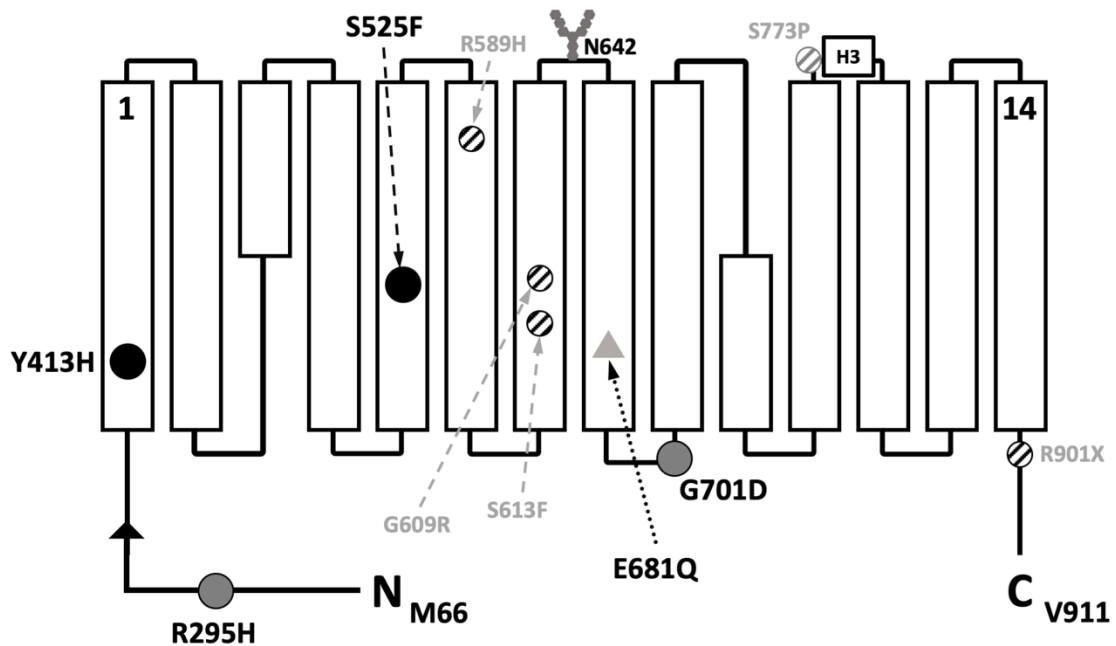


Figure 1.5: Topology model of kAE1 showing the location of mutations.

Linear topology model of kAE1 is illustrating the positions of the kAE1 mutations. The TMs are numbered from N-terminus (1) to C-terminus (14). The cytosolic side is at the bottom. Dominant dRTA mutations are indicated as black circles and recessive mutants are labeled as gray circles. The solid circles (black and gray) represent dRTA mutants investigated in this study (R295H, Y413H, S525F, and G701D). The hatched circles (black and gray) indicate dRTA mutants previously studied in mammalian cells and animal models. The gray triangle shows the location of the induced mutation E681Q. The N-glycosylation site at position N642 residue is indicated (modified from Almomani *et al.*, 2011).

In the kAE1 E681Q mutant, glutamine replaces the glutamate at position 681 in the AE1 peptide sequence, resulting in significant inhibition of monovalent anion exchange activity. Glutamate 681 (Glu⁶⁸¹) is located in TM8 and known as the binding site for H⁺ (Jennings & Smith, 1992). When the Glu⁶⁸¹ residue becomes protonated, AE1/kAE1 can transport divalent anions such as SO₄²⁻ instead of monovalent anions. Moreover, the AE1 E699Q knock-in mouse (equivalent to human E681Q) exhibited a proton independent Cl⁻/SO₄²⁻ exchange activity, indicating that this mutation converts the protein from an electroneutral to an electrogenic transporter which is much less sensitive to pH changes than the native protein. In HEK293 cells, kAE1 E689Q displays a cell surface localization and an impaired Cl⁻/HCO₃⁻ exchange activity, suggesting that Glu⁶⁸¹ is required as an active site for the Cl⁻/HCO₃⁻ exchange. However, the kAE1 E681Q

mutant is not clinically found and typically has been used as a transport-negative control (Chernova *et al.*, 2008; Jennings, 2005; Shnitsar *et al.*, 2013).

1.4.2 Controversy on the intracellular localization of kAE1 in dominant dRTA

Previously, *in vitro* studies using the kAE1 R589H mutant showed that it is retained in the ER as a homodimer and it can also lead to the retention of wild-type kAE1 into the ER by forming heterodimer (Reithmeier *et al.*, 2016). In HEK293 cells, kAE1 R589H mutant was predominantly retained in the ER despite being similarly folded as the wild-type protein (Quilty *et al.*, 2002). Further studies in MDCK cells also demonstrated the ER-retention of the mutant protein. However, the addition of the ER chaperon inhibitor castanospermine could rescue the kAE1 R589H mutant to the cell surface of MDCK cells, suggesting that inhibition of ER chaperones (such as calnexin) binding to the dominant dRTA mutant allows the escape of the mutant to the plasma membrane (Patterson & Reithmeier, 2010). In recent years, Mumtaz and colleagues performed a comprehensive study involving hetero- and homozygous knock-in mice carrying the dominant dRTA variant kAE1 R607H which corresponds to the human dominant dRTA kAE1 R589H mutant (Mumtaz *et al.*, 2017). A critical finding of the *in vivo* study was the regular targeting of functional kAE1 R607H variant to the basolateral membrane of α -intercalated cells, despite a low level of expression. This contradicts the concept of dRTA pathophysiology mechanisms previously obtained in MDCK cell studies, which based the development of autosomal dominant dRTA on the mistrafficking/mistargeting of the mutant (Figure 1.6). Besides, the study on dominant R607H dRTA knock-in mice suggests that the compromised pathological state observed in these mice is not caused by targeting or functional defects of kAE1, but due to the impaired targeting of V-H⁺-ATPase and a remarkably reduced number of α -intercalated cells in the kidney (Mumtaz *et al.*, 2017).

Previous model for kAE1-associated dRTA based on MDCK cells

New *in vivo* findings of dominant dRTA

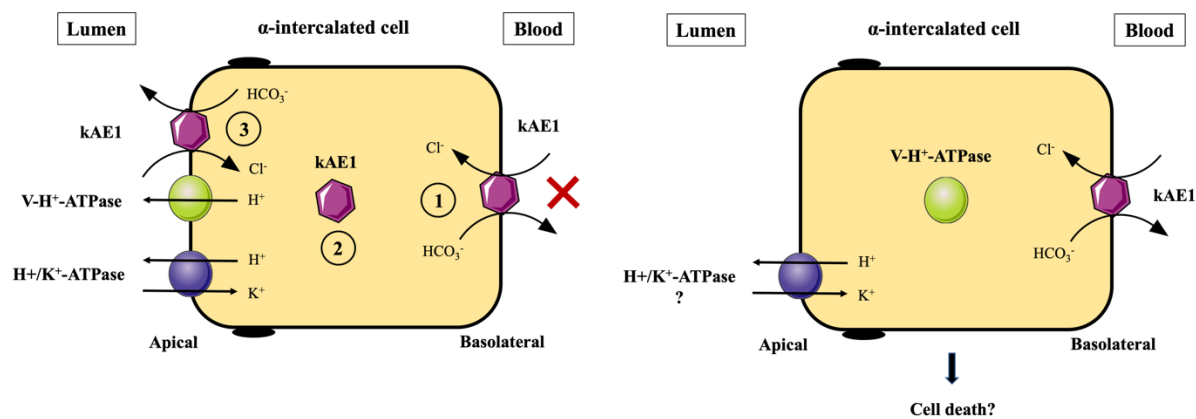


Figure 1.6: Schematic outline of previous and novel findings for kAE1-mediated dRTA. Left schema is showing the observed phenotypes of kAE1 mutants in MDCK cells. In MDCK cells, the dRTA causing kAE1 mutants were described as either (1) inactive, (2) intracellularly retained, or (3) mistargeted to apical membrane. Right diagram is depicting recent *in vivo* findings of the dominant dRTA kAE1 R607H variant. In kAE1 R607H knock-in mice, the missense mutation did not alter the trafficking of functional mutant protein to the basolateral membrane, but caused a secondary targeting defect of V-H⁺-ATPase to the apical membrane that potentially responsible for the dramatic loss of α -intercalated cells in the kidney. However, the precise reason for the α -intercalated cell depletion is still unknown (modified from Lashhab *et al.*, 2019).

As the dominant dRTA knock-in study was conducted in a mouse model, one has to be careful to hypothesize that dominant dRTA mutants are not mistrafficked in humans. In this context, biopsy data of human kidney tissue from patients suffering from dominant dRTA caused by the kAE1 mutation G609R displayed a similar phenotype as knock-in mice, showing a significant reduction of α -intercalated cells and a severe targeting defect of V-H⁺-ATPase (Vichot *et al.*, 2017). The *in vivo* patient data were pointing out that the phenotypic explanation of dominant dRTA from MDCK cells might not be correct, and the dominant dRTA mutant phenotype is based on the different genetic background between the MDCK cells and the α -intercalated cells. These findings illustrate the complexity of kAE1-related dRTA and highlight that the molecular and cellular mechanism of kAE1-related dRTA still remains obscure.

1.5 Alternative model systems for investigating kAE1 physiology

Many mammalian cells have been successfully employed as a model system for the study of renal proteins, but there is always the dilemma which cell type is the most suitable model. Since

α -intercalated cells could not be immortalized yet, other available kidney cell lines, including HEK293 and MDCK cells, were used to characterize dominant or recessive dRTA-causing mutations. The recent *in vivo* data of dominant dRTA patients as well as data from dominant dRTA knock-in mice contradict the findings from these kidney cell lines. Thus, the molecular mechanisms involved in dRTA need to be further investigated and clarified by using a cell model that is maximally close to α -intercalated cells. A promising cellular model system is mouse inner medullary collecting duct cells (mIMCD3) which are derived from individual tubules of the terminal inner medullary collecting duct (IMCD) in the kidney of transgenic mice expressing the early region of simian virus 40 (SV40) (Rauchman *et al.*, 1993). It has been reported that, when the kAE1 mutant R589H was expressed in mIMCD3 cells, the mutant exhibits unaltered trafficking to the basolateral membrane and a normal ion exchange activity. These observations are in line with the results obtained in *in vivo* knock-in mice (Mumtaz *et al.*, 2017). Moreover, these cells are capable of adapting to hypertonic medium (~910 mOsmol/kg H₂O). This particular characteristic of mIMCD3 cells makes them highly favorable for the study of cellular adaptation to osmotic conditions similar to the natural *in vivo* state of the renal medulla (Madsen *et al.*, 1988). Therefore, all the features mentioned above highlight that mIMCD3 cells are a well-fitting cellular model for imitating *in vivo* dRTA conditions. In addition to mammalian cell lines, other model systems are available for investigating renal proteins, including baculovirus-infected insect cells and *Xenopus* oocytes. The latter are widely used in electrophysiology studies of numerous renal transporters and membrane proteins. Still, biochemical techniques utilizing this system are laborious, and the number of available materials is also limited (Kolb *et al.*, 2011). The usage of insect cells for heterologous gene expression makes it necessary to generate recombinant baculoviruses that render this system technically challenging as well (Junge *et al.*, 2008). However, genetic manipulation of mammalian cells may not be secure and can be very time-consuming, and since the previous section revealed that the molecular basis of dRTA is far more complex than initially expected, it is important to comprehend the molecular mechanism of kAE1 trafficking in kidney cells in a more specific manner. From this perspective, alternative model organisms are useful tools to address various cellular aspects of kAE1-physiology. In this thesis, the potential of the yeast *Saccharomyces cerevisiae* (*S. cerevisiae*) has been emphasized as a model organism to investigate intracellular transport and functionality of kAE1.

S. cerevisiae has been widely used to analyze a variety of renal proteins in order to investigate their expression, trafficking, structural and functional activity, or to identify interacting partners and degradation pathways (Kolb *et al.*, 2011). Several fundamental features make yeast an excellent model system to study a renal protein like kAE1. Firstly, most of the cellular processes are conserved between *S. cerevisiae* and higher eukaryotic organisms. Therefore, data obtained from studies in *S. cerevisiae* can be translated into the situation of higher organisms. Secondly, yeast is a unicellular organism that can exist in a haploid and a diploid state, giving the opportunity for either clonal division or sexual crossing and allowing for genetic manipulation and screening. Thirdly, yeast can be cultivated in a large quantity in a speedy and cheap way. Fourthly, the transformation of heterologous genes in *S. cerevisiae* is a straightforward process and a given protein of interest can be expressed either from an episomal plasmid or through chromosomal integration. In addition, it is a relatively easy process to insert, mutate or delete any genomic sequence in yeast because of its highly efficient homologous recombination machinery. Fifthly, a wide range of genetic manipulation tools is available for *S. cerevisiae* in comparison with other model systems, such as the collection of non-essential gene knock-out mutants (about ~85% of all genes) and the collection of temperature-sensitive mutants which is about ~50% of total essential genes. Moreover, *S. cerevisiae* was the first eukaryotic organism whose complete genome was sequenced in 1996 (Goffeau *et al.*, 1996). High-throughput data from functional genomic resources including metabolome, transcriptome, proteome and lipidome analysis provide the availability of beneficial information that makes it the organism with an extensively available dataset. Finally, since genetic modifications can be attained in yeast in a facilitated way, large-scale screens of genetic interactions are feasible, which permits efficient assessment of genetic interaction maps (Kolb *et al.*, 2011; Petranovic & Nielsen, 2008).

Although important discoveries have undoubtedly been made using other model systems, there is always a requirement for a faster, cheaper, easier, and more genetically amenable system. Notably, the membrane domain of eAE1/kAE1 (361–911 aa, also known as B3mem) has already been expressed at high levels in *S. cerevisiae* and was found functional at the plasma membrane (Groves *et al.*, 1996). Therefore, yeast stands out as a prospective model organism for investigating trafficking machineries, protein-protein interactions and subcellular localization of wild-type kAE1 and its dRTA-causing mutants.

1.6 Aims of this study

kAE1 significantly contributes to renal acid secretion by promoting HCO_3^- reabsorption into the blood produced by the renal tubular H^+ secretion. Malfunctioning of this protein disrupts the renal acid-base regulation process and leads to dRTA. Since it is known that dRTA is not simply caused by the mistrafficking of kAE1 but is based on a more complicated process, it is necessary to understand the proper maturation and trafficking process of kAE1 under normal physiological conditions. The first aim of this study was to dissect the expression and trafficking of kAE1 in a fast and inexpensive manner by using *S. cerevisiae* as a model organism. In order to achieve this ambitious goal, a variety of full-length kAE1 variants should be generated. After optimizing the expression in yeast, the subcellular localization of kAE1 was extensively analyzed by fluorescence-based and confocal laser-scanning microscopy. The functionality of the full-length protein was further investigated by the cytosolic pH measurement assay and the ion-exchange chromatography.

Until now, mIMCD3 cells are reported as the closest cellular model for α -intercalated cells. The second aim of this thesis was the characterization of dRTA mutants in mIMCD3 cells. For this purpose, the half-life of three novel dRTA mutants, one recessive (kAE1 R295H) and two dominant mutants (kAE1 Y413H and S525F), were determined in a stably transduced mIMCD3 cell system. Since defective autophagy was seen in dominant dRTA knock-in mice, the effect of these mutants on the autophagy process was investigated by assessing the protein level of its regulator named p62. Lastly, the impact of dRTA mutants on the proliferation of mIMCD3 cells was analyzed.

2. Materials and Methods

2.1 Organisms

In this research project, different cells from distinct species were used to explore the localization, function and degradation of wild-type kAE1 and its mutants.

2.1.1 Bacterial strains

Escherichia coli strain indicated in Table 1 was taken from the strain collection of the Department of Molecular and Cell Biology at Saarland University.

Table 1: Information of used bacterial strain, its genotype and source

Strain	Genotype	Source
TOP10	F ⁻ <i>mcrA</i> Δ (<i>mrr-hsdRMS-mcrBC</i>) Φ 80 <i>lacZ</i> Δ M15 <i>ΔlacX74 recA1 deoR araD139 Δ(ara-leu) 7697</i> <i>galU galK rpsL (Str^R) endA1 nupG</i>	Invitrogen

2.1.2 Yeast strains

Saccharomyces cerevisiae strains mentioned in Table 2 were taken from the strain collection of the Department of Molecular and Cell Biology at Saarland University.

Table 2: Information of used yeast strains, their genotypes and sources

Strain	Genotype	Source
BY4742	MAT α ; <i>his3</i> Δ 1; <i>leu2</i> Δ 0; <i>lys2</i> Δ 0; <i>ura3</i> Δ 0	Open Biosystems/ Winzeler <i>et al.</i> , 1999
Δ <i>bor1</i>	MAT α <i>his3</i> Δ 1 <i>leu2</i> Δ 0 <i>lys2</i> Δ 0 <i>ura3</i> Δ 0 Δ <i>bor1</i>	Open Biosystems
Δ <i>end3</i>	MAT α <i>his3</i> Δ 1 <i>leu2</i> Δ 0 <i>lys2</i> Δ 0 <i>ura3</i> Δ 0 Δ <i>end3</i>	Open Biosystems

2.1.3 Mammalian cell lines

Mammalian cell lines specified in Table 3 were taken from the cryoculture collection of the Department of Physiology at the University of Alberta (UofA), Canada.

Table 3: Information of used mammalian cell lines, their genotypes and sources

Cell line	Features	Source
mIMCD3	Mouse, transgenic, medulla or collecting duct of kidney, SV40 transformed, epithelial, adherent	ATCC® (CRL-2123™)
mIMCD3 kAE1	pLVX-TRE3G kAE1, pLVX-Tet3G	Cordat lab, UofA, Canada
mIMCD3 kAE1 R295H	pLVX-TRE3G kAE1 R295H, pLVX-Tet3G	Cordat lab, UofA, Canada
mIMCD3 kAE1 Y413H	pLVX-TRE3G kAE1 Y413H, pLVX-Tet3G	Cordat lab, UofA, Canada
mIMCD3 kAE1 S525F	pLVX-TRE3G kAE1 S525F, pLVX-Tet3G	Cordat lab, UofA, Canada

2.2 Growth media and culture condition

Culture media used in this study were prepared by dissolving particular components in distilled water (dH₂O), followed by autoclaving at 121 °C for 20 min at 15 psi. For bacteria and yeast, liquid and solid media were stored at room temperature (RT) and at 4 °C, respectively. The media used for mammalian cell culture were stored at 4 °C.

2.2.1 Bacteria

Lysogeny broth (LB) medium composed of the following ingredients was used to culture bacterial strains.

LB Medium	
Components	Amount
Trypton	1.0% (w/v)
Yeast extract	0.5% (w/v)
NaCl	0.5% (w/v)
Agar (only for plates)	1.5% (w/v)

Bacterial cultures in liquid media were maintained in a shaking incubator about 220 rpm at 37 °C, whereas cultures on solid media were kept in an incubator at 37 °C overnight (unless otherwise indicated).

2.2.2 Yeast

Yeast peptone dextrose (YPD) medium

YPD medium composed of the following components was used for the maintenance and propagation of yeast cells.

YPD medium	
Components	Amount
Glucose	2% (w/v)
Peptone	2% (w/v)
Yeast extract	1% (w/v)

To prepare YPD medium, peptone and yeast extract were dissolved in 800 ml of dH₂O, while glucose was dissolved in 200 ml of dH₂O. Subsequently, both solutions were autoclaved separately and mixed.

Synthetic complete medium (SC-medium)

SC-medium, commonly utilized for the auxotrophic yeast growth, was prepared by mixing of solutions A, B, and C.

Solution A		Solution B		Solution C	
Components	Amount	Components	Amount	Components	Amount
Glucose /	2% /	Ammonium	0.5% (w/v)	YNB	0.17% (w/v)
Raffinose /	2% /	sulfate			
Galactose /	3% (w/v)	SC-Mix	0.087% (w/v)		
Agar (for plates)	1.5% (w/v)				

SC-Mix

Components	Amount	Components	Amount	Components	Amount
Adenine	0.2 g	Leucine	1.0 g	Tryptophan	0.2 g
Arginine	0.2 g	Lysine	0.3 g	Tyrosine	0.3 g
Asparagine	1.0 g	Methionine	0.2 g	Uracil	0.2 g
Histidine	0.2 g	Phenylalanine	0.5 g	Valine	1.5 g
Isoleucine	0.3 g	Threonine	2.0 g		

Solutions A, B, and C were prepared separately by dissolving the above-mentioned ingredients in 700 ml, 250 ml and 50 ml of dH₂O, respectively. Then, the solutions A and B were autoclaved while the solution C was sterilized by filtration (0.2 µm sterile filter, Merck). The liquid media were kept at RT, and the solid media plates containing agar were stored at 4 °C. To prepare a particular drop-out (d/o) medium, the appropriate amino acids or bases were omitted in the SC-Mix. The SC- or drop-out mix was stored at 4 °C.

2.2.3 Mammalian cells

Stably transduced mIMCD3 cells were cultured in Dulbecco's Modified Eagle Medium/Nutrient Mixture F-12 (DMEM/F12 = 1:1) medium containing the below-listed components.

Growth medium

Components	Amount
DMEM/F12	500 ml
FBS	10% (v/v)
Penicillin/Streptomycin	1% (v/v)
G418	2 mg/ml
Puromycin	4 µg/ml

DMEM/F12 medium was supplemented with 10% fetal bovine serum (FBS), 1% penicillin/streptomycin, 2 mg/ml G418 and 4 µg/ml puromycin for maintaining the stably transduced mIMCD3 cells. The cells were incubated in culture flasks, dish or well-plates at 37 °C with 5% CO₂. To split confluent cells, culture medium was removed and the adherent

cell monolayer was washed with 1x PBS. The cells were detached by adding 1x Trypsin/EDTA solution and subsequent incubation in the incubator for the duration of 2–5 min, depending on the cell line. The reaction was stopped by adding two volumes of cell culture medium. The cells were then resuspended, and a portion of the cell suspension (depending on the proliferation rate of cells) was transferred into a cell culture flask with fresh medium.

2.3 Cryopreservation

Cryopreservation technique is used to store structurally intact living cells or tissue at very low temperatures. Cryoprotectants like glycerol or DMSO were added to protect the intact cells or subcellular structures (Day & McLellan, 1995).

2.3.1 Cryopreservation of bacteria and yeast

Bacteria and yeast cells were grown overnight in a 5 ml culture tube. 1 ml of a fresh overnight culture was then mixed with 1 ml sterile glycerol (99% v/v). The tubes were then kept at $-80\text{ }^{\circ}\text{C}$ in the freezer.

2.3.2 Cryopreservation of mammalian cells

Cryopreservation samples were prepared from freshly grown cells with a confluency of about 70–80%. Cells were washed with 1x PBS and detached by applying 1x trypsin/EDTA solution. Next, cell density was counted by a hemocytometer and an appropriate amount was centrifuged at 300 g for 5 min at $4\text{ }^{\circ}\text{C}$. After aspiration of the supernatant, the cell number was adjusted to 1×10^6 cells/ml in an equal part of both DMEM/F12 and freezing medium (composition listed below). Afterward, 1 ml of cell suspension was transferred to a cryotube. A freezer box (CryoSaveTM, Scienceware) was utilized for controlling the freezing rate of the cells ($-1\text{ }^{\circ}\text{C}/\text{min}$) by placing at $-80\text{ }^{\circ}\text{C}$ for 24 h. Finally, to ensure the long-term preservation of the cells, all tubes were kept in liquid nitrogen.

Freezing medium

Components	Amount
FCS	60%
DMSO	20%
DMEM:F12	20%

2.4 Plasmids

Plasmids used in this study and their characteristics are described in Table 4.

Table 4: Information of plasmids used in yeast, their characteristics and sources

Plasmid	Characteristics	Source
pYES2.1 V5-His-TOPO	<i>S. cerevisiae</i> expression vector, <i>GAL1</i> promoter, <i>URA3</i> and <i>Amp^R</i> gene, TOPO-Cloning site, V5-epitope (C-terminus), polyhistidine (6xHis) -tag (C-terminus)	Thermo Scientific
pYES2.1 hkAE1 ^{V5}	pYES2.1 with a human wild-type kAE1 sequence containing a V5 tag at the C-terminus	This study
pYES2.1 Kar2 ^{SS} - hkAE1 ^{V5}	pYES2.1 with a human wild-type kAE1 sequence containing a Kar2 ^{SS} at the N-terminus and a V5 tag at the C-terminus	This study
pYES2.1 ykAE1 ^{V5}	pYES2.1 with a yeast codon-optimized sequence of wild-type kAE1 sequence containing a V5 tag at the C-terminus	This study
pYES2.1 ykAE1	pYES2.1 with an untagged wild-type yeast codon-optimized kAE1 sequence	This study
pYES2.1 ykAE1-yeGFP	pYES2.1 with a yeast codon-optimized wild-type kAE1 sequence fused to a yeGFP at its C-terminus	This study
pYES2.1 yeGFP-ykAE1	pYES2.1 with a yeast codon-optimized wild-type kAE1 sequence connected to a yeGFP at the N-terminus through a flexible GGGGS linker.	This study
pYES2.1 ykAE1 ^{HA}	pYES2.1 with a yeast codon-optimized wild-type kAE1 sequence containing a HA tag within third extracellular loop between Asn ⁵⁵⁶ and Val ⁵⁵⁷	This study
pYES2.1 ykAE1- G701D ^{FLAG}	pYES2.1 with a yeast codon-optimized kAE1 sequence containing the G701D mutation and a FLAG tag within third extracellular loop between Asn ⁵⁵⁶ and Val ⁵⁵⁷	This study

pYES2.1 ykAE1-E681Q	pYES2.1 with an untagged yeast codon-optimized kAE1 sequence containing the E681Q mutation	This study
YIplac128	Yeast integrating plasmid vector, <i>LacZα</i> , <i>URA3</i> and <i>Amp^R</i> gene,	(Malínská <i>et al.</i> , 2003)
YIplac128 Pma1-mRFP	YIplac128 with a yeast proton pump sequence attached to a mRFP at the C-terminus	(Malínská <i>et al.</i> , 2003)
pPGK 6His/Xa/GST	<i>S. cerevisiae</i> expression vector, <i>PGK1</i> promoter, <i>URA3</i> and <i>Amp^R</i> gene, polyhistidine (6xHis) -tag (C-terminus), GST-tag (C-terminus).	(Kang <i>et al.</i> , 1990)
pPGK ykAE1	pPGK with an untagged wild-type yeast codon-optimized kAE1 sequence inserted between <i>XhoI</i> and <i>BamHI</i> restriction sites.	This study
pMS109	<i>HAC1</i> gene of <i>S. cerevisiae</i> inserted between the promoter and terminator of <i>PGK1</i> gene into the <i>S. cerevisiae</i> single-copy vector pKK1 carrying a <i>LEU2</i> auxotrophic marker gene.	(Valkonen <i>et al.</i> , 2003)
pAct1-GEV	β -estradiol inducible activator Gal4dbd.ER.VP16 (GEV) sequence inserted in the <i>S. cerevisiae</i> plasmid vector pAGL containing <i>ACT1</i> promoter.	(McIsaac <i>et al.</i> , 2011)

2.5 Polymerase chain reaction (PCR)

kAE1 variants were constructed by using polymerase chain reaction (PCR). For that purpose, the FastStart High Fidelity PCR system (Merck) was used which contains a proof-reading *Taq* polymerase. PCR was performed by using a thermocycler (Mastercycler nexus, Eppendorf) with adapting specific parameters according to the length of the product, the annealing temperature of the primers, or both. Amplified products were then checked by agarose gel electrophoresis. For a single application, the components listed below were added into a PCR tube.

Components	Amount
10x PCR buffer	5.0 μ l
Primer forward (100 mM)	0.25 μ l
Primer reverse (100 mM)	0.25 μ l
Template-DNA	100 ng
dNTPs (10 mM)	1.0 μ l
DNA Polymerase (5 U/ μ l)	0.5 μ l
dH ₂ O (sterile)	Up to 50 μ l

PCR reactions were carried out by following subsequent parameters in the thermocycler.

Cycle steps	Temperature (°C)	Time	Cycle
Initial denaturation	95	2 min	1
Denaturation	95	30 sec	} 30
Annealing	55	30 Sec	
Elongation	72	3 min	
Final elongation	72	7 min	1
Cooling	4	∞	

Primers were used to generate untagged ykAE1 (ykAE1) and N-terminus yeGFP fused ykAE1 (yeGFP-ykAE1), and are listed in Table 5. Primer sequences written with capital letters represent the target DNA sequence, small letters refer to the restriction sites, and small underlined letters indicate the linker sequence (GGGGS).

Table 5: Overhang primers for *in vivo* recombination in yeast

Primer name	Overhang complementary with	Sequence 5'–3'
5' ykAE1	pYES2.1	CGACTCACTATAGGGAATATTAAGCTCGCctcgaggaattc ATGGACGAAAAGAATCAAGAATTGAGATG
3' ykAE1	pYES2.1	ACCTTCGAATGGGTGACCTCGAAGCTCGCCgtcgacggatcc TTAAACTGGCATAGCAACTTCATCGTATTC
5' yeGFP	pYES2.1	ACTATAGGGAATATTAAGCTCGCctcgag ATGTCTAAAGGTGAAGAATTATTCAC
3' yeGFP	5' ykAE1	CATCTCAATTCTTGATTCTTTTCGTCactaccaccaccacc TTTGTACAATTCATCCATACCA

kAE1 variants generated by PCR were routinely sequenced by Eurofins Genomics and data were analyzed using DNASTAR Lasergene 7.0 software.

2.6 Site-directed mutagenesis

Site-directed mutagenesis is a widely used method for introducing a point mutation in a DNA sequence (Hutchison *et al.*, 1978). This technique is very beneficial for generating DNA sequences with mutated codons, insertions and sequence deletions. In this study, mutants were generated by using the “Q5 site-directed mutagenesis kit” (NEB) with the mutagenic primers listed in Table 6. Primer sequences shown as capital letters refer to the target DNA sequence. The nucleotides altered from the native sequence are marked in red and mutated codons are underlined.

Table 6: Mutagenic primers (for yeast codon-optimized sequence of kAE1)

Primer name	Sequence 5'–3'
5' E681Q	GAT ATT CTT <u>GCA</u> ATC CCA AAT CAC
3' E681Q	AAG ATA AAA ACC AAT AAA GCT G
5' G701D	AAG GGT TCT <u>GAT</u> TTT CAC TTG
3' G701D	GAC CAT CTT TCT TTC AGG

First, PCR was accomplished with the Q5 Hot Start High-Fidelity DNA Polymerase for introducing the particular mutation in the kAE1 sequence. Later on, the amplified PCR product was incubated with the Kinase-Ligase-*DpnI* (KLD) enzyme-mix at RT for 5 min. The kinase phosphorylates the amplified PCR product at the 5' end enabling the product to be circularized by the ligase. The *DpnI* restriction enzyme then removed the template DNA by cleaving methylated DNA. Finally, the obtained product was transformed into high-efficiency NEB 5- α competent *E coli* cells. The PCR cycles were performed by applying the following parameters in the thermocycler.

Cycle steps	Temperature (°C)	Time	Cycle
Initial denaturation	98	30 sec	1
Denaturation	98	10 sec	} 25
Annealing	57	30 Sec	
Elongation	72	4 min	
Final elongation	72	7 min	1
Cooling	4	∞	

2.7 TOPO TA cloning

pYES2.1 (Thermo Scientific) expressing vector was used for the yeast expression of kAE1 variants. A synthetic cDNA string of human or yeast codon-optimized kAE1 sequence was inserted into pYES2.1 by TOPO cloning. TOPO cloning reaction was accomplished using the following components.

Components	Amount
3' poly-A overhangs DNA	2.0 μ l
pYES2.1/V5-His-TOPO [®] vector	0.5 μ l
Salt solution (1.2 M NaCl, 0.06 M MgCl ₂)	0.5 μ l

As the plasmid vector is linearized and has thymidine (T) overhangs, the insert should have 3' adenine (A) overhangs for ligation. Extension of 3' poly-A overhangs at cDNA string was carried out with *Taq* polymerase using the following reaction mixture.

Components	Amount
Synthetic cDNA (20 ng/μl)	8.0 μl
<i>Taq</i> polymerase	1.0 μl
10x reaction buffer	1.0 μl
dATP	0.1 μl

The reaction was performed in PCR tubes in a thermocycler (Mastercycler nexus, Eppendorf) at 72 °C for 15 min. Then, tubes were placed on ice for subsequent DNA precipitation. After the addition of the poly-A overhangs, DNA strings were sedimented using phenol-chloroform extraction by adding 10 μl of phenol:chloroform:isoamyl alcohol (25:24:1) solution with gentle mixing. Next, 2 μl of 3 M sodium acetate and 44 μl of absolute ethanol were added, followed by gently mixing. The mixture was centrifuged at 13,000 rpm for 5 min. After the supernatant was aspirated, the pellet was rinsed with 80% ethanol and air-dried. Finally, DNA the pellet was resuspended into 5 μl dH₂O.

2.8 Restriction digestion

Restriction cloning is the insertion of a gene of interest within a plasmid vector. An expression vector usually carries the information of replication and expression for the target gene. A variety of endonucleases is used to create sticky ends of the vector and insert fragments that subsequently ligate by utilizing the ligase enzyme. For the constitutive expression of kAE1 in *S. cerevisiae*, the unmodified kAE1 (ykAE1) sequence was inserted into the pPGK vector through *Xho*I and *Bam*HI restriction sites. ykAE1 insert and pPGK vector were individually double digested with the relevant restriction enzymes for 3 h at 37 °C. 50 μl digestion mixture for both vector and insert were arranged as indicated below.

Components	Amount
10x buffer	5.0 μ l
<i>Bam</i> HI (10 unit/ μ l)	1.0 μ l
<i>Xho</i> I (10 unit/ μ l)	1.0 μ l
RNase A	0.5 μ l
Vector/Insert DNA	5.0 μ g
dH ₂ O	add 50 μ l

Digested DNA fragments were separated by agarose gel electrophoresis and extracted by using the “Gel Extraction Kit” (Omega Bio-tek) following the manufacturer’s protocol. Both vector and insert were separately eluted in nuclease-free water. Purified digested insert and vector were then ligated by using “T4 DNA ligase kit” (Roche). The amount of insert and vector can differ depending on the length of the insert. Ligation was carried out into a total volume of 20 μ l containing the following components.

Components	Amount
Insert	8 μ l (variable)
Vector	8 μ l (variable)
Buffer 10x	2 μ l
T4 DNA ligase	1 μ l
dH ₂ O	Up to 20 μ l

Reaction mixture was incubated overnight at 16 °C. To remove salt from the mixture, the ligated product was dialyzed by using a dialysis filter (0,025 μ m, Millipore) floating on 10% glycerin solution for 1 h. The dialyzed ligation mixture was then used for electroporation.

2.9 Agarose gel electrophoresis

Amplified PCR products or digested plasmids were analyzed by agarose gel electrophoresis. For the sample preparation, 20 μ l PCR product or digested plasmid were mixed with 5 μ l of 5x GLB (gel loading buffer) solution and loaded into the wells of an agarose gel (1%) together with 5 μ l of HyperLadder™ 1kb (Bioline) DNA marker. The electrophoresis was performed at 160 V, 400 mA and 45 min with 1x TBE as the electrophoresis buffer using BlueMarine™

100 system (Serva Electrophoresis GmbH). To visualize DNA fragments, gels were soaked in ethidium bromide solution (2.5 µg/ml) for 10–15 min, and respective DNA bands were detected by using the ChemiDoc XRS system (Bio-Rad). Captured images were analyzed by the Quantity One 4.6.2 (Bio-Rad) software. Following electrophoresis, the DNA fragments were reisolated by using “E.Z.N.A. gel extraction kits” (Omega) according to the manufacturer’s protocol. 10x TBE buffer and 5x GLB buffer were prepared as mentioned below.

10x TBE buffer

Component	Amount
Tris-HCl, pH 8,0	0.89 M
Boric acid	0.89 M
Na ₂ EDTA	0.02 M

5x GLB buffer

Component	Amount
Glycerin	50% (v/v)
SDS	1% (w/v)
Na ₂ EDTA	125 mM
Bromophenol blue	0.05% (w/v)
Xylene cyanol	0.05% (w/v)

2.10 Transformation of microorganisms

2.10.1 Electroporation of *E. coli*

Preparation of electrocompetent cells

To prepare electrocompetent TOP10 cells, 200 ml of LB medium was inoculated with 1% of a fresh overnight culture and incubated at 37 °C until culture density reached OD₆₀₀ = 0.7. Afterward, cells were placed on ice for 15 min and then centrifuged at 8,000 rpm for 5 min at 4 °C. Cells were then washed two times by using 10% sterile glycerin and the cell pellet was resuspended in the remaining liquid. The cell suspension was transferred into a new reaction tube and centrifuged in a similar procedure. Supernatant was aspirated and pellet was

resuspended in an equal volume of 10% glycerol. Finally, 40 μ l of cell suspension were aliquoted in a microcentrifuge tube and stored at -80 °C.

Electroporation

The recombinant plasmids were transformed in TOP10 competent cells via electroporation. One aliquot (40 μ l) of electrocompetent cells was thawed and mixed gently with the ligated product. After 5 min incubation on ice, the mixture was placed into an electroporation cuvette (Bio-Rad). Electroporation was carried out using the “Gene Pulser Xcell™” (Bio-Rad) at 200 Ω , 2.5 kV/cm and 2.5 μ F. Immediately after the pulse, cells were resuspended in 1 ml SOC medium (composition provided below) and incubated for 1 h at 37 °C. Later on, cells were plated on LB-agar plates containing antibiotics as a selection marker for positive transformants and cultivated overnight at 37 °C.

SOC medium	
Component	Amount
Yeast extract	0.5%
Peptone	2.0%
Sodium chloride	10 mM
Glucose	20 mM
Potassium chloride	10 mM
Magnesium chloride	10 mM
Magnesium sulfate	2.5 mM

Plasmid selection

Antibiotic used for bacterial strain selection is specified in the list below. Sterilization was accomplished by filtering the solution through 0.2 μ filter.

Substance	Concentration	Solvent
Ampicillin	50 mg/ml	50% (v/v) ethanol

Selection for positive bacterial transformants was achieved by adding 400 µg/ml Ampicillin in liquid or solid medium.

2.10.2 Transformation of *S. cerevisiae*

2.10.2.1 Lithium acetate transformation

Lithium-acetate transformation is a simple and fast method to introduce exogenous DNA into *S. cerevisiae* (Gietz *et al.*, 1995; Ito *et al.*, 1983). To accomplish the procedure, four elements are necessary: divalent alkali cations, polyethylene glycol (PEG), single-stranded carrier DNA (Herring sperm), and a heat shock at 42 °C. In order to perform a single transformation, 2 ml fresh overnight yeast culture were centrifuged at 8,000 rpm for 5 min. Supernatant was aspirated and pellet was then washed two times with 500 µl of 1x LiAc/TE solution. After the wash, cells were finally resuspended in 100 µl of 1x LiAc/TE. Yeast cell suspension was mixed with 10 µl denatured carrier DNA (Herring sperm), 1 µg plasmid DNA and 600 µl PEG solution. After incubation for 30 min at 30 °C, the heat shock was performed in a water bath for 15 min at 42 °C. Cells were then centrifuged at 13,000 rpm for 1 min, and the pellet was washed two times with 500 µl of 1x TE solution. Finally, cells were resuspended in 500 µl 1x TE solution and the cell suspension was plated onto a suitable d/o glucose-agar plate. Plates were incubated at 30 °C for 3 d and checked for the growth of the appropriate yeast colonies. Reagents used for yeast transformation were prepared as mentioned below.

Polyethylene glycol (PEG 50%)

Component	Amount
PEG-4000	50% (w/v)

TE-Buffer (10x)		Lithium acetate (10x LiAc)	
Components	Amount	Components	Amount
Tris	100 mM	Lithium acetate	1.0 M
Na ₂ EDTA	10 mM		

pH of TE-buffer and LiAc solution was adjusted to 7.5 with acetic acid.

PEG solution		LiAc-TE solution	
Components	Amount	Components	Amount
PEG (50%)	80% (v/v)	10x TE buffer	10% (v/v)
10x TE buffer	10% (v/v)	10x LiAc	10% (v/v)
10x LiAc	10% (v/v)	dH ₂ O (sterile)	80% (v/v)

2.10.2.2 *In vivo* recombination in yeast

S. cerevisiae has a unique feature of combining ectopic linear DNA fragments inside the cell (Gibson *et al.*, 2008; Jinks-Robertson *et al.*, 1993). In this process, the fragment of DNA requires to bear homology of the plasmid sequence that can be directly ligated with the linearized vector sequence. Previously, Manivasakam and his colleagues reported that 15 bp of the overlapping region of DNA fragments are sufficient for effective integration in yeast (Manivasakam *et al.*, 1995). It is a straightforward cloning method that avoids multiple-steps involved in restriction cloning, such as enzymatic digestion, and subsequent ligation of insert and vector. In this study, two expression plasmids pYES2.1-ykAE1 and pYES2.1-yeGFP-ykAE1 were generated via *in vivo* recombination. Primers were designed with a homologous region between 25–30 bp of the pYES2.1 vector and the kAE1 yeast codon-optimized sequence (Table 5). Unmodified kAE1 (ykAE1) was amplified by performing PCR, using pYES2.1-ykAE1-yeGFP as template and appropriate forward and reverse primers. Next, the pYES2.1-yeGFP plasmid was enzymatically digested with *Xho*I and *Bam*HI. Finally, the PCR fragment (ykAE1) and linearized vector (pYES2.1) were transformed by Li/Ac transformation technique into yeast cells. The ligation of pYES2.1-ykAE1 plasmid was carried out by yeast itself through *in vivo* recombination. For pYES2.1-yeGFP-ykAE1 plasmid, yeGFP was generated by PCR with the designated primers (Table 5) using pYES2.1-yeGFP as a template. In the end, the PCR product and linearized pYES2.1-ykAE1 plasmid (digested with *Xho*I) were transformed into yeast and DNA fragments ligated via *in vivo* recombination.

2.10.2.3 GEV yeast strain construction

The BY4742-GEV strain was generated by transforming cells with the linearized plasmid pAct1-GEV digested with *Eco*RV. Clones with successful homologous recombination were selected on leucine d/o plates. The positive transformants were finally transformed with

pYES2.1-ykAE1 to generate BY4742-GEV [pYES2.1-ykAE1] strain, in which kAE1 was expressed upon β -estradiol induction.

2.11 Lentiviral transduction of mammalian cells

Transduction is a process where a foreign DNA molecule is introduced to host cells by a virus or viral vector. In recent years, the lentiviral transduction system becomes a very efficient tool for delivering transgenes into mammalian cells to create stable cell lines for robust expression of target proteins. The system uses a recombinant lentivirus, incorporating the genetic materials of human immunodeficiency viruses (HIV) to deliver the target gene. By exploiting the host's cellular machinery, viruses are amplified and packed their genetic material together with the transgene. The packed transgene is then transported via membrane fusion to the target cells (Elegheert *et al.*, 2018; Naldini *et al.*, 1996). The Lenti-X™ Tet-On® 3G (Clontech) Inducible Expression System uses a regulator vector, pLVX-Tet3G and a response vector, pLVX-TRE3G. The regulator plasmid is responsible for constitutive expression of the Tet-on 3G transactivator protein under the control of the P_{CMV} promoter (Figure 2.1 A). In contrast, the response plasmid contains an inducible promoter P_{TRE3GV} which controls transcription of the gene of interest (Figure 2.1 B). Plasmid vectors map are depicted below:

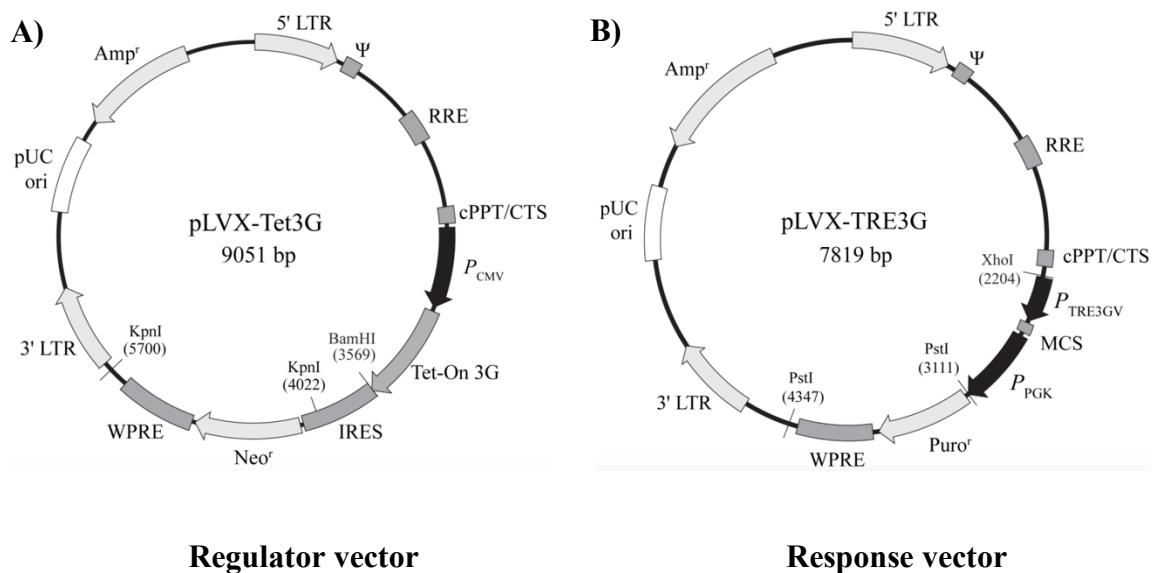


Figure 2.1: Overview of vectors used in lentiviral transduction system.

(A) pLVX-Tet3G regulator vector consisting of markers (Neo^r and Amp^r), origin of replication (pUC ori), promoter (P_{CMV}) and viral elements (5' LTR, 3' LTR, WPRE, RRE, IRES).

Continued Figure 2.1: (B) pLVX-TRE3G response vector comprising of markers (Puro^r and Amp^r), promoter (P_{TRE3V} and P_{PGK}), origin of replication (pUC ori), MCS (multiple cloning site) and viral elements (5' LTR, 3' LTR, WPRE, RRE, IRES). Besides MCS, restriction sites are indicated on the vector map (Clontech).

In the presence of doxycycline, the Tet-on 3G protein undergoes for structural modification and then binds at the tet-operator sequence located in the P_{TRE3GV} promoter, which initiates the transcription process. The P_{TRE3GV} promoter ensures not only the least basal expression but also delivers the highest degree of target protein expression after induction (Loew *et al.*, 2010; Zhou *et al.*, 2006). Thus, the lentivirus transduction system classifies as an effective tool for heterologous protein expression in mammalian cells. In this study, all response plasmids containing kAE1 variants and the stably transduced mIMCD3 cell lines were generated in cooperation with the Cordat's lab at the University of Alberta, Canada.

2.11.1 Construction of the response plasmid

The pLVX-TRE3G kAE1 plasmid was constructed by inserting the human cDNA of kAE1 carrying a HA tag within the third extracellular loop between Val⁵⁵⁷ and Leu⁵⁵⁸ into the vector pLVX TRE3G. The insert was enzymatically digested in 3' and 5' of the open reading frame with *Mlu*I. Vector was linearized with the same restriction enzyme and ligated with the insert utilizing the T4 DNA ligase enzyme (5 U/ μ l; Thermo Scientific) according to the manufacturer's protocol. The kAE1 R295H, kAE1 Y413H and kAE1 S525F mutants were constructed by using "Q5 site-directed mutagenesis kit" (NEB) with the mutagenic primers (shown in Table 7). The cDNA of HA-tagged kAE1 was used as the template. In Table 7, the primer sequences denoted in capital letters referring to the target DNA sequence, modified nucleotides are labeled in red, and mutated codons marked as underlined.

Table 7: Mutagenic primers (for human sequence of kAE1)

Primer name	Sequence 5'–3'
5' R295H	AGG GTG TTC <u>CAC</u> ATA GAT GCC
3' R295H	CTC TGA CAT GAG GGT GGC
5' Y413H	CAT CTT CAT <u>CCA</u> CTT TGC TGC ACT GTC ACC
3' Y413H	ACG GCA GCC AGG ACC TGG
5' S525F	GAG ATC TTC <u>TTC</u> TTC CTC ATT TCC C
3' S525F	CTG GGT ATA GCG GGA GAT G

Plasmids generated for mIMCD3 cells are listed in Table 8.

Table 8: Plasmids used in mammalian cells

Plasmid	Characteristics	Source
pLVX-TRE3G kAE1	pLVX-TRE3G with human wild-type kAE1 sequence containing a HA tag within third extracellular loop between Val ⁵⁵⁷ and Leu ⁵⁵⁸	Cordat lab, Canada
pLVX-TRE3G kAE1 R295H	pLVX-TRE3G with human kAE1 sequence containing the R295H mutation and a HA tag within third extracellular loop between Val ⁵⁵⁷ and Leu ⁵⁵⁸	Cordat lab, Canada
pLVX-TRE3G kAE1 Y413H	pLVX-TRE3G with human kAE1 sequence containing the Y413H mutation and a HA tag within third extracellular loop between Val ⁵⁵⁷ and Leu ⁵⁵⁸	Cordat lab, Canada
pLVX-TRE3G kAE1 S525F	pLVX-TRE3G with human kAE1 sequence containing the S525F mutation and a HA tag within third extracellular loop between Val ⁵⁵⁷ and Leu ⁵⁵⁸	Cordat lab, Canada

2.11.2 Generation of stable mIMCD3 cell lines

The “Lenti-X™ Tet-On® 3G” (Clontech) transducing kit was used to produce a stable cell line of mIMCD3 which inducibly expressed kAE1 in the presence of doxycycline. In the beginning, ~70% of fresh confluent Lenti-X 293T cells (Clontech) were separately transfected with 7 µg of either pLVX-Tet3G (regulator plasmid), pLVX-TRE3G-kAE1, pLVX-TRE3G-kAE1 R295H, pLVX-TRE3G-kAE1 Y413H or pLVX-TRE3G-kAE1 S525F (response plasmids) using the Lenti-X HTX Packaging mix and Xfect Transfection Reagent (Clontech).

Afterward, transfected cells were incubated in serum-free OptiMEM medium (Gibco) at 37 °C and 5% CO₂ for 48 h. Following incubation, supernatants containing lentiviruses were collected from each Lenti-X 293T cell culture and sterilized by using 0.45 µm filters. After that, ~70% confluent mIMCD3 were co-infected with lentiviruses containing both regulator (pLVX-Tet3G) and response (pLVX-TRE3G-kAE1, pLVX-TRE3G-kAE1 R295H, pLVX-TRE3G-kAE1 Y413H or pLVX-TRE3G-kAE1 S525F) plasmids plus 4 µg/ml of polybrene (Sigma, USA) for 48 h. Infected cells were selected by adding 4 µg/ml of Puromycin and 2 mg/ml of G418 into the growth medium. Finally, after 24 h of incubation with 1 µg/ml of doxycycline, robust expression of kAE1 protein was detected by Western blot analysis.

2.12 Plasmid isolation from microorganisms

2.12.1 Plasmid isolation from *E. coli*

Alkaline lysis

Alkaline lysis is a fast and simple method to extract plasmid DNA from bacteria (Bimboim & Doly, 1979). Initially, the overnight bacterial culture was prepared, and 1.5 ml of the sample was taken into a 2 ml tube for centrifugation at 13,000 rpm for 1 min. After centrifugation, the supernatant was removed and the pellet was resuspended in 100 µl of GTE-solution (glucose-tris-EDTA solution). Next, 200 µl of NaOH/SDS-solution were added, mixed by inversion, and the suspension was incubated at RT for 5 min. Afterward, 150 µl of potassium acetate-solution were added into the tube, and appropriately mixed. After an incubation of 3 min on ice, cellular debris was removed by centrifugation at 13,000 rpm for 10 mins. Supernatant was then collected and 800 µl ethanol were added to precipitate plasmid DNA. After centrifuging the solution, supernatant was discarded, and the pellet was air-dried. Finally, 20 µl dH₂O were added and plasmid DNA was stored at -20 °C.

GTE-Solution		NaOH/SDS-Solution	
Component	Amount	Component	Amount
Glucose	50 mM	NaOH	0.2 M
Tris-HCl pH 8,0	25 mM	SDS	1% (w/v)
Na ₂ EDTA	10 mM		

Potassium acetate-Solution	
Component	Amount
Acetic Acid	29.5 %

pH of the Potassium acetate-solution was adjusted with NaOH to 4.8. Solutions were subsequently autoclaved.

Plasmid Miniprep

Miniprep plasmid isolation was performed by using the “innuPREP Plasmid Mini Kit” (Analytik Jena) as per manufacturer’s instruction to have highly purified plasmid DNA from bacteria. The method is based on alkaline lysis with subsequent binding of plasmid DNA to silica membranes. The obtained plasmid DNA was stored at $-20\text{ }^{\circ}\text{C}$.

2.12.2 Extraction of plasmid from yeast

The recombinant plasmid generated from *in vivo* recombination were extracted by using “ZymoprepTM yeast plasmid Miniprep 1” (Zymo Research) following the manufacturer’s protocol. The isolated plasmid was then amplified by transforming it again into competent *E. coli* and re-isolated by using “innuPREP Plasmid Mini Kit”.

2.13 Determination of DNA concentration

Spectrometric assessment of isolated plasmids or fragmented DNA was carried out by using the NanoDrop 2000c (PEQLAB biotechnology).

2.14 Protein biochemical methods

2.14.1 Lysis of yeast cells

To collect the expressed kAE1 protein in yeast, overnight grown cells corresponding to $\text{OD}_{600} = 5$ or 10 were centrifuged at 8,000 rpm for 5 min. Cell pellet was washed twice with sterile water. After washing, 160 μl of lysis buffer (SUMEB buffer) and 40 μl of protease

inhibitor cocktail solution were added to the cell pellet, and the suspension was transferred into cell disruption tubes. Cell disruption was carried out in a homogenizer (Precellys® Evolution) by using 0.2 g of 0.7–1.0 mm diameter glass beads at 6,000 rpm for 2.5 min with 30 s pause after a 20 s cycle. Following cell lysis, the mixture was placed on ice for 15 min. Later, cell debris was removed by centrifuging at 13,000 rpm for 5 min and supernatants were used for further downstream analysis by SDS-PAGE mixed with 3x SDS sample buffer.

SUMEB Buffer

Component	Amount
SDS	1.0%
Urea	8.0 M
MOPS pH 6,8	10 mM
EDTA	10 mM
Bromophenol blue	0.01% (w/v)

MOPS (3-(N-morpholino)propanesulfonic acid) was sterilized by filtration and then added to the autoclaved buffer solution. The protease inhibitor cocktail solution was prepared by dissolving one tablet of EDTA-free Protease Inhibitor Cocktail (Roche) in 2 ml dH₂O (25x concentration).

3x SDS sample buffer

Components	Amount
dH ₂ O	4.0 ml
Tris-HCl pH = 6.8 (0.5 M)	2.0 ml
Glycerin 99% (v/v)	2.4 ml
SDS 10% (w/v)	1.0 ml
Coomasie blue 0.05% (w/v)	0.4 ml

2.14.2 Lysis of mammalian cells

mIMCD3 cells were grown in cell culture dishes/well-plates to 80–90 % confluency. Next, medium was aspirated and attached cells were washed with 1x PBS for one time. After washing, PBS was aspirated and 100–500 µl of cell lysis buffer was added into the dish/well-plates

(depending on the plate size and desired protein concentration). Following 15 min incubation on ice, the cells were scraped from the bottom by using a cell scraper and the cell suspension was transferred into microcentrifuge tubes. The solutions were centrifuged at 14,000 rpm for 15 min at 4 °C and supernatants were aspirated to new microcentrifuge tubes. If desired, the total protein concentration was determined by PierceTM BCA protein assay kit (Thermo Scientific) following manufacturer's protocol and the samples were stored at -80 °C for further analysis.

mIMCD3 cell lysis buffer

Components	Amount
PBS	1x
Triton X-100	0.1% (v/v)
EDTA-free Protease Inhibitor Cocktail (Roche)	1 tablet in 10 ml

2.14.3 SDS-PAGE

Sodium dodecyl sulfate-polyacrylamide gel electrophoresis (SDS-PAGE) is extensively used to separate proteins from the mixture based on their molecular weight (Shapiro *et al.*, 1967). SDS functions as an anionic surfactant, and the combination of SDS and polyacrylamide gel allows to exclude the influence of structure and charge of the protein during separation. In the SDS-PAGE, the linearized proteins migrate from the cathode towards the anode and high molecular weight proteins move slower than the smaller ones (Weber & Osborn, 1969). To analyze samples by SDS-PAGE, cells were lysed and supernatants were collected (as described in section 2.14.1 and 2.14.2). Samples were run on a 10% tris-tricine gel. Gels and buffers were prepared using the recipe stated below.

Tris-HCl/SDS

Component	Amount
Tris	3.0 M
SDS	0.3%

pH of the solution was adjusted to 8.45 by using hydrochloric acid (HCl), and the solution was stored at RT.

Resolving gel (10%)		Stacking gel	
Component	Amount (2 gels)	Components	Amount (2 gels)
Rotiphorese® gel 30	4.0 ml	Rotiphorese® gel 30	1.6 ml
Tris-HCl/SDS	5.0 ml	Tris-HCl/SDS	3.1 ml
dH ₂ O	4.0 ml	dH ₂ O	7.8 ml
Glycerin 80% (v/v)	2.0 ml	APS 10% (w/v) fresh	80 µl
APS 10% (w/v) fresh	80 µl	TEMED	25 µl
TEMED	25 µl		

Polyacrylamide gels were prepared by pouring the resolving gel solution into the Mini-PROTEAN® Tetra (Bio-Rad) hand-cast system. To remove bubbles and avoid drying of the upper surface, resolving gels were covered with 2-propanol. The isopropanol was removed completely after polymerization and stacking gel solution was poured over the resolving gel. Immediately, a comb was placed at the top of the cast system to form the desired number of wells for sample loading. Electrophoresis was conducted using a Mini-PROTEAN® 3 Cell (Bio-Rad) system. The inner chamber was filled with 1x cathode buffer and the outer chamber was filled with 1x anode buffer up to the mark on the chamber. Initially, the electrophoresis was accomplished at 80 V and 10 min to concentrate samples providing better resolution. After that, the electrophoresis settings were changed to 140 V for 50 min, or the required time to achieve desired protein separation. The samples were loaded with 7 µl of PageRuler™ Prestained protein marker (Thermo Scientific).

5x Anode buffer		5x Cathode buffer	
Components	Amount	Components	Amount
Tris-HCl, pH = 8.9	1.0 M	Tris	0.5 M
		Tricin	0.5 M
		SDS	0.5% (w/v)

pH of the 5x anode buffer was adjusted to 8.9 by using HCl and both buffers were stored at 4 °C.

Tris-glycine gels used for wet electroblotting were prepared as followed.

Resolving gel (8%)		Stacking gel	
Component	Amount (2 gels)	Component	Amount (2 gels)
Acrylamide solution 30%	5.3 ml	Acrylamide solution 30%	1.3 ml
Tris 1.5 M pH = 8.8, (Bio-Rad)	5.0 ml	Tris 0.5 M pH = 6.8, (Bio-Rad)	2.5 ml
dH ₂ O	9.5 ml	dH ₂ O	6.1 ml
SDS 10% (w/v)	200 µl	SDS 10% (w/v)	100 µl
APS 10% (w/v) fresh	100 µl	APS 10% (w/v) fresh	100 µl
TEMED	10 µl	TEMED	10 µl

10x Laemmli running buffer

Components	Amount
Tris	25 mM
Glycine	192 mM
SDS	0.1% (w/v)

2.14.4 Silver staining

Silver staining was performed using the “Pierce silver staining kit” (Thermo Scientific) to detect proteins in polyacrylamide gels. In brief, a gel was first washed with distilled water and fixed with a fixation solution (30% ethanol, 10% acetic acid, and 60% distilled water). After fixing, the gel was washed two times with 10% ethanol and two times with distilled water. Gel was then sensitized with a sensitizing working solution for 1 min (0.5 µl Sensitizer with 25 ml distilled water). Subsequently, the gel was washed two times with distilled water for 1 min and then stained with the stain working solution for 30 min (0.5 ml Enhancer with 25 ml Stain). Before detection, gel was washed again two times with distilled water. The protein bands were visualized with the developer working solution for 2–3 min (0.5 ml Enhancer with 25 ml Developer). Once the bands were clearly visible, the development was stopped by an incubation for 10 min with 5% acetic acid. Finally, image of the gel was acquired by Amersham Imager 600 (GE Healthcare).

2.14.5 Western blot analysis

Qualitative and quantitative detection of proteins after SDS-PAGE was determined by Western blot analysis (Towbin *et al.*, 1979). Target proteins were detected by respective antibody treatment and further visualized by the chemiluminescent detection produced from a substrate-conjugate reaction. In this study, Western blot was performed by using both semi-dry and wet transfer methods.

2.14.5.1 Semi-dry electrotransfer

The semi-dry blotting technique was used to transfer proteins from the SDS-PAGE gel matrix on a PVDF membrane. The membrane was incubated with methanol for 1 min prior to further use. Membrane, SDS-gel, and blotting paper were equilibrated with transfer buffer for 10 min. For a single transfer, a sandwich was prepared by sequential placement of blotting paper, membrane and gel. Protein transfer was carried out by using Trans-Blot Semi-Dry Electrophoretic Transfer Cell system (Bio-Rad). During a single blotting, a constant 54 mA current was applied for 1.5 h.

Transfer buffer	
Component	Amount
Tris	3.03 g
Glycine	14.4 g
SDS	0.1% (w/v)
Methanol	20% (v/v)
dH ₂ O	volume up to 1.0 L

2.14.5.2 Wet electrotransfer

To perform wet electroblotting, the SDS-PAGE was carried out according to Laemmli method (Laemmli, 1970). 8% SDS gels were made while the samples were mixed with 2x or 4x Laemmli sample buffer (Bio-Rad) containing 5% or 10% 2-mercaptoethanol, respectively. Afterward, samples were loaded into the gel alongside 5 µl of BLUelf prestained protein ladder (FroggaBio). Electrophoresis was performed at 200 V, 400 mA and 35 min with 1x Laemmli running buffer.

10x Transfer buffer

Components	Amount
Tris	25 mM
Glycine	192 mM
Methanol	20.0% (v/v)

2.14.5.3 Immunodetection

Following transfer, the PVDF membrane was incubated with blocking solution at 20 °C for 1 h to prevent unspecific antibody binding. Then, the membrane was incubated with primary antibody (dissolved in blocking solution) for overnight at 4 °C. The membrane was washed three times (10 min each) with wash buffer for removal of unbound antibodies and subsequently incubated with the secondary antibody conjugated with HRP at 20 °C for 1 h. Following incubation, the membrane was washed again with the washing solution for three times (10 min each). The target protein was visualized using the SuperSignal™ West Femto Maximum Sensitivity Substrate (Thermo Scientific), and signals were detected by using the Amersham Imager 600 (GE Healthcare).

10 x TBS

Component	Amount
Tris	1.0 M
NaCl	1.0 M

pH of the solution was adjusted to 7.5 by using HCl and stored at RT.

Wash buffer		Blocking solution	
Components	Amount	Components	Amount
TBS 10x	10.0% (v/v)	Non-fat dried milk	5.0% (w/v) in wash buffer
Tween 20	0.05% (v/v)		

Primary and secondary antibodies used for Western blotting are shown in table 9.

Table 9: Primary and secondary antibodies, their dilution and sources used for Western blotting

Antibody	Dilution	Source
anti-PGK1, mouse	1:1,000	LifeTechnologies (Novex)
anti-GFP, mouse	1:1,000	Roche
anti-V5, mouse	1:1,000	AbD SeroTec
anti-kAE1 _{Nter} , rabbit	1:1,000	E. Cordat, home-made
anti-HA, rat	1:1,000	Roche
anti-FLAG M2, mouse	1:1,000	Sigma
anti-mouse-HRP	1:10,000	Sigma
anti-rat-HRP	1:5,000	Cell Signalling Technology
anti-rabbit-HRP	1:10,000	Sigma

2.14.6 Determination of protein half-lives

Half-life of kAE1 mutants was determined from a densitometry analysis of immunoblots. Initially, relative kAE1 amount was calculated from the intensity ratio of the respective kAE1 band and β -actin band. Then, the starting time point was set as 100% and used to normalize the subsequent time points. A scatter plot was constructed by plotting time versus the percentage of relative kAE1 amount, and data were fitted by exponential regression. The half-life of mutants was estimated on the basis of the obtained equation shown below, where $y = 50$ h, $A =$ initial amount of protein and $k =$ decay constant:

$$x \text{ or } t_{1/2} = \frac{\ln \frac{y}{A}}{-k}$$

2.14.7 Cell surface biotinylation

Biotinylation is a common technique to determine protein located at the plasma membrane (PM). In order to attach biotin to a protein, a sulfo NHS-SS crosslinker was used that covalently binds primary amines present in peptides. Biotinylated proteins can then be isolated with avidin coated beads (Tarradas *et al.*, 2013). To perform cell surface biotinylation, yeast cells expressing wild-type kAE1 were grown to late log phase ($OD_{600} = 1-1.5$) and subsequently harvested. The experimental setup was performed as per previously reported protocol (Becker *et al.*, 2016). In brief, cells were first washed with cold PBS (pH 7.2) and labeled with EZ-link Sulfo-NHS-SS-Biotin (1 mg/ml in PBS) at 4 °C for 90 min. Then, cells were lysed after quenching the biotinylation reaction using quencher solution, and their lysates were immediately used for pull-down with avidin agarose beads (Pierce) with subsequent multiple washing steps with wash buffer (Pierce). Bound proteins (membrane fraction) were eluted in 3x SDS buffer containing 50 mM DTT and 5% 2-mercaptoethanol. Finally, the membrane fraction and aliquots of the cell lysate (input) were used for SDS-PAGE followed by Western blot analysis. The cellular integrity during the labeling step was checked by using antibodies against phosphoglycerate kinase 1 (Pgk1p), and the PM labeling of kAE1 was detected by using an anti-kAE1_{Nter} antibody.

2.14.8 Enzymatic deglycosylation

For the enzymatic deglycosylation, yeast cells were grown overnight and an aliquot of cells corresponding to $OD_{600} = 5$ was subsequently collected via centrifugation at 8,000 rpm for 5 min. Cells were lysed in a similar procedure as described in section 2.14.1 but using Tris-EDTA buffer as the lysis buffer. For one enzymatic digestion, 18 µl of cell extract was incubated with 2 µl of 10x denaturing buffer for 10 min either at RT for kAE1 protein or boiled at 100 °C for RNase B. After incubation, solutions were treated with either 1 µl endoglycosidase Hf (Endo Hf; NEB) or 1 µl Peptide:N-glycosidase F (PNGase F; NEB) with the respective Glycobuffer as indicated in the list below. Mixtures were then incubated at 37 °C for 1 h. The digested protein was analyzed by SDS-PAGE, followed by Western blot analysis.

Endo Hf digestion		PNGase F digestion	
Component	Amount	Component	Amount
Denatured protein mix	10 μ l	Denatured protein mix	10 μ l
10x Glycobuffer 3	2 μ l	10x Glycobuffer 2	2 μ l
Endo Hf (1,000,000 units/ml)	1 μ l	PNGase F (500,000 units/ml)	1 μ l
dH ₂ O	7 μ l	NP 40	2 μ l
		dH ₂ O	5 μ l

Tris-EDTA buffer

Component	Amount
Tris	10 mM
EDTA	1 mM
2-mercaptoethanol	0.1% (v/v)
PMSF	1 mM
Triton X-100	0.1% (v/v)

Phenylmethylsulfonyl fluoride (PMSF) is quickly degraded in aqueous solution. In order to solve this matter, a 100 mM stock solution of PMSF in absolute ethanol was prepared separately and mixed with other components just before the application.

2.15 Boric acid tolerance assay

The wild-type yeast strain BY4742 and its isogenic $\Delta bor1$ mutant containing either pYES2.1-ykAE1^{V5} or pYES2.1 (vector control) plasmid were grown to the stationary phase in uracil d/o glucose medium. Then, 1 ml of cell suspension was taken from the cultures, washed two times with uracil d/o raffinose medium, and the cell density was adjusted to OD₆₀₀ = 0.7. These density-adjusted cultures were further decreased by performing a ten-fold serial dilution with uracil d/o raffinose medium. Afterward, 5 μ l of cell suspension from each dilution were spotted on uracil d/o galactose agar plates containing 0, 10, 20, 40, and 80 mM boric acid. Cells were grown at 30 °C for 3 d and subsequently documented. To analyze boric acid tolerance in liquid culture, yeast cells were grown to the stationary phase. 1 ml of cell suspension was collected, washed twice, and diluted to OD₆₀₀ = 0.2 in uracil d/o galactose medium containing

0, 10, 20, 30, and 40 mM boric acid. 200 μ l of cell suspension from the diluted cultures were then placed in a 96-well plate. The plate was incubated at 30 °C, and the cell growth was measured at 600 nm by using a multi-mode plate reader (Molecular Devices).

2.16 Indirect immunofluorescence

The cell wall of yeast typically blocks the access of antibodies to the plasma membrane or intracellular organelles. Thus, cells were first spheroplasted via enzymatic treatment with Zymolase for the indirect immunofluorescence. To achieve spheroplasted cells, a fresh yeast culture was cultivated to $OD_{600} = 1$. Then, a final $OD_{600} = 10$ was harvested by centrifugation (8,000 rpm, 5 min at RT), washed twice with 1x PBS (0.1 M) and fixed with 3.7% formaldehyde for 1 h on a roller drum at 20 °C. After three washing steps with 0.1 M PBS, cells were washed two times with 1.2 M sorbitol, resuspended in 1 ml 1.2 M sorbitol supplemented with 10 μ l β -mercaptoethanol and 20 μ l zymolyase (5 mg/ml zymolyase 100T), and incubated at 30 °C for 45 min. Finally, cells were centrifuged at 2,000 rpm for 5 min, washed two times with 1.2 M sorbitol and used for antibody staining.

Prior to antibody staining, cells were permeabilized with 0.1% SDS at RT for 10 min. Then, 30 μ l of the sample were spotted on poly-L-lysine-coated coverslips, pre-incubated for 20 min, washed once with 1% BSA (dissolved in 1x PBS) and blocked for 30 min in 1% BSA. For detecting kAE1, cells were incubated at 20 °C for 1 h with primary antibodies and secondary antibodies conjugated with FITC for 1 h. After three washing steps with 1% BSA, cells were analyzed by fluorescence microscopy. Primary and secondary antibodies used for indirect immunofluorescence are shown in table 10.

Table 10: Primary and secondary antibodies, their dilution and sources used for indirect immunofluorescence

Antibody	Dilution	Source
anti-V5, mouse	1:40	AbD SeroTec
anti-kAE1 _{Nter} , rabbit	1:40	Against N-terminal region of kAE1 (65 to 80 aa) (Wu <i>et al.</i> , 2010).
anti-HA, rat	1:40	Roche
anti-FLAG M2, mouse	1:40	Sigma
anti-mouse-FITC, goat	1:160	Sigma
anti-rabbit-FITC, goat	1:160	Sigma
anti-rat-FITC, goat	1:160	Sigma

2.17 Microscopy techniques

2.17.1 Fluorescence microscopy

Dual-color images of proteins fused to yeGFP and mRFP were obtained by utilizing a Keyence BZ-8000 fluorescence microscope (100x Oil immersion Plan Apo VC objective [1.4 NA]). yeGFP signals were detected by BZ-X GFP filter (470 nm excitation, 535 nm emission) and mRFP signals were detected via using BZ-X TexasRed filter (560 nm excitation, 630 nm emission). To prevent cell movement, samples were spotted on poly-L-lysine-coated cover slips and pre-incubated for 15 min.

2.17.2 Confocal laser scanning microscopy

Confocal images of yeast cells were obtained by using inverted microscopy (CLSM 710 META, Carl Zeiss). Cell specimens were analyzed with a 100x Oil EC Plan-Neofluar objective. For yeGFP detection, GFP ChS1:496-554 channel was used. Captured images were further analyzed by using Zen 2.1 (Zeiss) image processing software.

2.17.3 Spinning disc confocal microscopy

Confocal images were captured using an inverted microscope (Ti-Eclipse, Nikon) fitted with a Yokogawa spinning disk unit (CSU-W1, Andor Technology). 100x Oil Plan Apo TRIF objective (Nikon) was used during image acquisition and recorded on a digital CSMOS camera (Orca-Flash 4.0, Hamamatsu). Finally, image analysis was carried out with Fiji software (Schindelin *et al.*, 2012). The figures were processed by separating the channels of each image and optimizing the signal level for better observation of dim structures.

2.18 pH measurement of the kAE1 expressing yeast cells

Intracellular pH (pHi) measurements of yeast cells were performed with the ratiometric pH-sensitive dye SNARF-5F AM (SNARF-5F 5-(and-6)-carboxylic acid, acetoxymethyl ester, acetate; Thermo Scientific). SNARF-5F is a naphthofluorescein derivative conjugated with an acetoxymethyl (AM) ester. The AM derivative easily penetrates the plasma membrane. It is then hydrolyzed by the nonselective esterases present in the cytosol and forms a nonpermeable charged fluorescence dye (Han & Burgess, 2010). In response to a single excitation wavelength, SNARF-5F AM has a dual emission property. Excitation of the dye at 543 nm generates both pH-sensitive (640 nm) and pH-insensitive (580 nm, isosbestic point) emission wavelengths. The elevation or reduction of fluorescence intensity depends upon the change in intracellular pH. This means that a pH increase causes a rise in SNARF-5F fluorescence emission at 640 nm with a corresponding decrease or constant fluorescence at 580 nm (Beane *et al.*, 2019). Finally, intracellular pH can be determined by the ratio of these two wavelengths. Figure 2.2 illustrates a schematic diagram of the cytosolic pH measurement of yeast cells.

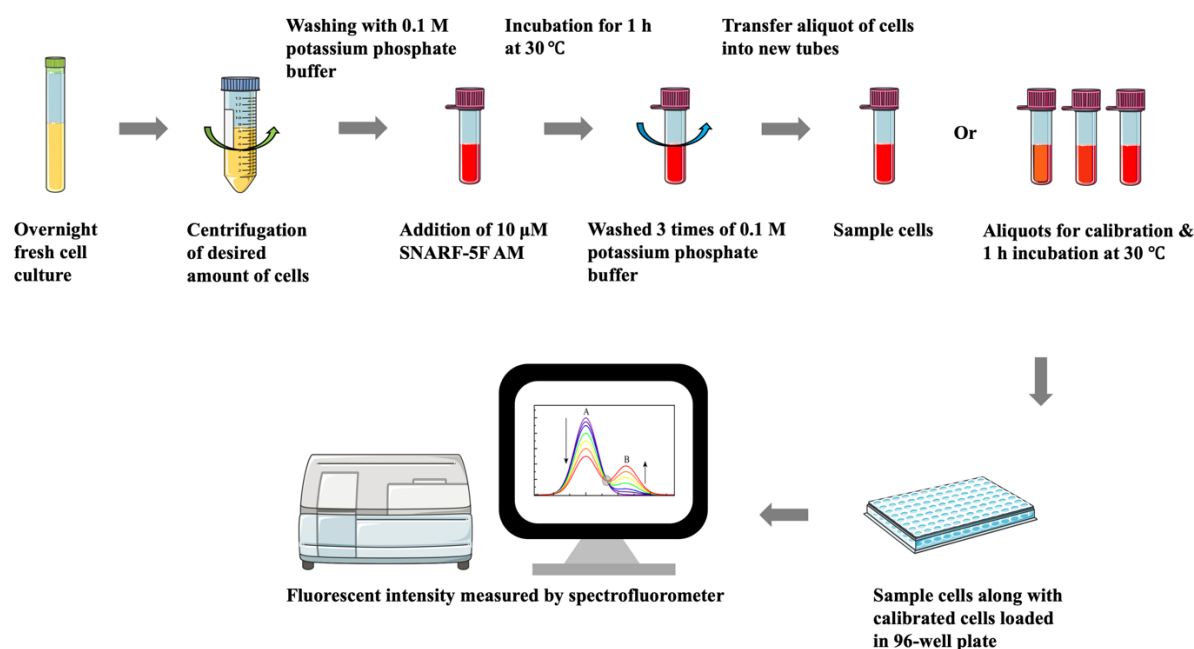


Figure 2.2: A simplified illustration of pHi measurement in yeast expressing kAE1.

kAE1 expressing yeast cells were grown overnight. A certain number of cells were taken from the culture and washed to remove culture medium. Then, cells were incubated with the pH-sensitive dye SNARF-5F AM for 1 h at 30 °C and shaking. After incubation, cells were washed carefully to remove excess amounts of extracellular dye. To determine cytosolic pH, calibrated sample cells were prepared by incubating cells with Nigericin and buffers with specific pH values for 1 h at 30 °C and shaking. Finally, a ratio of fluorescence from sample cells and calibrated cells were measured using a fluorometer.

In order to execute pHi measurement, 50 ml of yeast cells transformed with empty vector pPGK (negative control) or pPGK-ykAE1 were grown overnight in SC medium (pH = 6.4, 50 mM NaCl) to the stationary phase ($OD_{600} = 3-4$) and an aliquot of cells corresponding to $OD_{600} = 20$ was subsequently harvested by centrifugation at 8,000 rpm for 5 min. After washing the cells in 0.1 M potassium phosphate buffer (pH = 6.4, pH was adjusted by mixing specific volumes of 1.0 M K_2HPO_4 and KH_2PO_4 solutions), cells were incubated in 0.1 M potassium phosphate buffer containing 10 μ M SNARF-5F AM for 1 h at 30 °C and 220 rpm. To get rid of excess amounts of SNARF-5F AM, cells were washed three times with 0.1 M potassium phosphate buffer and resuspended in 400 μ l 0.1 M potassium phosphate buffer. 40 μ l aliquots ($OD_{600} = 2$) of cells expressing kAE1 or negative control were mixed with 160 μ l 0.1 M potassium phosphate buffer and placed into black 96-well plates (Nunc F96, Thermo Scientific) and fluorescence was measured by a fluorometer (Safire2, Tecan). For preparing an additional calibration curve, 40 μ l aliquots ($OD_{600} = 2$) were also taken from the 400 μ l cultures,

centrifuged at 8,000 rpm for 5 min and washed two times with the different calibration buffers with distinctive pH values (5.6, 6.4 and 7.2). Then, samples were incubated in 200 μ l of the corresponding calibration buffers supplemented with 40 μ M nigericin (Sigma) at 30 °C for 1 h (220 rpm). Finally, fluorescence of 200 μ l aliquots of the different calibration samples was measured in 96-well plates as described above. Excitation wavelength was set to 543 nm and dual emission was determined at 580 nm and 640 nm. Afterward, fluorescence emission ratios (640 nm/580 nm) and the corresponding mean fluorescence values were calculated for each sample ($n \geq 3$). A calibration curve was formulated by plotting the fluorescence ratio of calibrated samples versus corresponding extracellular pH and the data were fitted by a second-order polynomial regression. The quadratic equation is shown below:

$$y = ax^2 + bx + c$$

where, a , b and c are constants. To calculate unknown x (here, x corresponding to pH_i and y refers to 640 nm/580 nm emission ratio), subsequent equation was used:

$$x = \frac{\sqrt{4a(y - c) + b^2} - b}{2a} \quad \text{and } a \neq 0$$

Intracellular pH values of kAE1 expressing samples were determined by using the obtained equation from the calibration curve. All the samples were light-protected throughout the experiment to ensure the probe's stability.

2.19 Anion exchange chromatography

Intracellular and extracellular Cl⁻ concentration of BY4742 cells was measured by utilizing an anion exchange chromatography. BY4742 cells transformed with an empty vector control (pPGK) or expressing untagged wild-type kAE1 (pPGK-ykAE1) were grown to the stationary phase ($OD_{600} = 3-4$). To prevent kAE1 mediated chloride transport, constitutively ykAE1 expressing cells were pre-treated with 200 μ M DIDS (disodium 4,4'-diisothiocyanatostilbene-2,2'-disulfonate) dissolved in 10 mM HEPES buffer (pH = 7.4) for 30 min at 30 °C with shaking at 220 rpm. Afterward, empty vector expressing cells and ykAE1 expressing cells either pre-treated or non-treated with DIDS were collected with a final $OD_{600} = 200$. Cells were then incubated in 5 ml of HEPES buffer with 150 mM NaCl with or without DIDS for 1 h at 30 °C

with shaking. The cell density was measured again to confirm the number of cells present in each sample. Finally, an aliquot of each cell sample was taken for individual analysis of intracellular and extracellular Cl^- concentration.

Sample preparation for measuring extracellular Cl^- concentration: To collect supernatant for extracellular Cl^- ($[\text{Cl}^-]_{\text{ex}}$) determination, 1 ml cell suspension was centrifuged after 1h ($t_{1\text{h}}$). The collected supernatants were then diluted at a ratio of 1:10 with MiliQ water. Finally, 2 μl diluted supernatant were injected into an anion exchange chromatography for analyzing Cl^- concentration (Dionex Integrion HPLC system installed with a Dionex IonPac™ AS9-HC anion-exchange column, Thermo Scientific).

Sample preparation for measuring intracellular Cl^- concentration: The intracellular Cl^- concentration of yeast cells $[\text{Cl}^-]_{\text{in}}$ was determined using 1 ml of cell suspension. Cells were harvested by centrifugation, washed two times with wash buffer (150 mM sodium gluconate and 100 μM DIDS in HEPES buffer), and finally resuspended the cells into 1 ml of HEPES buffer. Cells were then lysed using a homogenizer (Precells Evolution, Bertin Corp.). Cellular debris was removed by centrifugation and the supernatant was collected for measuring Cl^- concentration. Lastly, 10 μl collected supernatants were injected into anion-exchange chromatography for analysis.

Calculation of Cl^- influx as well as intracellular Cl^- concentration: A chloride standard curve was prepared from standard solutions having Cl^- concentration of 0 mM, 50 mM, 100 mM, 150 mM and 200 mM for each experiment, and fitted with linear regression. Consequently, Cl^- concentration of the samples was determined by plotting the peak area of the samples against the peak areas of the chloride standards. To measure the total amount of Cl^- influx per hour into yeast cells, the extracellular Cl^- concentration at the beginning ($t_{0\text{h}}$) was additionally measured and calculated by following equation: $[\text{Cl}^-]_{\text{ex}}(t_{0\text{h}}) - [\text{Cl}^-]_{\text{ex}}(t_{1\text{h}})$. The obtained values were subsequently normalized to the total cell number where $\text{OD}_{600} = 1$ was set to $\sim 1 \times 10^7$ cells and depicted as Cl^- influx per cell per hour. To measure intracellular Cl^- concentration, the total intracellular Cl^- concentration $[\text{Cl}^-]_{\text{in}}$ as well as OD_{600} value were calculated from 1 ml aliquots, and then the intracellular Cl^- concentration was determined for a single cell.

2.20 MTS assay

2.20.1 Cell counting by hemocytometer

To achieve a certain cell concentration in culture dishes/well-plates, mammalian cells were counted by using a hemocytometer. In brief, ~70–80% confluent cells were trypsinized after washing with sterile 1x PBS and collected in a tube with 5 ml fresh culture medium. From the collection tube, 100 µl of cell suspension were transferred to a new microcentrifuge tube and diluted with the respective culture medium. Then, 10 µl of cell suspension were placed on the hemocytometer and cell density was calculated from the equation mentioned below:

$$\text{cell density} \left(\frac{\text{cells}}{\text{ml}} \right) = \frac{\text{number of cells in four squares}}{4} \times \text{dilution factor} \times 10^4$$

2.20.2 MTS assay for investigating mIMCD3 cell proliferation

To observe the effect of the kAE1 mutants on mIMCD3 cell proliferation, an MTS assay was performed by utilizing CellTiter 96[®] AQueous One-Solution Reagent (Promega). MTS is a tetrazolium compound [3-(4,5-dimethylthiazol-2-yl)-5-(3-carboxymethoxyphenyl)-2-(4-sulfophenyl)-2H-tetrazolium] which is reduced to a soluble formazan by the enzymatic activity of dehydrogenase enzymes, mainly involved in cellular metabolism. The solubilized formazan has a maximum absorbance of 490 nm (Cory *et al.*, 1991). One-Solution additionally consists an electron coupling reagent phenazine ethosulfate (PES) that helps to increase the stability of the solution combining with MTS.

First, mIMCD3 cells inducibly expressing wild-type and mutated kAE1 were grown to ~80% confluency. Cells were detached and 50,000 cells/well were split in 12-well plates containing growth medium in presence or absence of 1.0 µg/ml doxycycline. After 24 h, the culture medium was changed and cells were incubated into three different types of media: 1) standard growth medium, 2) growth medium containing 100 mM NaCl, and 3) growth medium containing of 200 mM Mannitol. The standard growth medium contains an osmolarity of ~300 mOsmol/kg H₂O. When 100 mM NaCl or 200 mM mannitol was added to the medium, its osmolarity was increased to ~500 mOsmol/kg H₂O and labeled as a hyperosmotic condition. In order to maintain a constant expression level of the kAE1 variants in the induced cells,

doxycycline was added into these three media. The initial time point of transferring cells into different media was counted as 0 h and cells were incubated until 72 h in the CO₂ incubator at 37 °C. MTS assay was performed at 0 h, 48 h and 72 h for determining the viability of mIMCD3 cells. For each measurement, cells were washed twice with fresh growth medium to remove dead cells and 240 µl of MTS-medium solution was added in each well. The MTS-medium solution was prepared by adding One-Solution into the growth medium at 1:5 ratio (One-Solution : growth medium) following the manufacturer's protocol. Then, cells were incubated for 20 min in a CO₂ incubator. Following incubation and gently mixing of the supernatant, 200 µl supernatant from each well was transferred to a new 96-well plate. The absorbance of the produced formazan was measured at 490 nm by using a Synergy Mx Plate Reader (BioTek).

For background correction, MTS-medium solution was added into empty wells (negative control) and incubated under identical conditions as samples. Finally, the relative absorbance of samples was calculated using the equation below, where the absorbance value of empty well was subtracted from the absorbance value of the sample.

$$\text{Corrected absorbance} = \text{Absorbance}_{\text{Sample}} - \text{Absorbance}_{\text{Negative control}}$$

2.21 Data analysis and statistics

Statistical analysis was carried out in Graphpad Prism 8. All pooled data were given as mean values ± standard error of the mean (SEM). Statistical significance was determined using either unpaired t-test, One-way or Two-way ANOVA based on biological replicates and at sample sizes of $n \geq 3$ (ns, not significant; *, $p < 0.05$; **, $p < 0.01$; ***, $p < 0.001$).

3. Results

Mutations in the kAE1-encoding gene *SLC4A1* lead to dRTA, a pathological condition characterized as a defect in urine acidification. Based on hereditary transmission, two types of dRTA can be clinically differentiated, an autosomal dominant and an autosomal recessive variant. The mutations are typically found in a heterozygous state in the case of the former, whereas homozygous and heterozygous mutations of the affected gene can be observed for autosomal recessive dRTA (Yenchitsomanus *et al.*, 2005). For characterizing kAE1-mediated dRTA mutants, many studies were previously carried out in MDCK cells, which are used as a model for renal intercalated cells (Gekle *et al.*, 1994). Studies in MDCK cells proposed that dRTA originates from either a complete dysfunction of kAE1 or a mistargeting of the respective mutated proteins to the apical membrane or the intracellular compartments (Cordat *et al.*, 2006). However, recent *in vivo* findings of dominant dRTA knock-in mice and biopsy data of dominant dRTA patients suggest that the origin of the disease is far more puzzling than anticipated. For example, in a kAE1 R609H knock-in mouse model, the mutant, although just expressed in minor amounts, was found to be correctly targeted to the basolateral membrane (Mumtaz *et al.*, 2017; Vichot *et al.*, 2017). These *in vivo* findings were in contrast to previous data obtained in MDCK cells on dRTA-causing kAE1 mutants, which eventually highlighted that the molecular mechanism of kAE1-mediated dRTA is still poorly understood.

To decipher the underlying reasons of kAE1-mediated dRTA, it is essential to address kAE1-related physiological questions in more detail. This study focused on the investigation of the intracellular trafficking and functionality of the anion exchanger and its mutant variants in yeast and mammalian cells. To achieve this goal, the capability of *Saccharomyces cerevisiae* to express full-length kAE1 was analyzed. A wide range of tagged and untagged full-length kAE1 variants was generated in order to attain a robust expression. After achieving an optimal expression level, intracellular localization and biological activity of full-length kAE1 variants in *S. cerevisiae* were determined. Moreover, the expression and localization of two kAE1 mutants (E681Q and G701D) were also investigated in yeast. Additional experiments were performed in mIMCD3 cells, the closest cellular model for α -intercalated cells at the moment. Three newly found dRTA mutants (kAE1 R295H, Y413H, and S525F) were characterized in this model cell line to investigate their half-life, effect on the cellular autophagy process and influence on cell proliferation.

3.1 Construction of different kAE1 derivatives for *S. cerevisiae*

Numerous attempts were previously made to express full-length human kAE1 (hkAE1) in yeast, but those efforts either failed or resulted in an inactive protein that did not get transported to the cell surface (Bonar & Casey, 2010; Groves *et al.*, 1999). In order to obtain a successful expression of full-length kAE1 in *S. cerevisiae*, two main approaches were applied in this study. First, the signal sequence of the fungal ER chaperon Kar2p was attached to the N-terminus of the human kAE1 sequence (Kar2^{SS}-hkAE1). This approach is commonly used to efficiently translocate heterologous proteins into the yeast ER (Chalfant *et al.*, 2019). Native hkAE1 and hkAE1 bearing the adapted ER import sequence were C-terminally fused with a V5 tag (hkAE1^{V5}, Kar2^{SS}-hkAE1^{V5}) to ease the detection process. Secondly, an adaptation of the human kAE1 cDNA sequence to yeast codon usage was conducted, and this untagged version of kAE1 was designated as ykAE1. The codon optimization technique is frequently used to facilitate recombinant protein production in *S. cerevisiae*, potentially overcoming inefficient translation due to the presence of rare codons in the target DNA sequence (Bai *et al.*, 2011; Quax *et al.*, 2015). In addition to an untagged ykAE1 derivative, two other variants were cloned carrying either a V5 tag (ykAE1^{V5}) or a yeast-optimized enhanced GFP (yeGFP) tag (ykAE1-yeGFP) at the C-terminus. A GFP tag can often simplify the visualization of proteins in living cells. In order to facilitate the cloning of all these constructs into different yeast expression vectors, *Xho*I and *Eco*RI restriction sites were inserted at the 5'-end, and *Bam*HI and *Sal*I restriction sites were introduced at the 3'-end of each construct. The vector pYES2.1 was used for expression of these constructs in the *S. cerevisiae* carrying *Amp*^R and *URA3* markers for positive selection in *E. coli* and *S. cerevisiae*, respectively. 2 μ origin of replication permits multi-copy autonomous replication of the plasmid in yeast, and the strong galactose-inducible promoter *P*_{GALI} drives expression of the different kAE1 variants (Figure 3.1).

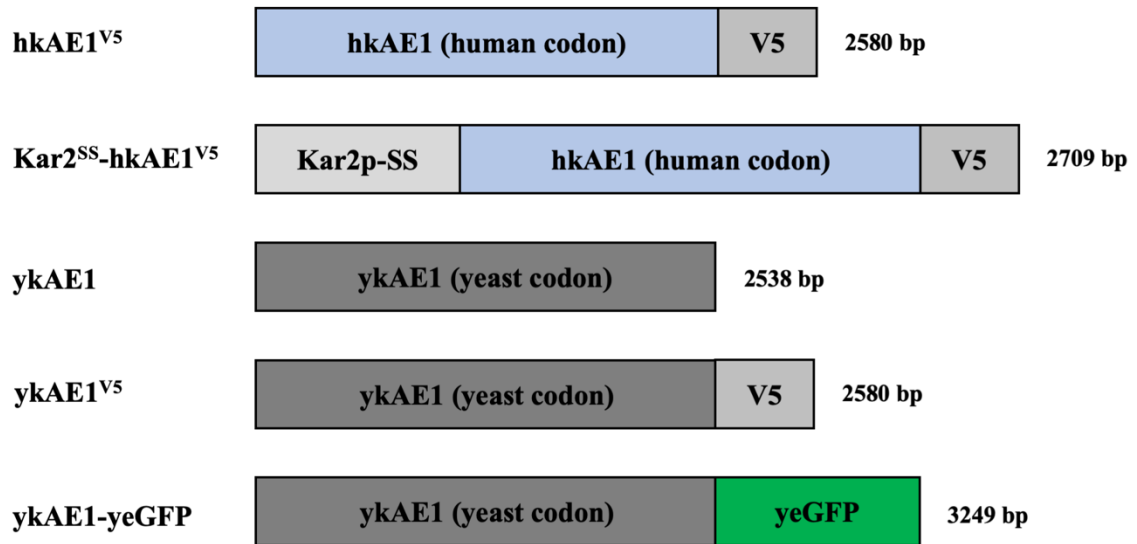


Figure 3.1: Schematic diagram of the kAE1 variants used for expression in *S. cerevisiae*. The native cDNA sequence of kAE1 (hkAE1) were C-terminally fused with a V5 tag (hkAE1^{V5}), whereas one variant was additionally carrying the ER signal sequence of yeast Kar2p at the N-terminus (Kar2^{SS}-hkAE1^{V5}). Further, an untagged yeast codon-optimized version (ykAE1), as well as its two derivatives with either a V5 tag (ykAE1^{V5}) or a yeast-optimized eGFP fusion at the C-terminus (ykAE1-yeGFP), were constructed. Calculated length of the variants is indicated (bp). Restriction sites: *Xho*I and *Eco*RI (5'), *Bam*HI and *Sal*I (3').

3.1.1 Expression profiles of the different kAE1 variants

The uracil auxotrophic *S. cerevisiae* BY4742 strain was used to investigate the expression of modified full-length kAE1 versions. The different recombinant plasmids pYES2.1-hkAE1^{V5}, pYES2.1-Kar2^{SS}-hkAE1^{V5}, pYES2.1-ykAE1^{V5}, pYES2.1-ykAE1 or pYES2.1-ykAE1-yeGFP were transformed into wild-type BY4742 cells by lithium-acetate transformation method (section 2.10.2.1). Expression of kAE1 variants was then initiated by culturing cells in medium with galactose as a carbon source (uracil d/o galactose medium). To analyze kAE1 expression, yeast cells were disrupted by using a cell homogenizer, and Western blotting analyses were performed. Depending on the type of protein tag in the different kAE1 constructs, blots were probed with an anti-V5 or anti-GFP primary antibody. The untagged ykAE1 variant was detected using an antibody that recognizes the N-terminus of the protein (anti-kAE1_{Nter}). Moreover, all blots were also incubated with anti-PGK1 antibody for identifying the loading control Pgl1p. The Western blot results are shown in Figure 3.2.

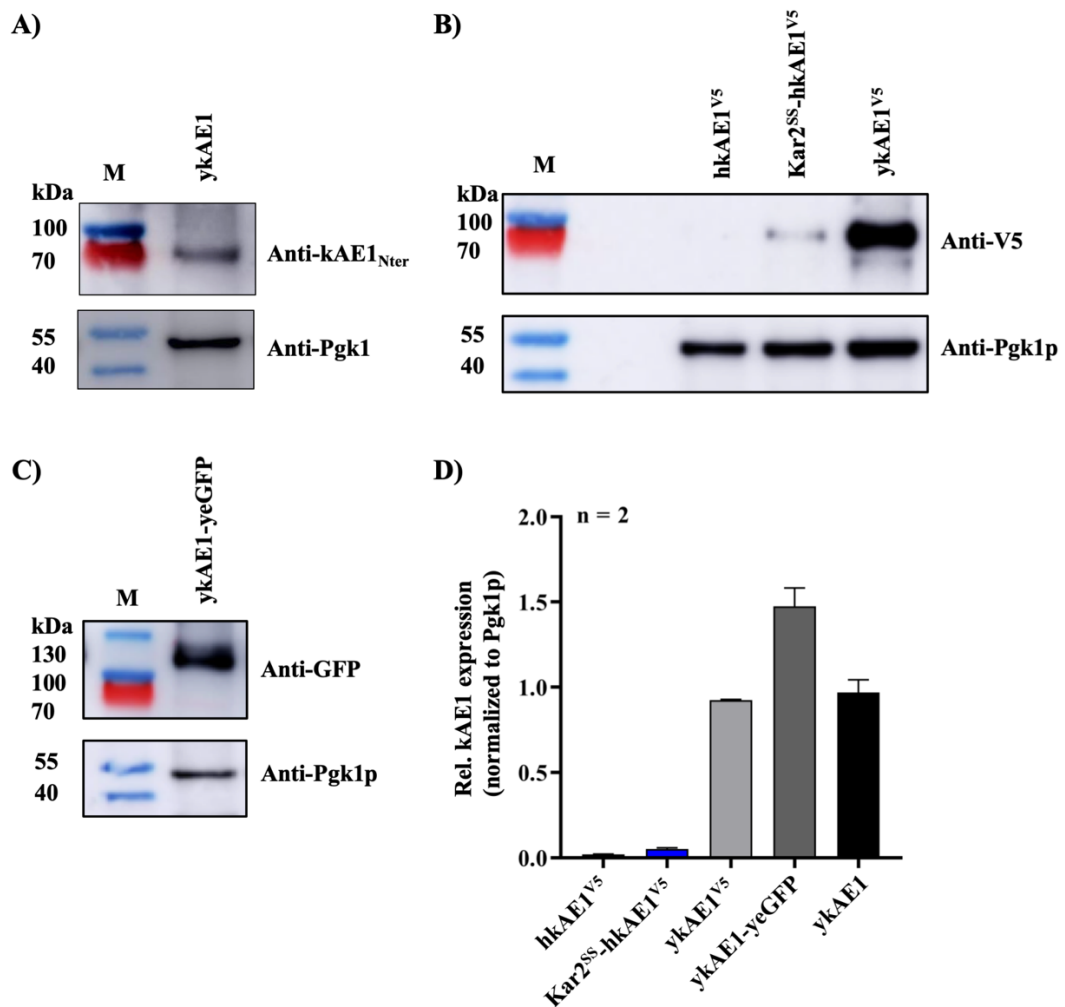


Figure 3.2: Expression analysis of different tagged and untagged kAE1 variants in *S. cerevisiae*.

Wild-type BY4742 cells were transformed with various kAE1 derivatives, expression was induced by incubation of the respective transformants in 3% galactose for 24 h. After cell lysis, Western blot analysis was conducted using the indicated primary antibodies. (A) Untagged ykAE1 was analyzed with an antibody recognizing the kAE1 N-terminus (anti-kAE1_{Nter}). (B) A V5-antibody was used for the respective V5-tagged constructs hkAE1^{V5}, Kar2^{SS}-hkAE1^{V5}, ykAE1^{V5}. (C) The expression of the yeGFP-fused variant (ykAE1-yeGFP) was detected with an anti-GFP antibody. The house-keeping protein Pgk1p was used as a loading control, and an HRP-coupled anti-mouse antibody was used as secondary antibody in all cases. Molecular weight marker is indicated (M). (D) Densitometry analysis of the different kAE1 variants. Each signal for the respective kAE1 variant was normalized to the corresponding signal of Pgk1p and the relative kAE1 signal was calculated. Data represent n = 2 separate experiments. The results are shown as mean ± SEM, (partially published in Sarder *et al.*, 2020).

In contrast to the untagged and V5-tagged yeast codon-optimized kAE1 constructs, no kAE1 signal could be detected for yeast cells expressing hkAE1^{V5} construct (Figure 3.2 A, B).

Untagged ykAE1 displayed a less intense band signal, which is possibly due to inefficient solubilization of the membranes during lysis. Notably, the addition of Kar2p^{SS} could not drastically increase the hkAE1 signal, although a faint signal of kAE1 at ~94 kDa was detected on the blot (Figure 3.2 B). Surprisingly, a very strong band signal of the ykAE1^{V5} variant at ~94 kDa size was observed that corresponds to the expected size of the V5-tagged kAE1. Similarly, a significant band at ~110 kDa was detected for the ykAE1-yeGFP variant equivalent to the expected size of the chimeric protein (Figure 3.2 C). Quantification of the bands by densitometric analysis also confirmed the strong expression of yeast-codon optimized ykAE1 variants comparing to both hkAE1^{V5} and Kar2^{SS}-hkAE1^{V5} (Figure 3.2 D). In addition, an increased level of expression for the ykAE1-yeGFP variant was observed compared to the ykAE1 and ykAE1^{V5} variants.

Altogether, these data suggested that the key factor for full-length kAE1 expression in yeast was the re-engineering of the human kAE1 cDNA sequence for yeast preferred codons. Based on these initial findings, only constructs optimized to yeast codon usage were used for further experiments.

3.1.2 Improvement of protein extraction

Since the signal intensity of untagged ykAE1 was not optimal on the immunoblots, different conditions for cell lysis buffers were tested. In general, membrane proteins are poorly soluble in aqueous solutions due to their hydrophobic nature (Seddon *et al.*, 2004). It was previously described that lysis buffer with Triton X-100 efficiently solubilizes kAE1 from mIMCD3 cell membranes (Lashhab *et al.*, 2019). Triton X-100 is a non-ionic detergent and extensively used to solubilize kAE1 variants expressed in mammalian cells. On the contrary, SDS combined with urea is used to solubilize yeast proteins (von der Haar, 2007). SDS is an anionic detergent commonly used to extract membrane proteins, whereas urea disrupts the secondary structure of proteins. To determine a suitable condition for protein extraction, BY4742 cells expressing untagged ykAE1 (ykAE1) were grown overnight at 30 °C in under inducing conditions (uracil d/o galactose medium) and subsequently three aliquots of cells (OD₆₀₀ = 5) were prepared. Cells were then lysed using three different SUMEB lysis buffer compositions (A, B and C) which additionally contained 20% of a protease inhibitor cocktail solution to inhibiting protein degradation. In condition-A, proteins were extracted using SUMEB buffer that was

supplemented with 1% SDS. In condition-B and -C, 2% dodecyl- β -d-maltopyranoside (a non-ionic detergent) and 1% Triton X-100 were added, respectively. Afterward, the solubilized protein was separated from insoluble cell debris by centrifugation at high speed. The amount of kAE1 present in the supernatant was compared to that in the pellet fraction via Western analysis using the polyclonal anti-kAE1_{Nter} antibody, and the results are shown in Figure 3.3.

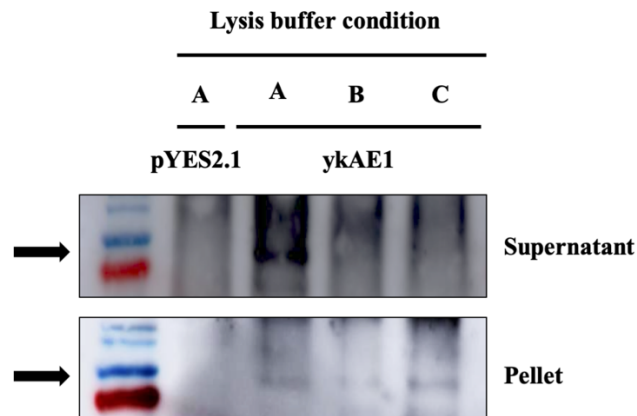


Figure 3.3: Comparison of yeast expressed ykAE1 solubility under different conditions. Wild-type BY4742 cells expressing the ykAE1 variant were incubated with 3% galactose for 24 h before lysis. To solubilize kAE1, three different compositions of SUMEB lysis buffer were compared: (A) 1% SDS, (B) 1% SDS plus 2% dodecyl- β -d-maltopyranoside and (C) 1% SDS plus 1% Triton X-100. The supernatant and pellets from each condition were collected and analyzed via Western blot. ykAE1 was identified by incubation with anti-kAE1_{Nter} and an appropriate secondary anti-rabbit antibody coupled with HRP. Protein bands referring to kAE1 on the blot are marked by black arrows. BY4742 cells expressing pYES2.1 were used as negative control.

As illustrated in Figure 3.3, samples treated with a SUMEB buffer containing only SDS showed the highest signal intensity correlating to kAE1 in the supernatant fraction compared to samples of the other two conditions (condition-B and -C). Moreover, a faint signal of kAE1 was detected in the pellet fraction among all three conditions. BY4742 cells expressing the corresponding empty vector (pYES2.1) were lysed, analyzed as a negative control, and as expected no kAE1-related signals could be determined. The data of these Western blot analyses suggest that the complete solubilization of kAE1 from yeast membranes could not be achieved by using these detergents. Nevertheless, the protein signal for yeast cells lysed under condition-A (1% SDS in SUMEB buffer) implied a slightly increased solubility of kAE1 in the supernatant than the other two conditions. Consequently, SUMEB buffer with 1% SDS was used as lysis buffer in the following experiments unless otherwise mentioned.

3.2 Intracellular localization of the kAE1 derivatives in *S. cerevisiae*

3.2.1 Localization of untagged ykAE1

To establish *S. cerevisiae* as an experimental system, an important criterion was the proper trafficking of kAE1 protein to the cell surface. A previous study reported that the detection of full-length AE1/kAE1 at the yeast cell surface was unsuccessful, and only the untagged membrane domain of AE1 (B3mem; further referred as AE1³⁶¹⁻⁹¹¹) could be targeted to the PM of yeast cells. In addition, AE1³⁶¹⁻⁹¹¹ protein was not carrying any tag within its sequence (Groves *et al.*, 1996). Therefore, the potential targeting of the untagged ykAE1 variant to the yeast plasma membrane was determined via indirect immunofluorescence. BY4742 cells expressing ykAE1 were analysed by fluorescence microscopy and subcellular localization of ykAE1 was detected with a primary anti-kAE1_{Nter} antibody succeeded by a secondary anti-rabbit antibody coupled with FITC (Figure 3.4).

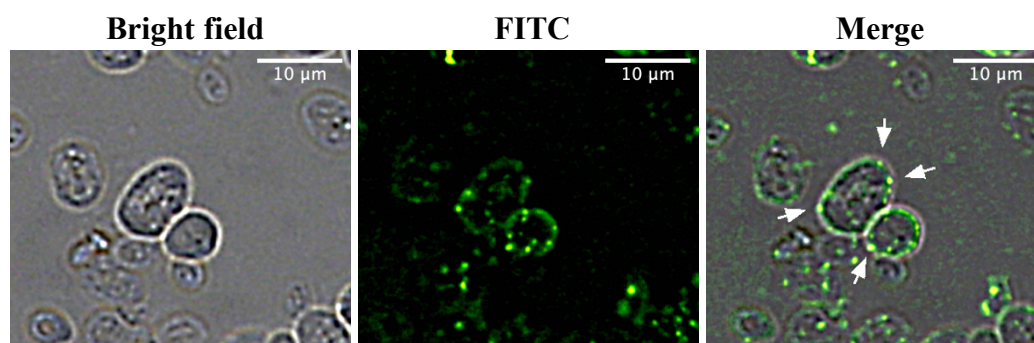


Figure 3.4: Indirect immunofluorescence images of wild-type yeast cells expressing ykAE1.

Wild-type BY4742 cells expressing the ykAE1 variant were incubated with 3% galactose for 24 h. Subcellular localization of kAE1 protein was detected by using anti-kAE1_{Nter} and a FITC-coupled secondary anti-rabbit antibody. The cells were analyzed via fluorescence microscopy (Keyence). Peripheral localized kAE1 signals are marked by white arrows. Objective: PlanApo VC 100x-1.4 Oil; Magnification: 50x; Filter: BZ-X GFP (470 nm excitation, 535 nm emission); Scale bar: 10 µm.

Figure 3.4 shows the subcellular localization of untagged ykAE1 protein in wild-type BY4742 cells. The green fluorescence signal corresponding to kAE1 was observed in intracellular structures and at the cell periphery. The intracellular signals likely resemble the localization of kAE1 in membranes of different organelles. In contrast, the obtained peripheral signals

correspond to the PM-localized kAE1 protein. Interestingly, the peripheral signals did not form a continuous ring-like structure, commonly noticed for PM located proteins, but a more punctured or dotted pattern. These observations suggest that only a minor pool of kAE1 can reach to the yeast cell surface.

3.2.2 Localization of tagged ykAE1 variants

Next, subcellular localization of the ykAE1^{V5} variant in *S. cerevisiae* was investigated by performing indirect immunofluorescence. BY4742 cells expressing ykAE1^{V5} were analyzed with a fluorescence microscope, and the subcellular localization of ykAE1^{V5} variant was detected with an anti-V5 antibody followed by a FITC conjugated anti-mouse antibody (Figure 3.5).

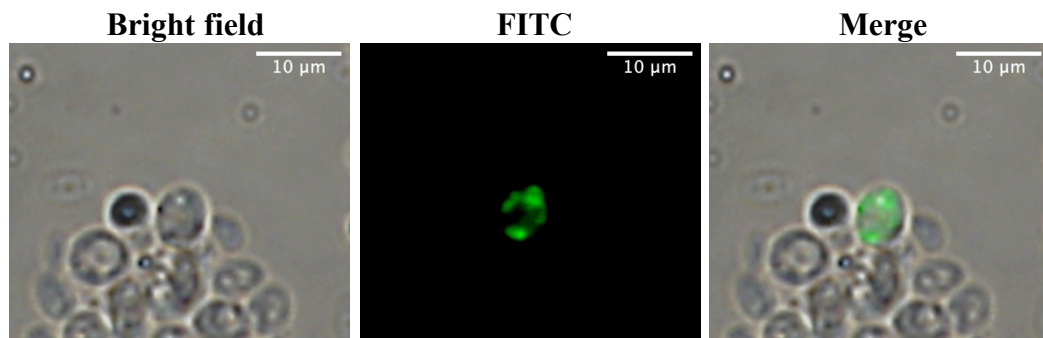


Figure 3.5: Indirect immunofluorescence images of wild-type yeast cells expressing the ykAE1^{V5} variant.

Wild-type BY4742 cells expressing ykAE1^{V5} variant (green) in an inducible manner were incubated with 3% galactose for 24 h. Then, cells were spheroplasted, fixed and permeabilized. Subcellular localization of kAE1 protein was detected by probing the cells with anti-V5 and anti-mouse coupled with FITC antibody. Cells were analyzed by fluorescence microscopy (Keyence). Merged image is showing the overlay of bright field and FITC channel. Objective: PlanApo VC 100x-1.4 Oil; Magnification: 50x; Filter: BZ-X GFP (470 nm excitation, 535 nm emission); Scale bar: 10 µm.

After visualizing cells by fluorescence microscopy, a completely intracellular kAE1 signal (green) was observed rather than a ring-like structure which would indicate a proper PM localization (Figure 3.5). Naturally, yeast-ER has two distinctive domains, the perinuclear ER and the cortical ER. Perinuclear-ER resides around the nucleus and cortical ER locates closely to the PM (West *et al.*, 2011). From the pattern of the detected signal, it could be

speculated that the majority of the expressed ykAE1^{V5} variant was trapped/accumulated at the perinuclear ER. Although, few peripheral kAE1 signals were found, which is most likely coming from the proteins resided in the cortical ER. However, to overcome the limitation of indirect immunofluorescence such as removal of the cell wall and to detect subcellular protein localization in living cells, a yeGFP was fused to the C-terminus of ykAE1 (ykAE1-yeGFP). The ykAE1-yeGFP variant was expressed in wild-type BY4742 cells upon galactose induction and localization of kAE1 was analyzed by CLSM (Figure 3.6).

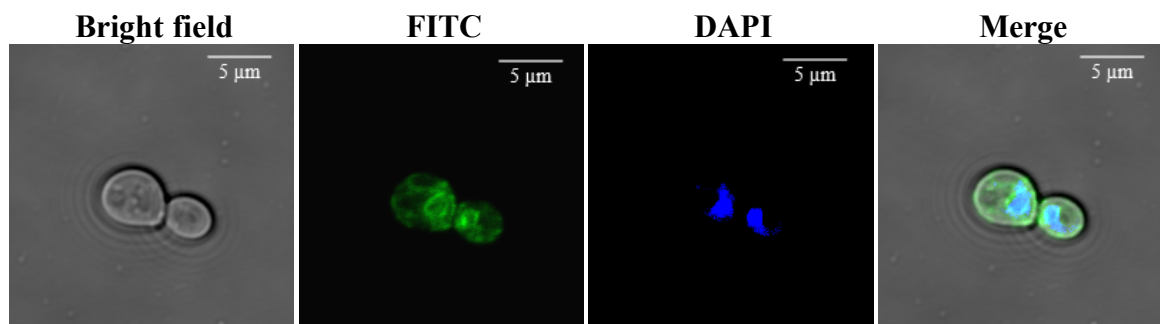


Figure 3.6: Live-cell imaging of wild-type yeast cells expressing ykAE1-yeGFP fusion protein.

Wild-type BY4742 cells expressing the ykAE1-yeGFP variant in an inducible manner were incubated with 3% galactose for 24 h. Live cells were incubated with DAPI for 15 min to stain DNA. After DAPI staining, cells were placed on poly-L-lysine coated glass slide to analyzed in CLSM microscopy (CLSM710, Zeiss). Green staining represents ykAE1-yeGFP protein and blue staining indicates the nucleus. Objective: C-Apochromat 63x; Filter: EGFP Ch2:500-582, DAPI Ch1:391-461. Scale bar: 5 μm.

Figure 3.6 shows the subcellular localization of ykAE1-yeGFP variant. DAPI (blue) was used to stain the nuclei of yeast cells. The green fluorescence signals corresponding to ykAE1-yeGFP were surrounding the nucleus resembling perinuclear ER-localized kAE1 protein. In addition, the green signals captured from the outer edge of cells were indicating the cortical ER-localized kAE1 protein. The distribution of ykAE1-yeGFP signal in BY4742 cells was similar to the ykAE1^{V5} variant. Therefore, these results suggest that C-terminal yeGFP fusion also leads to intracellular retention of kAE1 in yeast. In sum, these data show that kAE1 is predominantly located in the yeast ER when its C-terminus is masked by either V5 tag or yeGFP and is not able to reach the PM of *S. cerevisiae*.

3.3 Colocalization of kAE1 with the yeast plasma membrane protein Pma1p

3.3.1 Construction of N-terminally and intramolecularly tagged ykAE1 variants

It was previously reported that the cytosolic C-terminal domain of kAE1 interacts with different proteins such as GAPDH and AP-1 mu1A while being transported to the basolateral membrane (Junking *et al.*, 2014; Su *et al.*, 2011). In fact, the removal of the C-terminus domain leads to insufficient processing and massive intracellular retention of kAE1 protein (Quilty *et al.*, 2002). On the contrary, the addition of a peptide tag at the N-terminal domain or the third exofacial loop of kAE1 protein does not influence its trafficking and functionality (Beckmann *et al.*, 2002; Cordat *et al.*, 2006). To eliminate some potential negative effects of the initially tested C-terminally tagged constructs, ykAE1 variants with either an HA-epitope-tag or a yeGFP integrated to other intramolecular positions were used. Therefore, ykAE1 with an integrated HA tag within the third exofacial loop between Asn⁵⁵⁶ and Val⁵⁵⁷ (ykAE1^{HA}) and ykAE1 with an N-terminal fusion to yeGFP (yeGFP-ykAE1) were constructed. A schema of the new full-length kAE1 variants is shown in Figure 3.7.

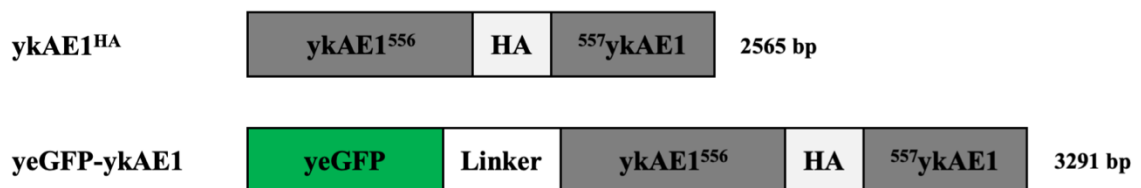


Figure 3.7: Schematic diagram of two different ykAE1 variants.

Schemas are showing yeast-codon optimized full-length kAE1 constructs containing either a HA tag or a yeGFP. Positions of the HA tag, yeGFP and GGGGS-linker are indicated. ykAE1^{HA} is carrying a HA tag within the third extracellular loop between Asn⁵⁵⁶ and Val⁵⁵⁷, and yeGFP-kAE1 contains a yeGFP fused to the N-terminus of the ykAE1^{HA} sequence with a flexible linker. Calculated length of the variants is shown (bp). Restriction sites: *Xho*I (5') and *Bam*HI (3').

yeGFP-kAE1 was constructed via *in vivo* recombination in yeast (section 2.10.2.2), and ykAE1^{HA} was synthetically generated by a company (GeneArt). These constructs were cloned into the expression vector pYES2.1 and transformed into BY4742 yeast cells. The expression of ykAE1^{HA} and yeGFP-kAE1 variants were detected by Western blot analysis using anti-HA and anti-GFP antibodies, respectively, and the results are shown in Figure 3.8.

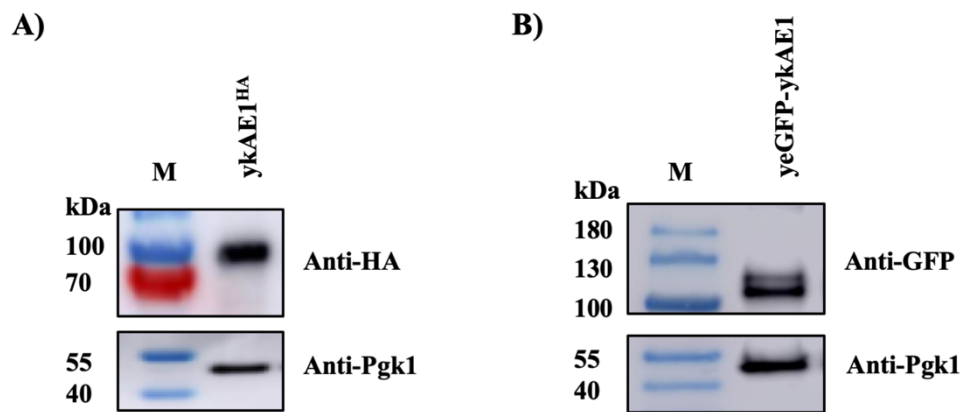


Figure 3.8: Expression of exofacial loop-3 HA-tagged or N-terminus yeGFP tagged kAE1 variants.

Wild-type BY4742 cells expressing different kAE1 variants were incubated with 3% galactose for 24 h before lysis. Representative images of the Western blot analysis of BY4742 cells expressing (A) exofacial loop-3 ykAE1(ykAE1^{HA}) and (B) N-terminal yeGFP fused to kAE1 (yeGFP-ykAE1). HA-tagged ykAE1 was identified by anti-HA antibody followed by anti-rat antibody conjugated with HRP. yeGFP fused ykAE1 was detected with anti-GFP antibody subsequently incubating with anti-mouse antibody coupled with HRP. Molecular weight marker is displayed (M). Pgk1p served as loading control (published in Sarder *et al.*, 2020).

Figure 3.8 shows a robust expression of both the ykAE1 variants (ykAE1^{HA} and yeGFP-ykAE1) after 24 h expression in wild-type yeast cells. However, there is a double band visible in the N-terminus yeGFP fusion construct. Since there was no other band pattern visible on the immunoblot, this double band is unlikely to be a degradation product of the fusion protein. A previous study reported that overexpression of GFP-tagged membrane protein could lead to misfolded proteins that exhibit different running behaviors during the SDS-PAGE (Geertsma *et al.*, 2008). Therefore, a portion of the expressed yeGFP-ykAE1 variant is in a misfolded state. Based on the molecular size of the bands, the upper band would correspond to a misfolded GFP-ykAE1 fused protein, whereas the lower band represents the properly folded chimeric protein. Wild-type BY4742 cells expressing empty vector (pYES2.1) were used as a negative control on the immunoblot.

3.3.2 Colocalization analysis

The subcellular localization of target proteins in a particular host organism is often determined by using a marker protein. To precisely verify the PM-localization of ykAE1, the PM-marker Pma1p-mRFP was expressed in *S. cerevisiae*. Pma1p works as a proton pump and is abundantly

present at the yeast cell surface (Ferreira *et al.*, 2001). To facilitate the visualization in living cells, a monomeric red fluorescence protein (mRFP) was fused to the C-terminus of *PMA1* gene to generate a PMA1-mRFP fusion construct (Malínská *et al.*, 2003). A schema of the PMA1-mRFP construct is shown in Figure 3.9.

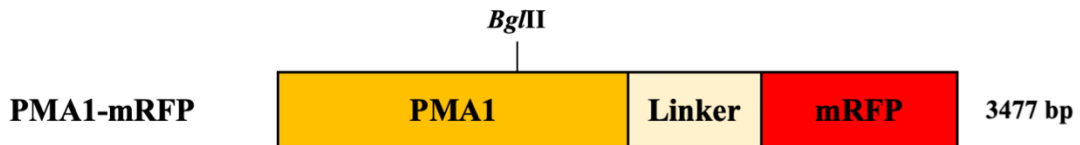


Figure 3.9: Schematic outline of PMA1-mRFP construct for integration into the yeast genome.

Schema is showing an illustration of the yeast PM marker Pma1p-mRFP variant. mRFP is fused to the C-terminus of Pma1p. The restriction site *Bgl*III in the construct is shown and is used for integration into the yeast chromosome. Position of the linker and the size of the construct (bp) are indicated.

PMA1-mRFP construct was cloned into the integrative shuttle vector pYIplac128, which carries an *Amp^R* and *LEU2* markers for *E. coli* and *S. cerevisiae*, respectively. Wild-type BY4742 cells and its isogenic mutant $\Delta end3$ cells were transformed with the linearized recombinant plasmid pYIplac128-PMA1-mRFP digested with *Bgl*III. The purpose of using $\Delta end3$ mutant was to examine whether a defective endocytosis mechanism could trap more PM-localized kAE1. Stable strains of BY4742-PMA1-mRFP and $\Delta end3$ -PMA1-mRFP were generated through the homologous recombination of PMA1-mRFP construct and positive transformants were selected in leucine d/o glucose medium. The chimeric Pma1p-mRFP protein was constitutively expressed under the control of the native P_{PMA1} promoter. Figure 3.10 shows the expression of the fusion protein in BY4742 and $\Delta end3$ cells. A clear ring-like structure at the periphery was observed via fluorescence microscopy resembling the plasma membrane of the cell. In addition, the internalization of Pma1p-mRFP leads to vacuolar transport permitting vacuolar staining. Wild-type yeast cells mostly displayed a single circle-like vacuolar structure. In contrast, the $\Delta end3$ mutant showed punctured multi-vacuolar like structures. This might be due to the defect of its endocytosis process.

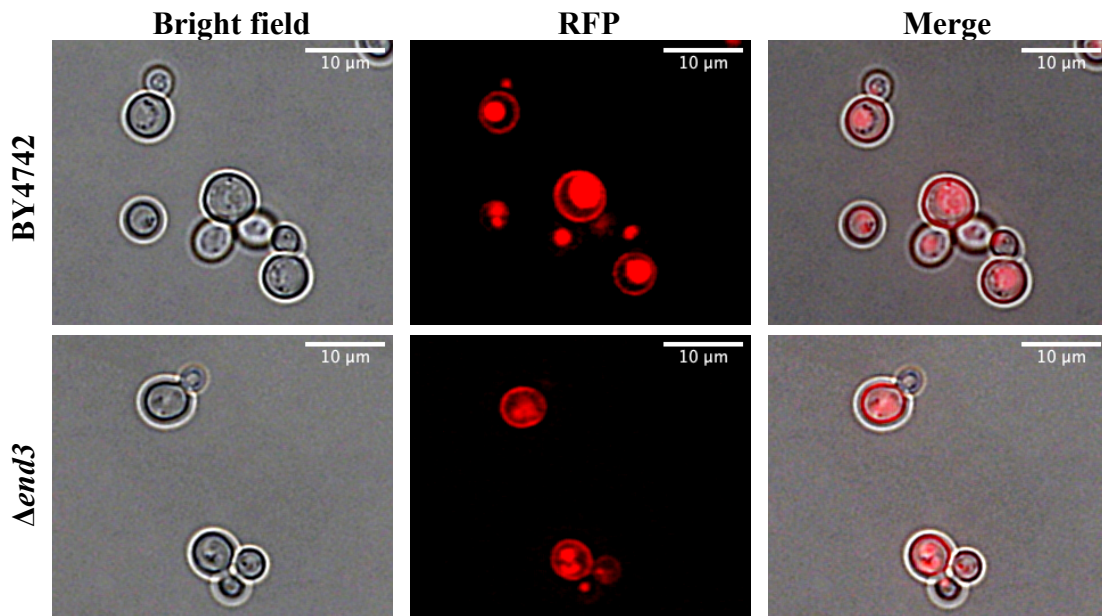


Figure 3.10: Fluorescence microscopy of stably transformed wild-type BY4742 and $\Delta end3$ yeast cells expressing the Pma1p-mRFP fusion protein.

BY4742 and its isogenic $\Delta end3$ mutant were transformed with linearized YIp128-PMA1-mRFP plasmid and stable cells constitutively expressing Pma1p-mRFP were generated via homologous recombination. Red signals correspond to Pma1p-mRFP. Pma1p signals located at the PM and vacuole were observed in living cells by fluorescence microscopy (Keyence). Objective: PlanApo VC 100x-1.4 Oil; Magnification: 50x; Filter: BZ-X TexasRed (560 nm excitation, 630 nm emission); Scale bar: 10 μ m.

After verifying the PM-localization of the Pma1p fusion protein, the transport of ykAE1 was further analyzed by a colocalization study. Therefore, a similar indirect immunofluorescence setup was used, but in order to enhance the image resolution, spinning-disk confocal microscopy was chosen. In this context, pYES2.1-ykAE1^{HA} was transformed into the BY4742-PMA1-mRFP strain, and the expression of ykAE1^{HA} was induced with 3% galactose for 24 h followed by immunostaining for ykAE1^{HA} with primary anti-HA antibody and secondary anti-rat antibody conjugated with FITC. The samples were then analyzed carefully by spinning-disk confocal microscopy (Figure 3.11).

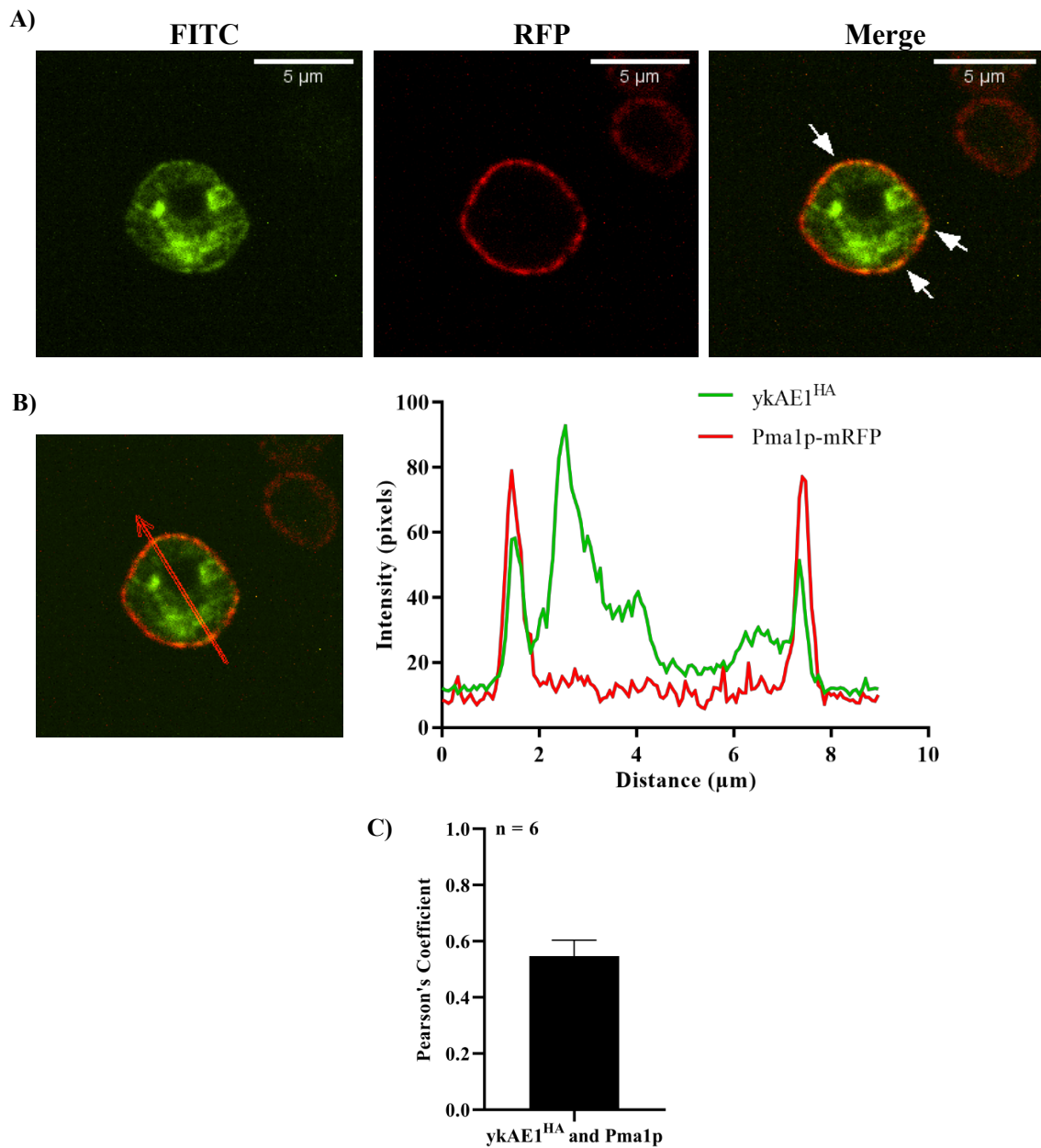


Figure 3.11: Colocalization study of ykAE1^{HA} with Pma1p-mRFP in *S. cerevisiae*.

Indirect immunofluorescence images of ykAE1^{HA} (green) and yeast PM-marker Pma1p-mRFP (red) in BY4742 cells. (A) To induce kAE1 expression, yeast cells were incubated in 3% galactose for 24 h. Then, cells were spheroplasted, fixed and permeabilized. Subcellular localization of kAE1 was detected by probing the cells with anti-HA antibody followed by FITC-coupled anti-rat antibody. The cells were analyzed using a confocal spinning disk microscope (Ti-Eclipse, Nikon). Green and red overlay signals are indicated by white arrows. Objective: 100x Oil Plan Apo TIRF objective (Nikon); Laser: CSU488 and CSU 561; Scale bar: 5 μ m (published in Sarder *et al.*, 2020). (B) Pixel intensities along the arrow in the image of merged channels displayed in A. Green intensities were obtained for kAE1 and red intensities were captured for Pma1p. (C) Average Pearson's correlation coefficient values for colocalization between kAE1 and Pma1p for n = 6 cells from four different samples.

Figure 3.11 shows the subcellular localization of ykAE1^{HA} expressed in the BY4742-PMA1-mRFP strain. Here, the green fluorescence signals correspond to kAE1, while red fluorescence signals represent Pma1p-mRFP. Notably, a few green signals are overlapping with the red signals at the cell surface, whereas the majority of green signals are visible intracellularly and do not colocalize with the red signals. These data demonstrate that the cell surface transport of kAE1 in *S. cerevisiae* is very inefficient and most of the expressed protein is accumulated or aggregated in the cellular organelles. Nonetheless, the evaluation of colocalization of kAE1 with Pma1p yielded a Pearson's coefficient of 0.5474 ± 0.051 (SEM, n = 6 cells), indicating that kAE1 and Pma1p colocalized to some extent (Figure 3.11 C). This evidence supported that a very limited amount of kAE1 protein is targeted to the yeast cell surface and the result was consistent with the previous observation of the untagged ykAE1 protein in this study.

In sum, indirect immunofluorescence data of HA-tagged kAE1 strengthen the evidence that a minor pool of kAE1 could reach the PM through the anterograde transport pathway. Nevertheless, these analyses are not sufficient to distinguish between the cortical-ER and the PM of yeast cells, as both are very tightly associated (West *et al.*, 2011). Therefore, it was not excluded that the observed kAE1 signal might be cortical-ER localized protein and further experiments were necessary to confirm the PM localization of kAE1.

3.4 Approaches for improving the kAE1 plasma membrane localization

Strong promoters are usually used to express foreign protein for high-yield production. However, this can lead to aggregation of the misfolded protein. Liu and colleagues reported that utilization of a strong promoter for synthesis of the insulin precursor protein or the α -amylase in *S. cerevisiae* leads to misfolded-proteins aggregating in the ER, and resulting in inadequate secretion (Liu *et al.*, 2012). In this study, kAE1 expression was controlled by a strong and inducible *P_{GALI}* promoter to facilitate robust protein synthesis. However, a strong overexpression, especially of larger transmembrane proteins, could induce cellular stress responses leading to reduced production and mistargeting of the desired protein. In order to boost plasma membrane localization, several approaches were taken into account. A reduction of the galactose concentration in the culture medium as well as the expression of ykAE1 in the endocytosis defective mutant $\Delta end3$ was conducted. Furthermore, the cultivation temperature

was lowered in an attempt to enhance the amount of PM-targeted kAE1 by increasing the cellular protein folding capacity. Lastly, the potential of a targeted induction of the cellular UPR by co-expression of Hac1p with ykAE1 to improve the localization of the transporter was analyzed.

First, live-cell imaging using fluorescence microscopy was performed with BY4742-PMA1-mRFP cells expressing yeGFP-ykAE1, where the expression of the kAE1 variant was induced by adding two different concentrations of galactose 1% and 3%, respectively, for 24 h at 30 °C (Figure 3.12).

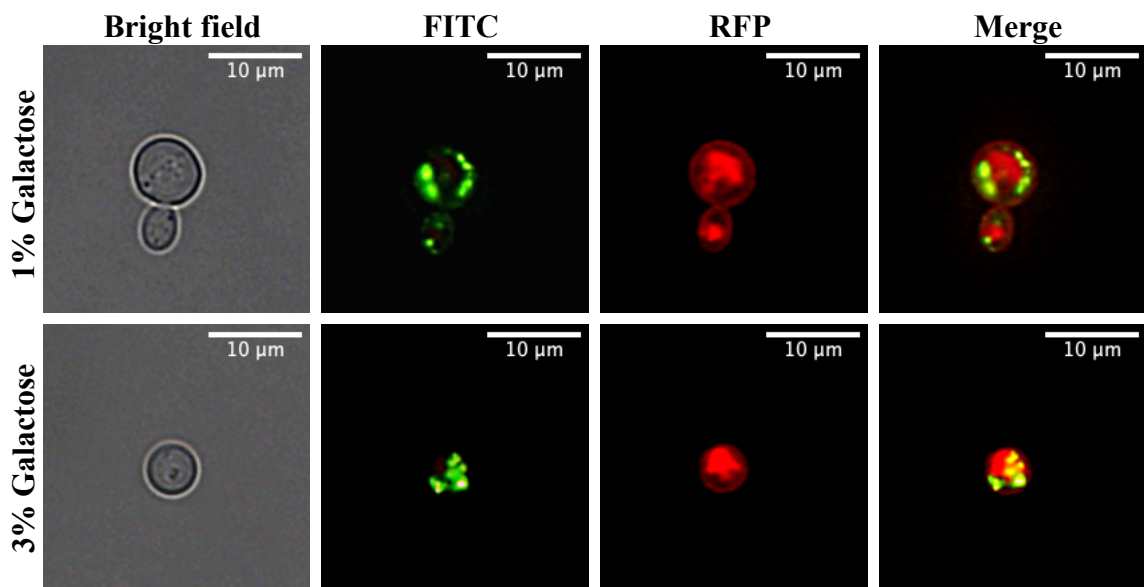


Figure 3.12: yeGFP-ykAE1 expression under different galactose concentrations in BY4742-PMA1-mRFP strain.

BY4742-PMA1-mRFP cells expressing yeGFP-ykAE1 variant in an inducible manner were incubated with either 1% or 3% galactose for 24 h. Intracellular localization of kAE1 protein (green) and Pma1p (red) was visualized in living cells by fluorescence microscopy (Keyence). Objective: PlanApo VC 100x-1.4 Oil; Magnification: 50x; Filter: BZ-X GFP (470 nm excitation, 535 nm emission) and BZ-X TexasRed (560 nm excitation, 630 nm emission); Scale bar: 10 µm.

As shown in Figure 3.12, a high amount of yeGFP-ykAE1 protein was produced in BY4742-PMA1-mRFP cells under both galactose concentrations where the majority of the protein localized in subcellular structures. A very intense yeGFP-ykAE1 signal was observed after the supplementation of 3% galactose compared to 1% galactose. These data suggest that a massive transcription of yeGFP-ykAE1 occurred under galactose induction and resulted in a

significant amount of protein synthesis. This overproduction of heterologous protein could be problematic for the yeast cells to process and subsequently induce cellular stress. In fact, the massive kAE1 production did not contribute to a higher PM targeting of kAE1 in yeast.

Since plasma membrane proteins are recycled back into the cells via endocytosis, the amount of PM-localized kAE1 protein could be increased by interfering with the endocytosis process and trapping kAE1 at the PM. In this background, a yeast strain lacking End3p (one of the key proteins responsible for endocytosis) was used to trap PM-located kAE1 (Raths *et al.*, 1993). The yeGFP-kAE1 variant was transformed into the $\Delta end3$ -PMA1-mRFP strain, and subsequent protein expression was induced by adding either 1% or 3% galactose. The subcellular localization of yeGFP-kAE1 in $\Delta end3$ -PMA1-mRFP cells was analyzed via fluorescence microscopy, and the obtained images are shown in Figure 3.13.

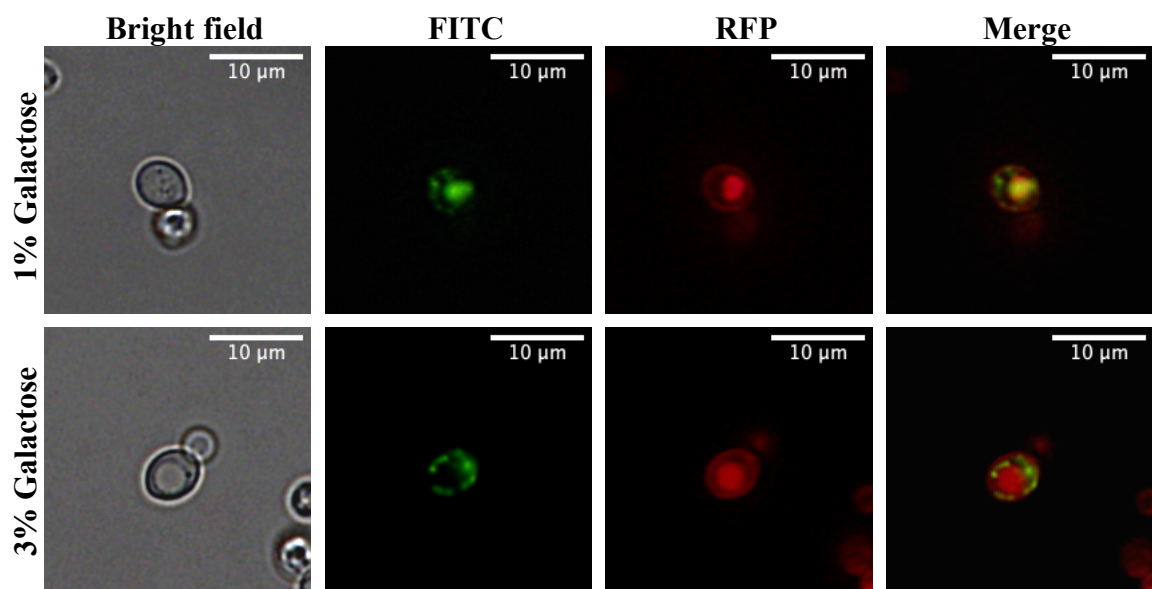


Figure 3.13: yeGFP-ykAE1 expression under different galactose concentrations in $\Delta end3$ mutated cells.

$\Delta end3$ -PMA1-mRFP cells expressing the yeGFP-ykAE1 variant in an inducible manner were incubated with either 1% or 3% galactose for 24 h. Intracellular localization of kAE1 protein (green) and Pma1p (red) was visualized in living cells by fluorescence microscopy (Keyence). Objective: PlanApo VC 100x-1.4 Oil; Magnification: 50x; Filter: BZ-X GFP (470 nm excitation, 535 nm emission) and BZ-X TexasRed (560 nm excitation, 630 nm emission); Scale bar: 10 μ m.

As shown in Figure 3.13, the PM localization of yeGFP-ykAE1 could not be dramatically improved using mutants with defects in endocytosis. However, a slightly increased kAE1 signal was observed under both galactose concentrations that overlapped with the marker protein signal, suggesting kAE1 is likely recycled via endocytosis processes in yeast. Therefore, the mutation of other genes coding for endocytic proteins could result in an improvement of kAE1 cell surface abundance.

A further attempt for optimizing kAE1 protein synthesis in *S. cerevisiae* was made by reducing the growth temperature. Cell growth rates at low temperatures not only slowed down but the protein synthesis rate is also reduced enhancing the protein-folding accuracy (Shi *et al.*, 2003; Vera *et al.*, 2007). In addition, low temperature reduces protein aggregation in *E. coli* by limiting the temperature-dependent hydrophobic interaction (Baldwin, 1986; Robertson & Murphy, 1997). To investigate a potentially similar effect of temperature on kAE1 synthesis in yeast, BY4742-PMA1-mRFP and $\Delta end3$ -PMA1-mRFP cells expressing yeGFP-ykAE1 were grown at 20 °C. In this experiment, kAE1 expression was induced using 0.5% galactose supplementation for a minimal level of protein synthesis to avoid the cellular burden due to heterologous protein overproduction. Yeast cells were analyzed via fluorescence microscopy. Respective images of the obtained results are shown in Figure 3.14.

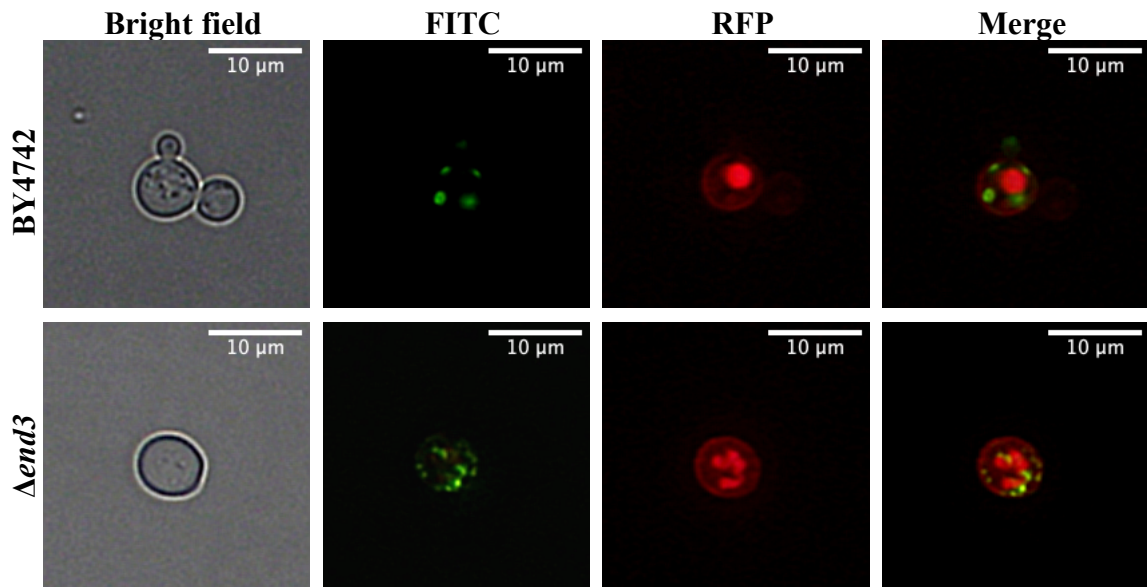


Figure 3.14: yeGFP-ykAE1 expression at low temperature in wild-type and $\Delta end3$ mutated cells.

BY4742-PMA1-mRFP and $\Delta end3$ -PMA1-mRFP cells expressing yeGFP-ykAE1 fusion protein in an inducible manner were incubated with 0.5% galactose for 24 h at 20 °C. Intracellular localization of kAE1 protein (green) and Pma1p (red) was visualized in living cells by fluorescence microscopy (Keyence). Objective: PlanApo VC 100x-1.4 Oil; Magnification: 50x; Filter: BZ-X GFP (470 nm excitation, 535 nm emission) and BZ-X TexasRed (560 nm excitation, 630 nm emission); Scale bar: 10 μ m.

A partial colocalization of yeGFP-ykAE1 (green) and Pma1p (red) was observed in endocytosis-defective $\Delta end3$ cells in a reduced temperature environment, whereas nearly no overlapped signal was observed in wild-type BY4742 cells. This result suggests that the amount of PM-localized kAE1 protein was slightly increased in $\Delta end3$ mutated cells at low temperature. However, the expression rate seemed to be relatively low compared to expression levels after supplementation with higher galactose concentrations.

As previously reported, recombinant proteins expressed in *S. cerevisiae* display a tendency to be retained in the ER, and usually, only a minor amount of the target protein reaches farther destinies of the secretory pathway. It is frequently observed that overexpression of heterologous proteins results in accumulation of improperly folded proteins leading to ER-overload (Mattanovich *et al.*, 2004). Such a phenomenon activates the unfolded protein response (UPR) in host cells, a stress response pathway. It was previously reported that Hac1p (a UPR regulator) is synthesized in response to UPR and ultimately regulates UPR genes such as ER-located

chaperones, foldase and proteases for ER-associated degradation (Mattanovich *et al.*, 2004). Finally, a potential improvement of kAE1 folding or a reduced intracellular accumulation of the anion transporter by the UPR activation was analyzed via Hac1p overexpression. It was previously reported that co-expression of Hac1p results in an increased intracellular protein and secretion level of the kringle fragment of human apolipoprotein-A in *S. cerevisiae* (Lee *et al.*, 2012). To achieve a continuous UPR activation, Hac1p was expressed under the control of a constitutive promoter P_{PGK1} on a single-copy yeast centromere vector pMS109 (Valkonen *et al.*, 2003). Hac1p was then co-expressed with yeGFP-kAE1 in order to analyze intracellular trafficking of kAE1 in yeast under UPR activation. Wild-type BY4742 and its isogenic endocytosis defective mutant $\Delta end3$ cells were co-transformed with pMS109-HAC1 and pYES2.1-yeGFP-kAE1. Expression of yeGFP-kAE1 was initiated by culturing cells in uracil/leucin d/o galactose medium and the intracellular distribution of kAE1 was determined by fluorescence microscopy (Figure 3.15).

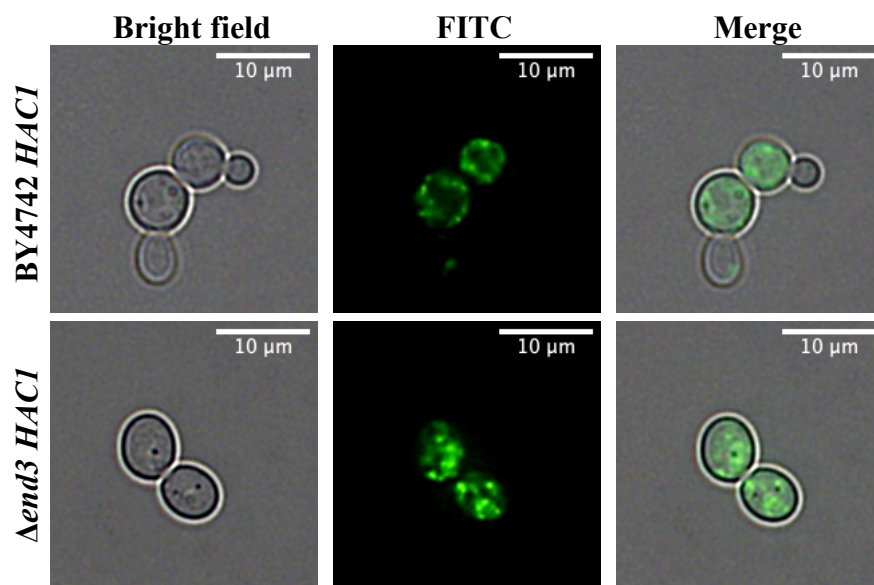


Figure 3.15: Expression of yeGFP-ykAE1 during continuous activation of the UPR.

BY4742 and $\Delta end3$ cells constitutively overexpressed Hac1p under control of P_{PGK1} promoter. Both cells were co-transformed with pYES2.1-yeGFP-ykAE1 plasmid. Expression was induced by culturing cells in 3% galactose-containing medium for 24 h at 30 °C. Intracellular localization of yeGFP-ykAE1 (green) was visualized in living cells by fluorescence microscopy (Keyence). Objective: PlanApo VC 100x-1.4 Oil; Magnification: 50x; Filter: BZ-X GFP (470 nm excitation, 535 nm emission); Scale bar: 10 μ m.

As shown in Figure 3.15, Hac1p co-expression had no profound influence on the ER-retained yeGFP-ykAE1 protein in wild-type and $\Delta end3$ cells. Green signals of yeGFP-ykAE1 were mostly visible in subcellular structures, corresponding to the previously observed ER-like localization of kAE1 variants. These data indicate that the majority of recombinant kAE1 protein could not escape the ER membrane during activation of the UPR. Therefore, Hac1p overexpression in both wild-type and $\Delta end3$ cells does not improve yeGFP-ykAE1 trafficking to the cell surface.

In short, all the aforementioned approaches taken in this study could not substantially improve the level of cell surface localization of the kAE1 variant in *S. cerevisiae*.

3.5 Biochemical detection of plasma membrane located kAE1

To biochemically validate the observed PM-localization of kAE1, cell surface biotinylation was performed in wild-type yeast cells expressing untagged ykAE1 variant. It was previously reported that biotinylation of yeast plasma membrane protein is extensively prevented by the cell wall barrier and, therefore, generally limited to the cell wall proteins (Becker *et al.*, 2016; Masuoka *et al.*, 2002; Mrsă *et al.*, 1997). However, a minor amount of kAE1 could be detected in the biotinylated cell surface fraction of wild-type yeast cells (Figure 3.16). This result was consistent with the aforementioned microscopic observation performed in this study (Figure 3.11). In contrast, there was no kAE1 signal observed in both of the fractions containing cells under non-induced conditions and cells expressing an empty vector (pYES2.1). The cytosolic marker Pgk1p was used to confirm cellular integration during the biotinylation process. As expected, the Pgk1p signal was detected from the whole cell lysate but not from the membrane fraction.

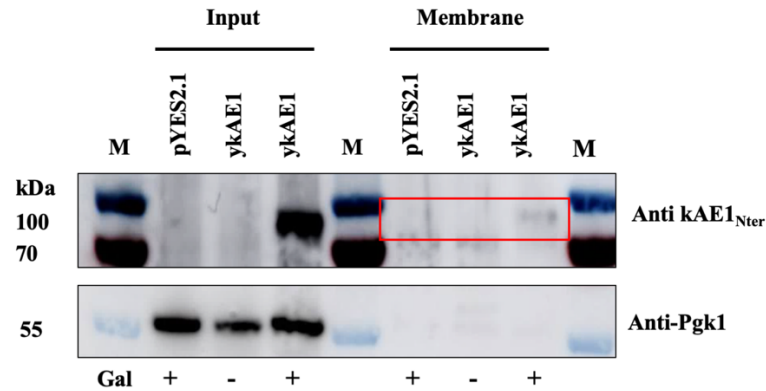


Figure 3.16: Cell surface biotinylation of wild-type yeast cells expressing ykAE1.

BY4742 cells expressing ykAE1 were biotinylated with Sulfo-NHS-biotin under induced (+, galactose) or non-induced (-) conditions and a subsequent pull-down with avidin beads. Whole yeast cell lysates (input) are represented as control to determine the total amount of kAE1. Membrane fraction (membrane) represents the pool of kAE1 located at the cell surface. kAE1 was detected by probing with anti-kAE1_{Nter} antibody followed by an anti-rabbit antibody coupled with HRP. Molecular weight marker is displayed (M). Pgk1p serves as a cytosolic marker protein used to validate cellular integrity during biotinylation (published in Sarder *et al.*, 2020).

3.6 Glycosylation analysis of ykAE1 variants with glycosidase enzymes

Human membrane proteins exhibit inadequate processing when expressed in yeast compared to the respective fungi or plant homologs (Tate, 2001). It was reported that truncated versions of AE1 or kAE1 protein expressed in yeast were not glycosylated (Groves *et al.*, 1999). kAE1 is N-glycosylated at a single site (Asn⁶⁴²) in mammalian cells. To verify whether yeast is able to perform N-glycosylation in kAE1, different full-length ykAE1 variants such as ykAE1, ykAE1^{HA} and yeGFP-ykAE1 were incubated with endoglycosidase enzymes. For this purpose, wild-type BY4742 and mutated $\Delta end3$ cells expressing above-mentioned ykAE1 variants were grown in selective medium under inducing conditions (uracil d/o galactose) for 24 h at 30 °C, and lysed. The extracted ykAE1 variants were then treated with either Endo Hf or PNGase F. Endo HF is a recombinant glycosidase enzyme cloned from *Streptomyces plicatus* that cleaves the chitobiose core of high mannose glycans (Trimble *et al.*, 1978). Alternatively, PNGase F, an amidase derived from *Flavobacterium meningosepticum*, hydrolyses the innermost core of any N-glycans (Plummer *et al.*, 1984). The glycosylation analysis of ykAE1 variants is shown in Figure 3.17.

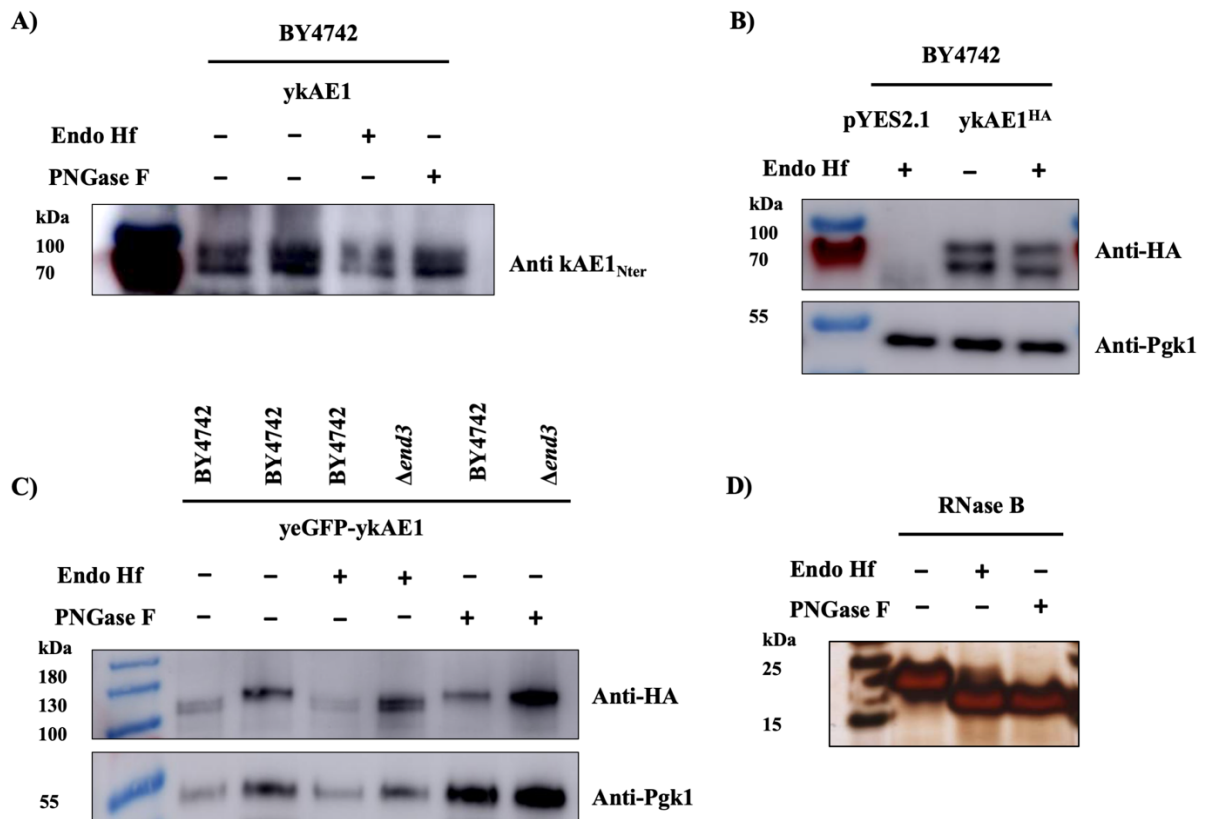


Figure 3.17: Enzymatic deglycosylation study of yeast expressed ykAE1 variants.

Wild-type BY4742 or $\Delta end3$ mutant cells expressing different ykAE1 variants were lysed and protein extracts were incubated either in the presence or absence of Endo HF or PNGase F for 1 h at 37 °C and analyzed via Western blot. Expression of ykAE1 variants was induced by culturing cells in medium containing 3% of galactose. (A) Lysate of BY4742 cells expressing untagged ykAE1 treated with Endo HF or PNGase F. (B) Lysate of BY4742 cells expressing HA-tagged ykAE1 (ykAE1^{HA}) treated with Endo HF. (C) Lysate of BY4742 cells or $\Delta end3$ mutant expressing yeGFP fused ykAE1 variant (yeGFP-ykAE1) treated with Endo HF or PNGase F. (D) A glycosylated protein RNase B was treated with Endo HF or PNGase F served as a positive control and detected through SDS-PAGE with subsequent silver staining. Pgk1p was served as loading control and cells expressing empty vector (pYES2.1) used as a negative control for kAE1 detection.

There was no difference found between the band signals of treated and untreated samples of ykAE1, ykAE1^{HA} and yeGFP-ykAE1 variants with both Endo Hf and PNGase F on immunoblot (Figure 3.17). Interestingly in each sample of kAE1 variants, a top band and a bottom band was observed, whereas the top band corresponds to the estimated molecular weight of the respective kAE1 variant. Since the bottom band found across all samples (treated and untreated), it should not be considered as a deglycosylated protein. To perform glycosylation analysis, kAE1 was incubated at room temperature for a certain period of time (section 2.14.8) and then run on

SDS-PAGE under reducing condition. These bottom bands likely correspond to the degraded products of kAE1. In addition, a positive control experiment with a glycoprotein ribonuclease B (RNase B) was performed under identical conditions (Figure 3.17 D). A clear downshifted band of RNase B was observed for the protein treated with one of the glycosidase enzymes compared to the non-treated condition. This result verified that both enzymes were active.

3.7 Functional analysis of full-length ykAE1 variants in yeast

3.7.1 Analyzing functional homology between kAE1 and Bor1p

It has been reported that Bor1p in yeast is the structural homolog protein of human AE1 (Jennings *et al.*, 2007; Thurtle-Schmidt & Stroud, 2016). Bor1p is an integral membrane protein located at the plasma membrane of *S. cerevisiae* that actively transports boron against a concentration gradient (Takano *et al.*, 2007). Therefore, to examine whether kAE1 could compensate for Bor1p functionality in *S. cerevisiae*, boric acid tolerance assays were performed. Wild-type BY4742 and $\Delta bor1$ mutated yeast cells transformed with either empty vector (pYES2.1) or pYES2.1-ykAE1^{V5} were spotted on solid selective medium containing different concentration of boric acid. Expression of kAE1 was induced by 3% galactose (uracil d/o galactose agar plate) and cell growth was monitored for three days. The corresponding results are shown in Figure 3.18.

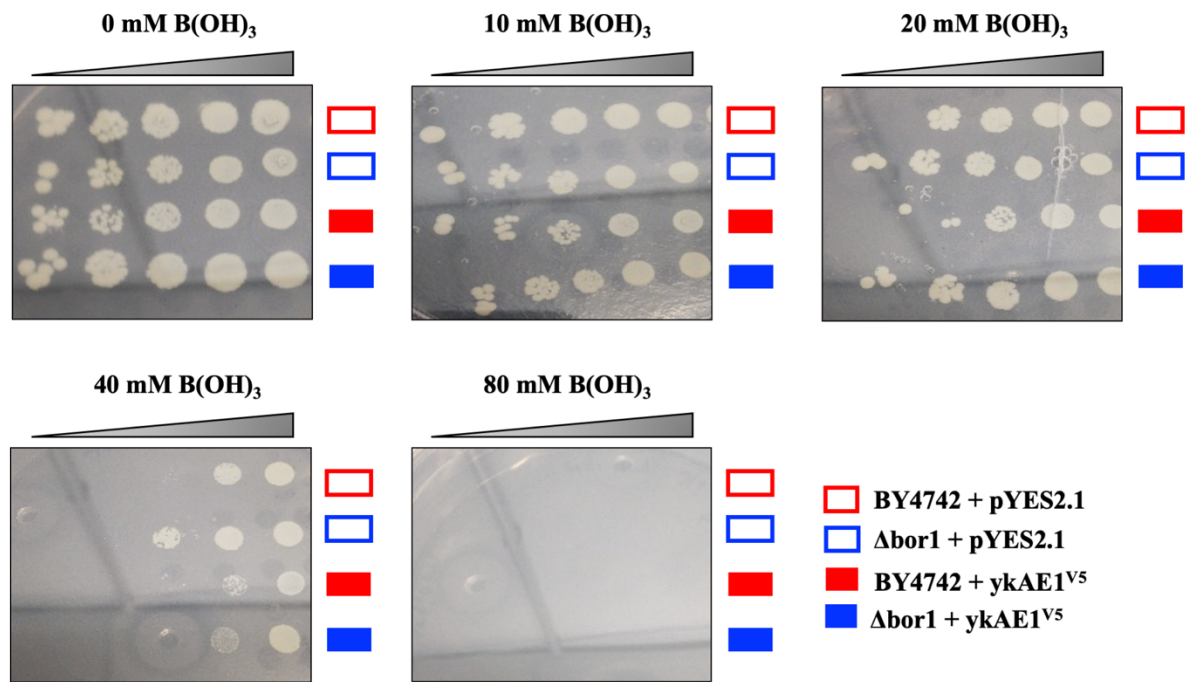


Figure 3.18: Boric acid tolerance assay for wild-type and mutated yeast cells expressing ykAE1^{V5} in solid medium.

BY4742 and $\Delta bor1$ cells expressing ykAE1^{V5} or empty vector were grown to stationary phase. The cell density was adjusted to $OD_{600} = 0.7$ and serially diluted. 5 μ l of cell suspension from the diluted cultures ($OD_{600} = 0.7 \times 10^{-5} - 0.7 \times 10^{-1}$) was spotted on uracil d/o galactose plates containing the indicated amount of boric acid. The plates were then incubated for 3 d at 30 °C and photographed.

The expression of ykAE1^{V5} did not improve the growth of BY4742 cells in the presence of a high concentration of boric acid in the medium. Additionally, kAE1 expression was also not able to rescue the growth defect of the $\Delta bor1$ mutant (Figure 3.18). Moreover, empty vector expressing $\Delta bor1$ cells displayed a less sensitive phenotype to boric acid (in the presence of 20 mM and 40 mM boric acid) compared to wild-type cells. For further investigation, boric acid tolerance assay in liquid medium was carried out and the obtained results are shown in Figure 3.19.

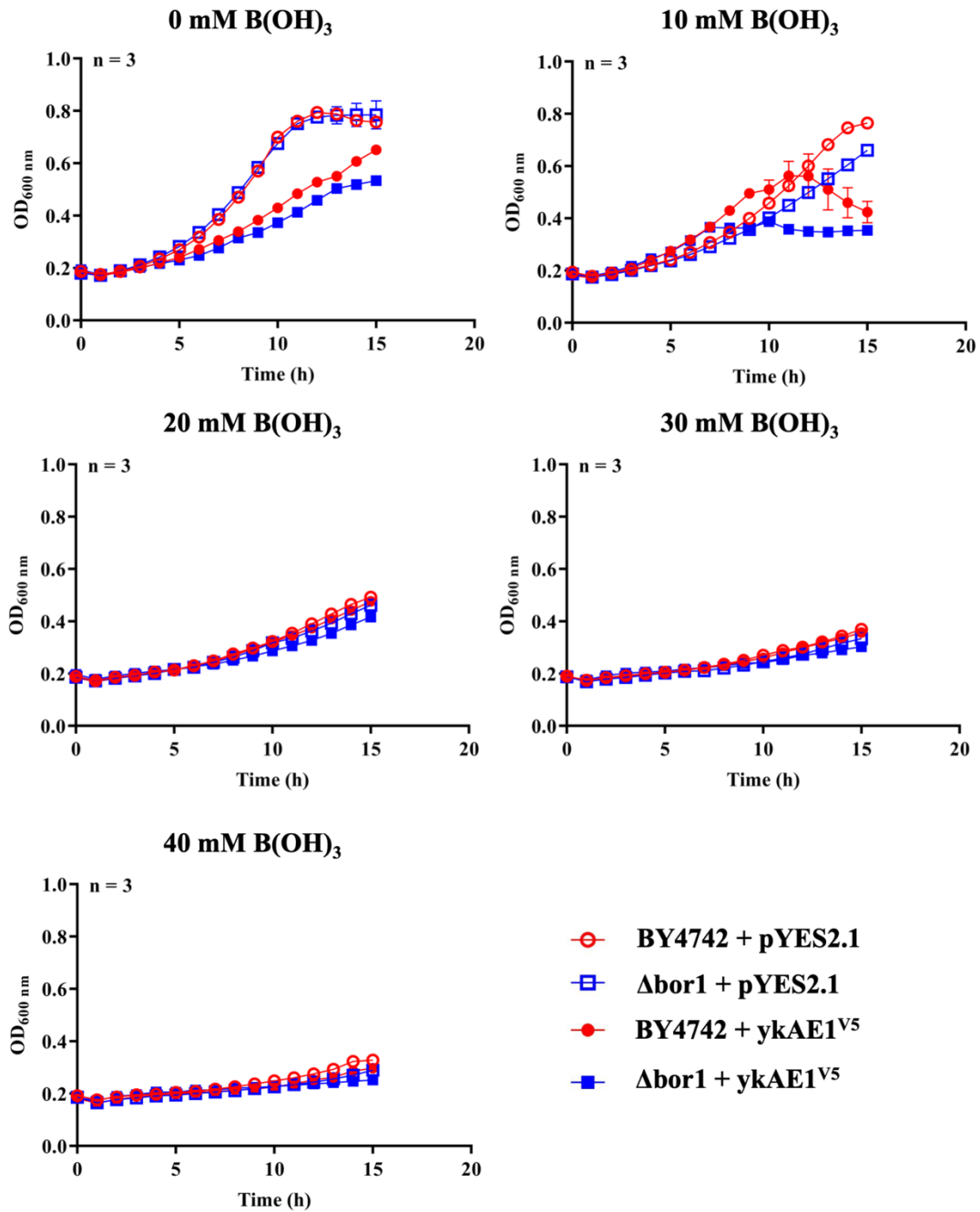


Figure 3.19: Boric acid tolerance assay for wild-type and $\Delta bor1$ yeast cells expressing ykAE1^{V5} in liquid medium.

Wild-type BY4742 and $\Delta bor1$ mutated cells containing pYES2.1 (empty vector) or pYES2.1-ykAE1^{V5} plasmid were first grown into uracil d/o glucose medium for overnight. Cultures were then diluted to OD₆₀₀ = 0.2 and placed into uracil d/o galactose medium containing the indicated amount of boric acid. Afterward, 200 μ l of the individual cell suspension was transferred into a 96-well plate. Finally, plates were incubated for 15 h at 30 °C and cell growth was recorded by a multi-mode plate reader at 600 nm. Data are shown as mean \pm SEM of n = 3 experiments.

In liquid medium, both wild-type BY4742 and $\Delta bor1$ cells expressing the ykAE1^{V5} variant displayed a strong reduction in cell growth in the presence of boric acid and the growth rate of these cells did not differ significantly from the empty vector expressing cells (Figure 3.19). Therefore, kAE1 expression did not improve the growth defect of yeast cells under high boric acid conditions, suggesting that kAE1 does not compensate for the function of Bor1p. However, in this experiment $\Delta bor1$ cells showed more sensitivity to boric acid in comparison to wild-type cells validating the experimental condition.

In brief, $\Delta bor1$ mutant expressing ykAE1^{V5} did not show an improved growth rate compared to empty vector containing cells in the presence of boric acid. Thus, kAE1 did not compensate for the function of Bor1p in $\Delta bor1$ mutated cells.

3.7.2 Correlation of intracellular pH and kAE1 expression

kAE1-mediated Cl^-/HCO_3^- exchange activity can alter cytosolic pH in mammalian cells. Rawad and colleagues recently found that expression of wild-type kAE1 in mIMCD3 cells resulted in a drastic reduction of cytosolic pH level compared to non-expressing cells (Lashhab *et al.*, 2019). To verify whether the expressed full-length kAE1 is active in yeast, the cytosolic pH of ykAE1 variant expressing cells was determined. BCECF-AM dye is commonly used to determine the cytosolic pH of mammalian cells (Chu *et al.*, 2010; Shnitsar *et al.*, 2013). On the contrary, yeast cells tend to transport BCECF-AM into the vacuole and this dye was previously used to measure the vacuolar pH of *S. cerevisiae* (Diakov *et al.*, 2013). Therefore, to measure the cytosolic pH of *S. cerevisiae* an alternative dye named SNARF-5F AM (a derivative of SNARF AM) was used in this study. SNARF AM is a naphthofluorecin derivative conjugated with acetoxymethyl ester, which was already utilized to determine cytosolic pH of *S. cerevisiae* (Valli *et al.*, 2005). Yeast cells loaded with SNARF-5F AM were analyzed under a fluorescence microscope to observe the intracellular distribution of the pH probe (Figure 3.20).

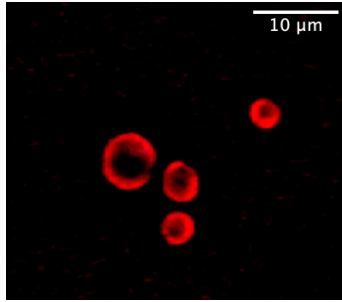


Figure 3.20: Wild-type BY4742 cells treated with SNARF-5F AM.

BY4742 cells were incubated with 10.0 $\mu\text{g/ml}$ SNARF-5F AM for 1 h at 30 $^{\circ}\text{C}$. Red signals resemble the cytosolic presence of the dye in yeast cells. Live-cells were analyzed by fluorescence microscopy (Keyence). Objective: PlanApo VC 100x-1.4 Oil; Magnification: 50x; Filter: BZ-X TexasRed (560 nm excitation, 630 nm emission); Scale bar: 10 μm .

As shown in Figure 3.20, a diffused intracellular red fluorescence signal was detected corresponding to the cytoplasmic distribution of SNARF-5F in yeast cells. In contrast, nearly no fluorescence signal was observed from the core of the cells, which resembles the nucleus of the cells. This result indicated that SNARF-5F AM was suitable to measure the cytosolic pH of yeast cells.

To avoid any effect due to alternating of carbon sources on the cytosolic pH analysis, the vector pPGK was utilized to express untagged ykAE1 in *S. cerevisiae*. The constitutive expression of ykAE1 was verified via Western blot analysis (data not shown). BY4742 cells expressing either wild-type kAE1 (pPGK-ykAE1) or empty vector (pPGK) were incubated with SNARF-5F AM for 1 h at 30 $^{\circ}\text{C}$. The fluorescence signal was detected using a fluorometer and cytosolic pH was calculated by plotting a standard curve. Cytosolic pH measurement data of yeast cells expressing empty vector and untagged ykAE1 variant is shown in Figure 3.21.

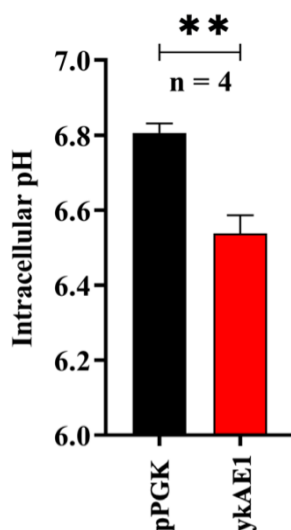


Figure 3.21: Cytosolic pH measurement of *S. cerevisiae* during kAE1 expression.

BY4742 cells expressing empty vector (pPGK) or wild-type ykAE1 were grown in 2% glucose for 24 h. Cells were treated with SNARF-5F AM and intracellular pH was measured. Intracellular pH values are displayed. Measurements were performed from $n = 4$ independent experiments and represent as mean \pm SEM; *, $p < 0.05$; **, $p < 0.01$ using unpaired t-test (published in Sarder *et al.*, 2020).

The mean cytosolic pH value of cells expressing an empty vector was 6.81 ± 0.02 (SEM) (Figure 3.21), which is in agreement with the previously reported cytosolic pH value of the wild-type yeast cells (Valkonen *et al.*, 2013). Surprisingly, a significant drop of cytosolic pH to 6.54 ± 0.04 (SEM) occurred under ykAE1 expression ($p < 0.01$).

3.7.3 Dose-dependent correlation of cytosolic pH and kAE1 expression

To further verify the link between the cytosolic pH drop and kAE1 activity in yeast, a dose-dependent expression of ykAE1 using β -estradiol was performed in BY4742-GEV cells. Gal4dbd.ER.VP16 (GEV) is a chimeric transcriptional activator composed of a Gal4p DNA binding domain, a hormone-binding domain of the human estrogen receptor as well as an eukaryotic transcriptional activator domain of herpes simplex virus VP16 (McIsaac *et al.*, 2011). The BY4742-GEV strain contains an integrated copy of GEV driven by a constitutive promoter P_{ACT1} . In absence of β -estradiol, GEV is inactive and located in the cytosol coupled with the heat sensor protein HSP-90 complex. When β -estradiol is added to the growth medium, it diffuses through the cell membrane and binds to the estrogen binding site of GEV, which results in a dissociation of HSP-90 complex and relocation of GEV from the cytosol to the

nucleus. In the nucleus, GEV attaches to the UAS_{GAL} consensus sequence and initiates the transcription of the target protein by its VP16 domain. kAE1 induction in BY4742-GEV cells in a dose-dependent manner by β -estradiol is shown in Figure 3.22.

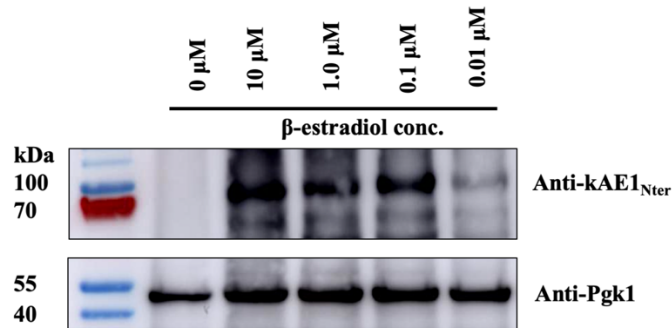


Figure 3.22: Dose-dependent induction of ykAE1 expression in BY4742-GEV cells.

BY4742-GEV cells were incubated with different concentrations of β -estradiol to induce expression of untagged ykAE1. After cell lysis, Western blot analysis was performed to verify the levels of kAE1 expression in the presence of β -estradiol. Blots were probed with primary anti-kyAE1_{Nter} antibody and secondary anti-rabbit antibody coupled with HRP (published in Sarder *et al.*, 2020).

BY4742-GEV cells were transformed with the pYES2.1-ykAE1 plasmid and the positive transformants were selected by culturing cells in selective medium (uracil d/o glucose). ykAE1 expression was stimulated by adding β -estradiol for 18 h at 30 °C. The expression level of ykAE1 was directly proportional to the amount of β -estradiol in the medium (Figure 3.22). No kAE1 expression was detected on the immunoblot in cells without β -estradiol, which served as negative control. This result showed that kAE1 expression levels in the BY4742-GEV strain could be manipulated by simply providing a certain amount of β -estradiol to the respective growth medium. In order to determine whether the decrease in cytosolic pH had a direct connection to the level of kAE1 expression in yeast cells, cytosolic pH measurement of ykAE1 expressing BY4742-GEV cells was performed by using SNARF-5F AM. ykAE1 expression was induced by adding defined amounts of β -estradiol ranging from 0.01 μ M to 10.0 μ M, and cells were incubated for 18 h at 30 °C. The cells were then treated with SNARF-5F AM for 1 h, and cytosolic pH was measured using a fluorometer (Figure 3.23).

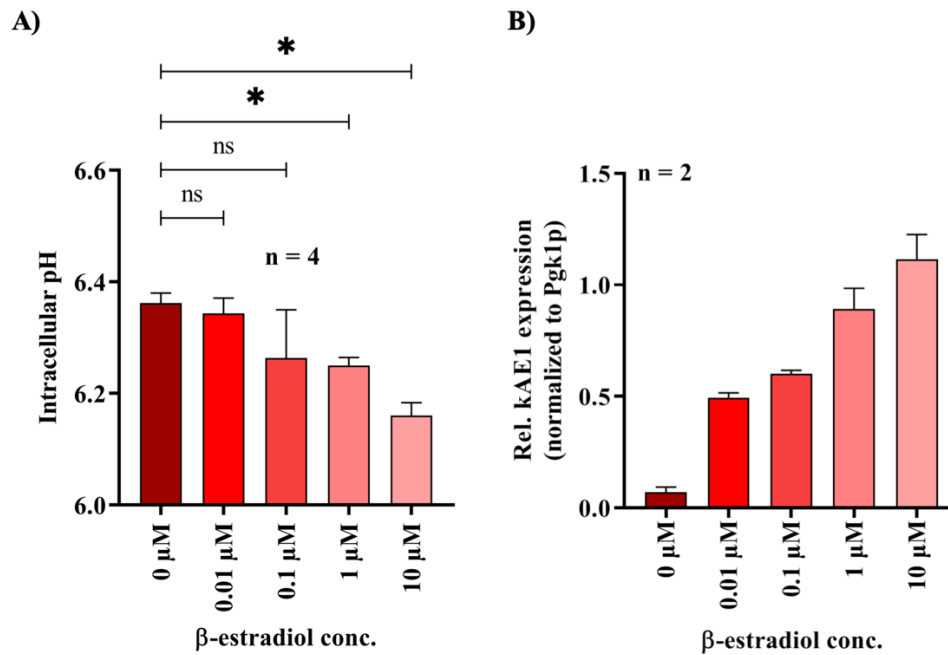


Figure 3.23: Correlation between intracellular pH and kAE1 expression level in wild-type yeast cells.

(A) Intracellular pH measurement of BY4742-GEV cells expressing ykAE1 induced by the indicated concentration of β -estradiol. Intracellular pH values are displayed. Measurements were performed from n = 4 independent experiments and represented as mean \pm SEM; *, $p < 0.05$ using One-Way ANOVA. (B) Densitometry analysis of the ykAE1 expression in BY4742-GEV cells corresponding to the indicated amount of β -estradiol. Each signal for kAE1 was normalized to the respective signals of Pgk1p and relative kAE1 signals were calculated. Data are shown as mean \pm SEM of n = 2 separate experiments (published in Sarder *et al.*, 2020).

Figure 3.23 shows graphs of the cytosolic pH measurement of BY4742-GEV cells expressing ykAE1 (A) and the densitometry analysis of kAE1 expression level with the corresponding cells (B). A cytosolic pH value of 6.36 ± 0.02 (SEM) was detected from negative control cells (without β -estradiol), whereas cytosolic pH values of 6.34 ± 0.02 , 6.26 ± 0.07 , 6.25 ± 0.01 and 6.16 ± 0.02 (SEM) were measured from cells incubated with 0.01 μ M, 0.1 μ M, 1.0 μ M and 10 μ M β -estradiol, respectively. Interestingly, an elegant correlation was found between cytosolic pH and the kAE1 expression level in yeast cells (Figure 3.23). Cells expressing a high amount of kAE1 (1.0 μ M and 10 μ M of β -estradiol) displayed a significant drop of cytosolic pH ($p < 0.05$). In contrast, cells expressing a low level of kAE1 (0.1 μ M and 0.01 μ M of β -estradiol) showed no significant difference in cytosolic pH versus the negative control cells (cells without β -estradiol). The highest kAE1 expressing cells displayed the lowest cytosolic pH and vice-versa. Therefore, these results indicate that the drop of cytosolic pH is associated

with the level of kAE1 expression in wild-type yeast cells and are, therefore, in line with the previously observed data from mammalian cells.

3.7.4 Determination of intracellular chloride transport in dependency of kAE1 expression

The basic function of kAE1 is the exchange of $\text{Cl}^-/\text{HCO}_3^-$ in the kidney, hence the Cl^- transport rate by kAE1 expressing yeast cells was determined for analyzing the biological activity of the protein. kAE1-mediated Cl^- influx was measured via anion exchange chromatography in wild-type yeast cells expressing either empty vector (pPGK) or untagged kAE1 (ykAE1) (Figure 3.24).

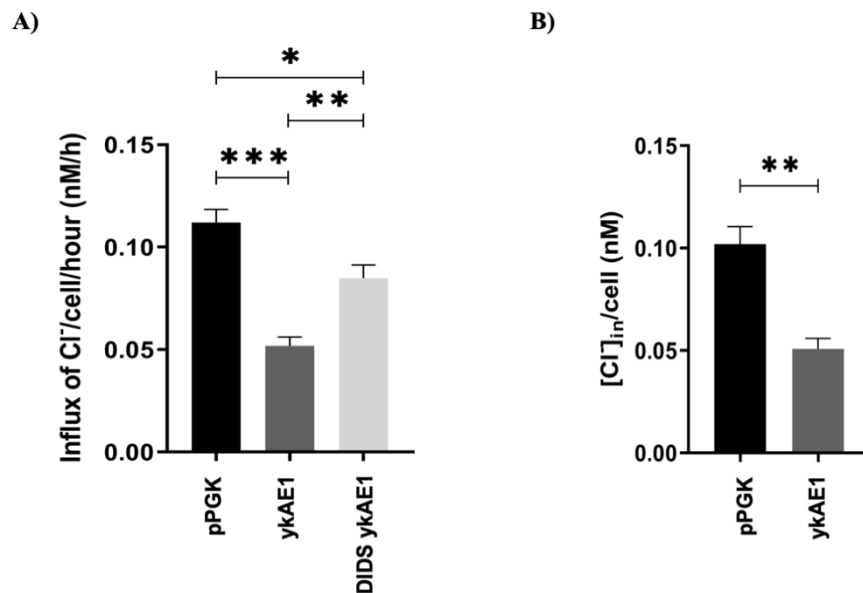


Figure 3.24: Cl⁻ influx rate measurement of wild-type yeast cells expressing pPGK or ykAE1.

(A) Cl⁻ influx rate of BY4742 cells expressing pPGK or ykAE1 in the presence or absence of 200 μM DIDS. Data is showing the Cl⁻ influx rate per hour per cell as nanomolar per hour (nM/h) for $n = 6$ measurements and mean \pm SEM; *, $p < 0.05$; **, $p < 0.01$; ***, $p < 0.001$ using One-Way ANOVA. The Cl⁻ influx rate was normalized to the total cell number ($\text{OD}_{600} = 1$, equivalent to 1×10^7 cells). (B) Relative intracellular Cl⁻ concentration ($[\text{Cl}^-]_{\text{in}}$) of BY4742 cells expressing pPGK or ykAE1 indicated in nanomolar (nM). Each measurement was normalized to corresponding total cell numbers. Data represent the mean \pm SEM of $n = 3$ separate experiments and; *, $p < 0.05$; **, $p < 0.01$; using One-Way ANOVA (published in Sarder *et al.*, 2020).

Under hyperosmotic conditions (150 mM NaCl), a reduced Cl⁻ influx rate together with a decreased intracellular Cl⁻ concentration was detected in cells expressing ykAE1. In contrast,

the empty vector expressing cells exhibited an elevated level of Cl^- influx, leading to a higher intracellular Cl^- concentration (Figure 3.24). Surprisingly, the diminished Cl^- influx rate observed in kAE1 expressing cells was opposite to a previous $^{36}\text{Cl}^-$ uptake study performed in yeast cells expressing the truncated AE1³⁶¹⁻⁹¹¹ variant (Groves *et al.*, 1996). However, restriction of kAE1 activity with the kAE1 inhibitor DIDS expectedly led to a high level of Cl^- influx, resulting in the prevention of kAE1-mediated Cl^- efflux compared to kAE1 expressing cells. Although increased Cl^- influx by the kAE1 expressing cells was anticipated, the significant differences between the empty vector and kAE1 expressing cells strongly indicate a kAE1-mediated Cl^- transport in yeast cells.

Altogether, the occurrence of cytosolic pH drop along with the increased rate of Cl^- efflux in kAE1 expressing cells is pointing towards the biological activity of the heterologously expressed anion exchanger in yeast.

3.8 Expression and localization analysis of kAE1 mutants in *S. cerevisiae*

In order to validate yeast as a model organism to dissect pathophysiologic characteristics of kAE1, mutants of kAE1 were generated, such as E681Q and G701D, and their expression level and subsequent localization were investigated. kAE1 E681Q showed an impaired chloride-bicarbonate exchange but was localized at the cells surface of HEK293 cells (Shnitsar *et al.*, 2013). Alternatively, kAE1 G701D displayed a complete retention in the ER of MDCK cells (Cordat *et al.*, 2006). An untagged E681Q mutant was generated using pYES2.1-ykAE1 as template by PCR amplification (section 2.6). Similarly, the G701D^{Flag} was created from pYES2.1-ykAE1^{Flag} plasmid in the same way. A Flag tag was placed at the third exofacial loop between Asn⁵⁵⁶ and Val⁵⁵⁷ of G701D^{Flag} mutant to facilitate the detection process. Unfortunately, the construction of a Flag-tagged kAE1 E681Q was not successful.

Wild-type BY4742-GEV cells were transformed with pYES2.1-E681Q or pYES2.1-G701D^{Flag} recombinant plasmid, and expression of the mutants was induced by adding 10 μM of β -estradiol hormone into the selective medium. Protein levels of kAE1 E681Q and G701D^{Flag} mutants were analyzed via immunoblotting by probing with anti-kAE1_{Nter} antibody and anti-Flag antibody, respectively (Figure 3.25). A robust signal at ~94 kDa was detected for both untagged kAE1 E681Q and Flag-tagged kAE1 G701D^{Flag} mutants on the immunoblot which is the expected molecular weight of the mutants. Expression level of the kAE1 E681Q mutant was

similar to the expression level of wild-type protein. Besides, the protein level of kAE1 G701D^{Flag} was also comparable to wild-type protein (data not shown). This result demonstrated that heterologous expression of kAE1 mutants at a high level is possible in *S. cerevisiae*.

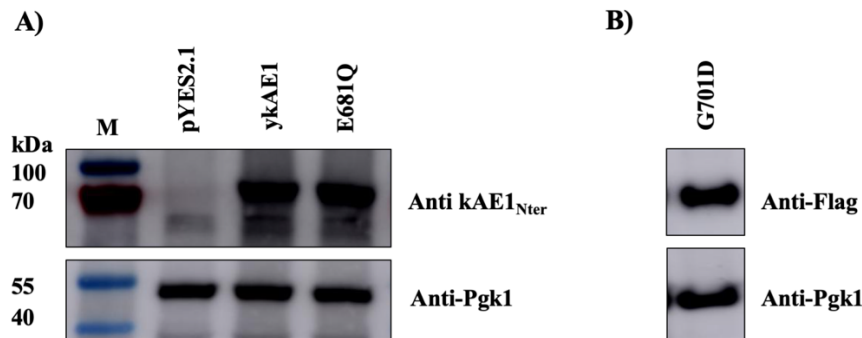


Figure 3.25: Expression analysis of kAE1 E681Q and G701D^{Flag} mutant in yeast.

BY4742-GEV cells expressing kAE1 E681Q and G701D^{Flag} in an inducible manner were incubated with 10 μ l of β -estradiol for 24 h prior to lysis. (A) Representative immunoblot of kAE1 E681Q probed with anti-kAE1_{Nter} antibody followed by an anti-rabbit antibody coupled with HRP. Empty vector (pYES2.1) expressing cells represent as negative control and untagged kAE1 (ykAE1) expressing cells represent as positive control. (B) Representative immunoblot of kAE1 G701D^{Flag} probed with primary anti-flag antibody and secondary anti-mouse antibody coupled with HRP. Pgk1p serves as a loading control.

Investigation of kAE1 mutants' trafficking in yeast cells was crucial for elucidating the role of mutants in pathological condition. Hence, indirect immunostaining was performed in order to detect subcellular localization of both kAE1 E681Q and G701D mutant. BY4742-GEV cells expressing E681Q or G701D^{Flag} were incubated with 10 μ M β -estradiol for 24 h at 30 °C and indirect immunostaining was performed. To determine intracellular localization of the mutants, cells expressing kAE1 E681Q or kAE1 G701D^{Flag} were probed with the appropriate primary and secondary antibodies. By performing fluorescence microscopy, a peripheral ring-like structure (green) was observed in cells expressing kAE1 E681Q mutant (Figure 3.26), indicating a possible PM localization. In addition, fluorescence signals detected from intracellular structures resemble the localization at the intracellular membranes. Since kAE1 E681Q was previously detected at the PM of mammalian cells (Shnitsar *et al.*, 2013), this outcome from yeast cells was expected. However, it could not be clarified that the detected peripheral signal of the kAE1 E681Q mutant was not from the cortical-ER localized protein. In

contrast, the cells expressing kAE1 G701D^{Flag} displayed a prominent diffused intracellular signal, which most likely arose from the protein located at the ER-like structure.

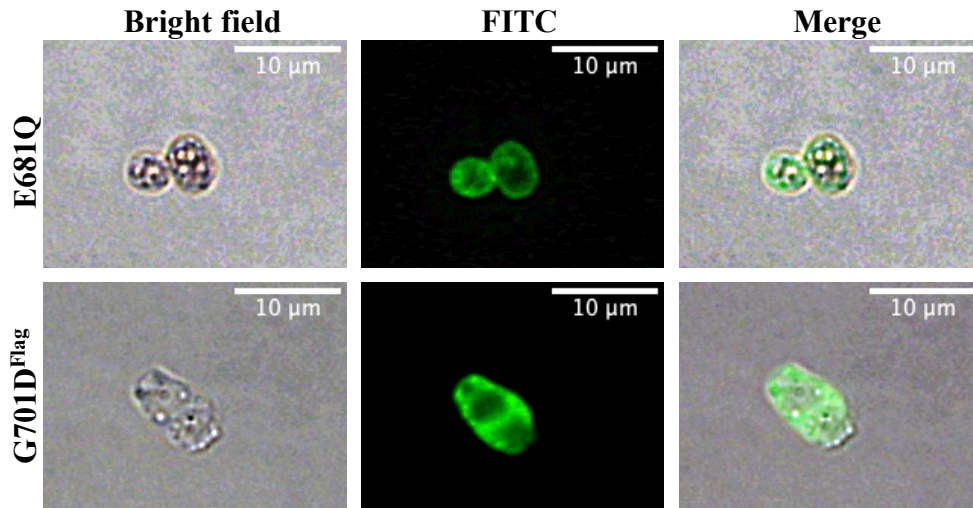


Figure 3.26: Intracellular localization of kAE1 E681Q and G701D^{Flag} in yeast.

Indirect immunofluorescence images of kAE1 E681Q and G701D^{Flag} in BY4742-GEV cells. Yeast cells were induced by 10 μ M β -estradiol for 24 h. Intracellular localization of E681Q mutant was detected by using anti-kAE1_{Nter} followed by anti-rabbit antibody coupled with FITC. G701D^{Flag} was visualized by probing with a primary anti-flag antibody and a secondary anti-mouse antibody coupled with FITC. Cells were analyzed using fluorescence microscopy (Keyence). Objective: PlanApo VC 100x-1.4 Oil; Magnification: 50x; Filter: BZ-X GFP (470 nm excitation, 535 nm emission); Scale bar: 10 μ m. The pictures were taken during the bachelor thesis of Elisa Bertin (2017).

In sum, these data demonstrate a robust expression of the two kAE1 mutants in *S. cerevisiae*. kAE1 E681Q mutant was found at the cell periphery, whereas kAE1 G701D^{Flag} mutant was localized intracellularly. In fact, the localization of kAE1 E681Q mutant can be compared to the localization of wild-type kAE1 in BY7472 cells. However, further experiments are needed with marker protein for addressing the detailed subcellular localization of the mutants in yeast.

3.9 Characterization of novel dRTA mutants in mammalian cells

In the second part of this project, three newly found dRTA mutants were characterized in mouse inner medullary collecting duct cells (mIMCD3): a recessive dRTA mutant kAE1 R295H and two dominant dRTA mutants kAE1 Y413H and S525F. It was previously reported that the

majority of dRTA mutants show mistrafficking rather than altered function in MDCK cells (Almomani *et al.*, 2011). On the contrary, evidence from dominant dRTA patients (kAE1 G609R) and a mouse model with the dominant dRTA mutation kAE1 R607H revealed that the mutated protein locates at the basolateral membrane of α -intercalated cells, but in a reduced amount. In addition, a secondary mistrafficking of V-H⁺-ATPase was detected with an overall depletion of α -intercalated cells in the kidney. The expression of kAE1 R589H mutant in polarized mIMCD3 cells resulted in the functional localization of the mutant at the basolateral membrane (Mumtaz *et al.*, 2017). This preliminary finding suggests that in mIMCD3 cells, kAE1 mutant behaves similarly as the wild-type protein in terms of localization and functionality. Therefore, to characterize the novel dRTA mutants, mIMCD3 cells were used in this study which likely imitated the *in vivo* situation.

3.9.1 Half-life of the three novel kAE1 mutants

To express wild-type and mutated kAE1 variants, stable mIMCD3 cell lines were generated. Therefore, mIMCD3 cells were transduced with lentiviruses carrying the wild-type or a mutated kAE1 cDNA using the Clontech Lenti-X inducible expression system. Notably, after passages of the infected cells, the expression of kAE1 was not affected and the expression level was found to be identical. This strategy provides the opportunity to bypass the continuous loss of kAE1 when constitutively expressed (Chu *et al.*, 2010). Wild-type kAE1 and its mutants were carrying an HA tag at the third extracellular loop between Val⁵⁵⁷ and Leu⁵⁵⁸. To assess the stability of the kAE1 mutants, protein expression was induced in presence of 1.0 μ g/ml of doxycycline for 24 h. After removal of doxycycline, the relative amount of protein was measured at four time points such as 0, 8, 24, and 48 h by performing Western blot analysis and results are shown in Figure 3.27.

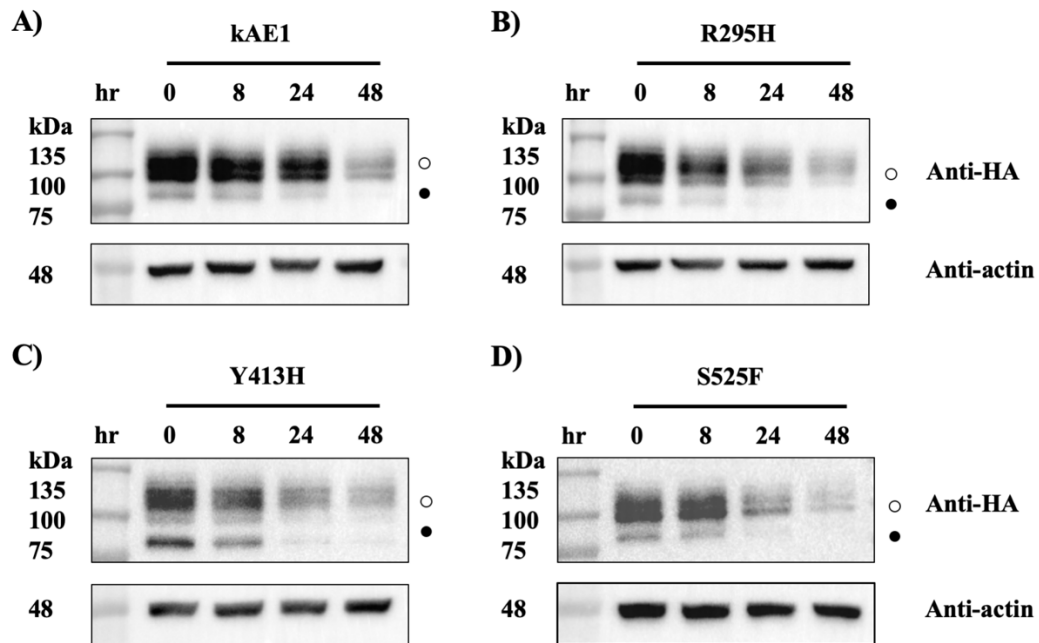


Figure 3.27: Degradation profile of wild-type and mutated kAE1 in mIMCD3 cells.

Stably transduced mIMCD3 cells expressing wild-type and mutated kAE1 in an inducible manner were incubated with 1.0 $\mu\text{g/ml}$ of doxycycline. After 24 h of induction, doxycycline was removed at the indicated time points and replaced with fresh medium. Cells were lysed and then analyzed by immunoblot. kAE1 variants were detected by using an anti-HA antibody succeeded by an anti-rat antibody coupled with HRP (upper panel). Representative immunoblot for (A) wild-type kAE1, (B) kAE1 R295H, (C) kAE1 Y413H, and (D) kAE1 S525F are shown. β -actin serves as a loading control (lower panel). White circle (top) corresponds to kAE1 carrying a complex oligosaccharide and black circle (bottom) represents kAE1 carrying a high-mannose oligosaccharide.

On the immunoblot, two distinct bands of kAE1 (closely spaced) were detected where the top band corresponds to the protein carrying a complex oligosaccharide and the bottom band resembles the protein carrying a high-mannose oligosaccharide (Figure 3.27). Wild-type kAE1 displayed an overall higher expression level compared to the three mutants. Therefore, the expression level of kAE1 and the mutants was normalized to the endogenous expression level of β -actin for each condition. After 8 h, there was no noticeable difference observed in protein levels between wild-type kAE1 and the three mutants. In contrast, after 24 h and 48 h removal of doxycycline from the medium, a significant reduction of protein level was observed for all the three mutants compared to wild-type kAE1. This result showed that all the novel dRTA mutants are degraded in a faster manner than the wild-type protein. In addition, the mutants

kAE1 Y413H and S525F displayed an increased amount of high-mannose carrying protein (bottom) compared to wild-type kAE1. These data indicate that the processing of these two mutants is affected in mIMCD3 cells. The dominant mutants were able to escape from the ER to the median Golgi, but not as efficiently as wild-type kAE1. In contrast, the complex- and high-mannose carrying protein band for the recessive kAE1 R295H was similar to that of the wild-type protein. This result suggests similar processing of the mutant occurred compared to wild-type kAE1 in the secretory pathway. In addition, the half-life of the mutants was calculated, and the results are shown in Figure 3.28.

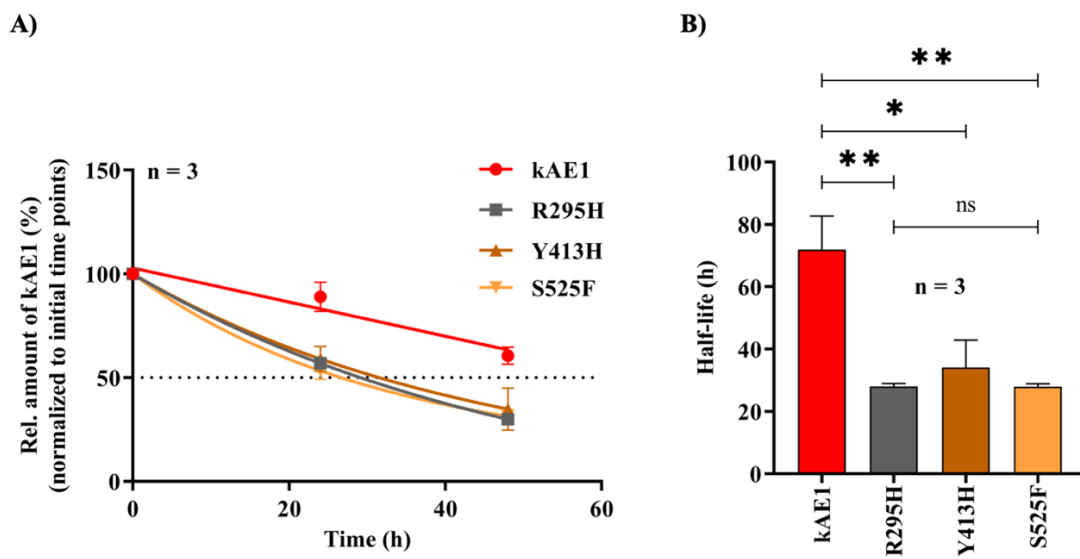


Figure 3.28: Half-life of kAE1 mutants compared to wild-type kAE1.

(A) Densitometry analysis of the immunoblots to determine the relative amount of kAE1 variants expressed in mIMCD3 cells. The relative amount of kAE1 was primarily determined by dividing the kAE1 band intensity with the corresponding β -actin band intensity. The initial time point was then set as 100% and used for normalization of the following time points. Data are shown as mean \pm SEM of $n = 3$ independent experiments and are fitted by exponential regression. (B) Half-life of wild-type and mutated kAE1 was generated by using the equation obtained from the graph represented in A. Data represent the mean \pm SEM of $n = 3$ separate experiments and; *, $p < 0.05$; **, $p < 0.01$ using One-Way ANOVA.

Figure 3.28 shows a graphical representation of the half-life of three novel dRTA mutants. The detected half-life for kAE1 R295H, Y413H and S525F was 28.01 ± 0.91 , 34.13 ± 8.73 and 27.94 ± 0.91 h (SEM), respectively. In contrast, half-life for wild-type kAE1 was 71.94 ± 10.76 h (SEM). As expected, the half-life of all three dRTA mutants was significantly lower than the wild-type protein ($p < 0.05$). These data indicated that dRTA-causing mutants

are likely recognized as misfolded proteins and are prematurely degraded aligning with the previously obtained result of dRTA mutants characterized in kidney cell lines (Chu *et al.*, 2014a; Kittanakom *et al.*, 2004).

3.9.2 Impact on p62 level in mIMCD3 cells

The amount of α -intercalated cells was found to be remarkably depleted in dominant dRTA kAE1 R607H knock-in mice (Mumtaz *et al.*, 2017). Moreover, kidney tissue immunostaining of these mice revealed that p62, a classical marker for autophagy, was highly accumulated in cells, suggesting an impairment in the autophagy process. To determine the effect of the expression of kAE1 mutants on p62 in mIMCD3 cells, the relative p62 level was examined by Western blot analysis. Wild-type and mutated kAE1 expression was initiated by incubating the stably transduced mIMCD3 cells with 1.0 $\mu\text{g/ml}$ of doxycycline for 24 h. The p62 protein level upon mutant expression was detected by probing the blot with anti-HA, anti- β -actin and anti-p62 antibody, and the results are shown in Figure 3.29.

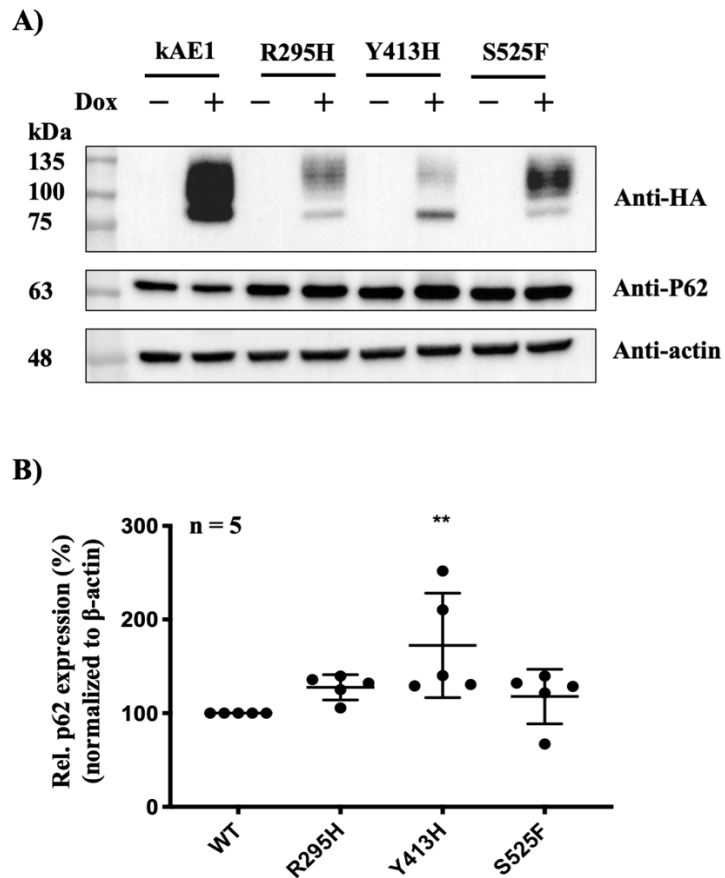


Figure 3.29: Investigation of p62 level in mIMCD3 cells expressing wild-type kAE1 and dRTA mutants.

mIMCD3 cells expressing wild-type or mutated kAE1 were incubated either in the absence or presence of doxycycline (1.0 μ g/ml) for 24 h. Cells were lysed and protein abundance was determined by performing Western blot. (A) Representative immunoblots for wild-type kAE1, kAE1 R295H, kAE1 Y413H and kAE1 S525F. The blot was probed with mouse anti-HA to detect kAE1 (upper panel), followed by mouse anti-p62 antibody for p62 (middle panel) or mouse- β -actin for β -actin (lower panel) detection. (B) Densitometry analysis of relative amount of p62 level (%) in mIMCD3 cells after expressing wild-type kAE1 and mutants. Each measurement of p62 was normalized to the corresponding signal of β -actin, and the relative p62 signal was calculated. The p62 signal of cells expressing wild-type kAE1 was set to 100 %. Data represented as mean \pm SEM of n = 5 different experiments and; *, $p < 0.05$; **, $p < 0.01$ using One-Way ANOVA. The column graph and four replicates among five were kindly generated by Lalie Vergnaud (2019).

Figure 3.29 shows the immunoblot and densitometry analysis of the relative p62 level in mIMCD3 cells expressing wild-type kAE1 and the mutants. The overall p62 level was higher

in mIMCD3 cells expressing the dRTA mutants. However, the p62 level was found to be significantly higher only for the dominant Y413H mutant compared to the wild-type protein ($p < 0.01$). Since the p62 level in mIMCD3 cells was not significantly higher when expressing R295H and S525F mutants ($n = 5$), this could be due to technical error while performing Western blot analysis. This issue might be solved by increasing sample numbers.

3.9.3 Effect on mIMCD3 cells viability

In dRTA patients or knock-in mice, a dramatic decline is seen in the viability of α -intercalated cells (Mumtaz *et al.*, 2017; Vichot *et al.*, 2017). Now an interesting point would be to know if the viability of mIMCD3 cells is also affected by expressing dRTA mutants. Therefore, an MTS-based assay was used to analyze the viability of mIMCD3 cells under the expression of the recessive kAE1 R295H or the dominant kAE1 S525F mutant in combination with different osmotic conditions. kAE1 is highly expressed in α -intercalated cells of the distal nephrons where the tubular fluid osmolality is very high reaching up to 1200 mOsmol/kg H₂O (Gottschalk, 1960). On the contrary, mIMCD3 cells are typically *in vitro* cultivated under a relatively low osmotic pressure as the osmolality of the growth medium is roughly ~300 mOsmol/kg H₂O. To reduce this osmotic discrepancy, 100 mM NaCl or 200 mM Mannitol were added to growth media to reach a final osmolarity of ~500 mOsmol/kg H₂O, representing hyperosmotic conditions. Stably transduced mIMCD3 cells were initially induced with 1.0 μ g/ml of doxycycline (+Dox) to express wild-type kAE1, kAE1 R295H and kAE1 S525F mutant for 24 h. Later on, the kAE1 expressing mIMCD3 cells along with non-induced (-Dox) mIMCD3 cells were grown under three different conditions: 1) standard growth medium, 2) 100 mM NaCl in growth medium, and 3) 200 mM Mannitol in the growth medium. The viability of mIMCD3 cells was measured using MTS reagent at 0, 48, and 72 h after placing cells under the indicated culture condition and the results are shown in Figure 3.30.

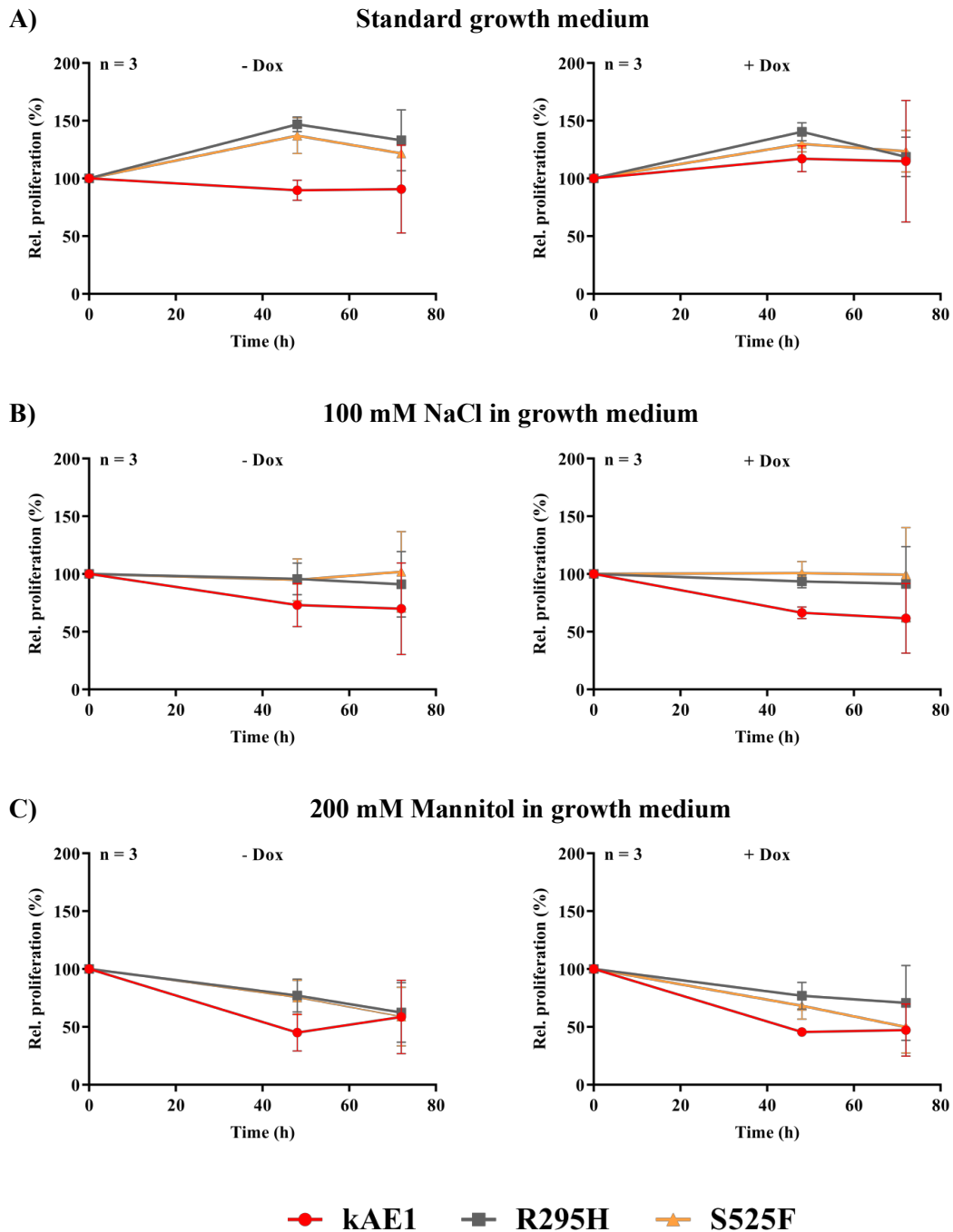


Figure 3.30: mIMCD3 cell proliferation analysis by MTS assay in non-induced (–Dox) and induced (+Dox) situation.

Stably transduced mIMCD3 cells were incubated into growth medium with or without 1.0 $\mu\text{g/ml}$ of doxycycline for 24 h at 37 $^{\circ}\text{C}$ in 5% CO_2 supplied incubator. In presence of doxycycline, cells were expressing wild-type kAE1, recessive kAE1 R295H, and dominant kAE1 S525F mutant. Afterward, cells were placed into three different osmotic mediums, and cell viability was measured after 0, 48, and 72 h. Cells were incubated in (A) standard growth medium, (B) 100 mM NaCl containing growth medium and (C) 200 mM Mannitol containing growth medium. The MTS absorbance of cells at 0 h was set to 100% and used for normalization of the following time points. Data are shown as mean \pm SEM of $n=3$ independent experiments.

The viability of mIMCD3 cells expressing the kAE1 R295H and S525F mutants was not significantly different compared to cells expressing wild-type kAE1 in standard growth medium (Figure 3.30 A). In addition, a similar phenomenon was observed when cells were incubated into the hyperosmotic medium. The viability of mIMCD3 cells expressing kAE1 R295H and S525F mutant was found to be similar in comparison to the wild-type kAE1 expressing mIMCD3 cells under both hyperosmotic media (Figure 3.30 B, C). Simultaneously, the viability of non-induced mIMCD3 cells was found to be comparable to the induced mIMCD3 cells under identical conditions. Thus, data from MTS-based cell proliferation assay showed no significant difference in proliferation of mIMCD3 cells expressing wild-type kAE1 and the mutants. The statistical analysis between -Dox and +Dox group in each condition were carried out by two-way ANOVA (data are not shown).

4. Discussion

Ion homeostasis is one of the fundamental processes in cell physiology for regulating numerous cellular mechanisms, ranging from cell division to cell death. In order to pass impermeable ions through the cell boundary, membrane transporters are used and their expression varies between different cell types (Dubyak, 2004; Gautier & Hinner, 2015). Such transporters consist of a diverse group of proteins where $\text{Cl}^-/\text{HCO}_3^-$ exchangers play a decisive role in the acid-base homeostasis in the human body. The anion exchanger 1 protein controls $\text{Cl}^-/\text{HCO}_3^-$ exchange in a sodium-independent manner and is considered the founding member of the solute carrier SLC4 superfamily (Alper, 2006; Cordat & Casey, 2009). In the distal nephron, the kidney isoform of AE1, kAE1, facilitates bicarbonate reabsorption into the interstitium across the basolateral membrane of α -intercalated cells. Thus, the anion transporter plays a crucial role in the urine acidification process. Interestingly, mutations in the kAE1 encoding gene *SLC4A1* result in faulty acidification of urine, which is known as distal renal tubular acidosis. dRTA patients usually suffer from various complications that eventually arose from defective urine acidification, such as metabolic acidosis, hyperchloremia, hyperkalemia, kidney stone formation and failure to thrive (Shayakul & Alper, 2000). So far, only the structure of the AE1/kAE1 membrane domain (381–887 aa, except three exofacial loops region) has been revealed (Arakawa *et al.*, 2015). In addition to the lack of a structural model of the full-length variant, there is also relatively little known about its cellular trafficking pathway. Heterologous expression of disease-causing kAE1 mutants in MDCK cells demonstrated that the mutant proteins were either mistargeted or intracellularly retained in ER-Golgi structures, thereby displaying improper function (Cordat *et al.*, 2006; Devonald *et al.*, 2003). For example, kAE1 R589H mutant expressed in MDCK cells exhibited a complete intracellular retention in the ER compartment (Toye *et al.*, 2004). In contrast, Mumtaz and colleagues reported that in α -intercalated cells from kAE1 R607H knock-in mice (corresponding to human kAE1 R589H variant), the mutant protein was targeted to the basolateral membrane and was found to be functional, albeit a secondary mistrafficking of apically located V-H⁺-ATPase was observed. These observations from kAE1 R607H knock-in mice are consistent with the biopsy report of patients with dominant dRTA kAE1 G607R mutation, where trafficking of the mutant was unaffected and found at the basolateral membrane of α -intercalated cells (Vichot *et al.*, 2017). However, the level of kAE1 expression was strongly reduced along with a severe depletion of α -intercalated cells in the patient's kidneys. All these findings are pointing towards the fact that

the cellular model systems formally used for investigating kAE1 mutants were inadequate to dissect precise molecular mechanisms of the disease. Therefore, the use of a new model organism for addressing kAE1-related research questions in a fast and economical manner becomes inevitable.

In the present study, analysis of intracellular transport and functionality of kAE1 and its mutant variants was performed in yeast and mammalian cells. The first part of the study highlights the capability of yeast as a model system for addressing kAE1 physiology-related questions. *Saccharomyces cerevisiae* is widely recognized as a model organism for analyzing various renal proteins such as epithelium sodium channel (ENaC), cystic fibrosis transmembrane conductance regulator (CFTR) and Na⁺-K⁺-ATPase (Buck *et al.*, 2010; Kolb *et al.*, 2011). Moreover, *S. cerevisiae* was previously used for the heterologous expression of kAE1, whereas only truncated kAE1 variants could be successfully expressed (Groves *et al.*, 1996). The attempts to express full-length kAE1 in yeast were either unsuccessful or resulted in the accumulation of inactive protein in organelle membranes (Groves *et al.*, 1999). In this study, several full-length kAE1 derivatives were constructed and expressed in *S. cerevisiae*. In addition, the potential plasma membrane localization of the variants was determined by various microscopic and biochemical techniques such as fluorescence microscopy, CLSM and a cell surface biotinylation assay. Furthermore, the functionality of selected full-length kAE1 derivatives was analyzed by the measurement of cytosolic pH as well as the Cl⁻ influx rate. Besides, the kAE1 mutants E681Q and G701D were expressed in yeast, and their cellular localization was determined by fluorescence microscopy. The second part of the study focused on the characterization of three novel dRTA mutants (recessive kAE1 R295H, dominant kAE1 Y413H, and kAE1 S525F mutant) in mouse inner medullary collecting duct cells (mIMCD3). The stability of these mutants in mIMCD3 cells was investigated via Western blot analysis, and the effect of their expression on mIMCD3 cell viability was analyzed by MTS assay.

Expression of full-length kAE1 in yeast

In the present study, two different strategies were used to express full-length kAE1 in yeast. Firstly, a signal peptide of Kar2p (Kar2^{SS}) was introduced at the N-terminal position of the human kAE1 sequence (hkAE1) to improve ER import of the newly synthesized protein. Secondly, the human cDNA sequence of kAE1 was optimized for the synonymous yeast codon

(ykAE1). So far, a few truncated versions of AE1/kAE1, such as AE1³⁶¹⁻⁹¹¹ (361–911 aa), AE1¹⁸³⁻⁹¹¹ and AE1³⁸⁸⁻⁹¹¹, were expressed in baker's yeast. However, only AE1³⁶¹⁻⁹¹¹ was able to exchange anions and could partially reach the cell surface, whereas other short versions AE1¹⁸³⁻⁹¹¹ and AE1³⁸⁸⁻⁹¹¹ were retained into intracellular compartments (Bonar & Casey, 2010; Groves *et al.*, 1996; Sekler *et al.*, 1995). The idea behind introducing a Kar2^{SS} was the attachment of a yeast signal peptide to the human protein, which has already been shown to facilitated ER translocation. For example, a fusion of Kar2^{SS} to TorsinA, a human AAA+ ATPase, increased its ER translocation and stability in *S. cerevisiae* (Chalfant *et al.*, 2019). Besides, the generation of mRNA transcripts is one of the critical factors for an effective translation rate. Each organism uses a specific set of preferred codons during translation (64 different codon triplet combinations are generally possible). It was proposed that the codon usage variability is determined by either the codon decoding rate or the codon reading ability of a particular organism (Chu & Haar, 2012; Routledge *et al.*, 2016).

Immunoblot results of the full-length kAE1 variants showed that the human cDNA sequence of kAE1 failed to be expressed in *S. cerevisiae*. This finding is in line with previous studies suggesting a failure to express the human sequence of kAE1 in yeast (Groves *et al.*, 1999). Interestingly, it could be shown that the yeast codon-optimization of the human kAE1 sequence led to robust expression of the full-length kAE1, whereas addition of Kar2^{SS} at the N-terminus of kAE1 only had a weak impact on the protein synthesis (Figure 3.2). Thus, the Kar2^{SS}-hkAE1^{V5} variant was not considered for further experiments. Notably, the yeast codon-optimized sequence of kAE1 seems to be expressed efficiently by yeast cells. It means that codon optimization has significantly improved the translation accuracy as well as the translation rate of the kAE1 mRNA in yeast. The human codon usage was found to be the restriction factor for the synthesis of full-length kAE1 in yeast cells. Therefore, it proposes that the codon optimization technique provides a valid possibility to express a variety of tagged and untagged full-length versions of kAE1 in *S. cerevisiae*.

Plasma membrane localization of full-length kAE1 in yeast

To study ykAE1 protein trafficking, the C-terminal end of kAE1 was tagged either with a V5 tag or yeGFP. Indirect immunofluorescence results of wild-type yeast cells expressing ykAE1^{V5} showed a complete intracellular localization of the protein (Figure 3.5). Similarly,

confocal microscopy images of BY4742 cells expressing ykAE1-yeGFP resulted in intracellular retention of the fusion protein at a comparable level to the ykAE1^{V5} variant (Figure 3.6). It has been reported that any alteration at the C-terminus of kAE1 may affect its functional targeting to the basolateral membrane (Cordat *et al.*, 2003). The untagged ykAE1 was generated to investigate the trafficking of the wild-type protein in yeast. Unlike the C-terminally tagged kAE1, indirect immunofluorescence data of untagged ykAE1 displayed few peripheral fluorescence signals (Figure 3.4). Although a substantial amount of the anion transporter was in the membrane of subcellular structures, this data showed a first hint of the plasma membrane localization of full-length kAE1. Several features on the C-terminal end of kAE1 are important for trafficking to the cell surface, and thus, tags could somehow interfere with proper recognition of kAE1 by transport machinery of the secretory pathway. The kAE1 C-terminus contains a tyrosine-based sorting motif Y⁹⁰⁴DEV⁹⁰⁷ and a class-II PDZ-binding domain A⁹⁰⁸MPV⁹¹¹. It has been reported that the tyrosine-based sorting motif (YxxΦ; Y represents tyrosine, x represents for any amino acid and Φ represents a hydrophobic amino acid) is crucial for the basolateral membrane targeting of kAE1. AP-1 -mu1A directly interacts with the tyrosine-based motif at the trans-Golgi network and mediates the basolateral sorting process of kAE1 (Almomani *et al.*, 2012; Junking *et al.*, 2014). In addition, the last four amino acids of the kAE1 polypeptide chain (A⁹⁰⁸MPV⁹¹¹) act as a class-II PDZ-binding domain (xΦxΦ-COOH; x represents any amino acid and Φ represents any hydrophobic amino acid). As reported previously, the class-II PDZ-binding domain also plays a role in the basolateral targeting of the kAE1 protein. The dominant kAE1 M909T mutant displayed both correct basolateral targeting and abnormal apical membrane targeting in polarized MDCK cells (Fry *et al.*, 2012). Therefore, any alteration in the kAE1 C-terminal region could potentially interfere with the plasma membrane targeting of the transporter.

On the contrary, insertion of an epitope tag at the third extracellular loop or modification of the N-terminus neither affects kAE1 function nor its localization to the plasma membrane in mammalian cells (Beckmann *et al.*, 2002; Parker & Tanner, 2004). Therefore, a third extracellular loop HA-tagged ykAE1 (ykAE1^{HA}) and an N-terminal yeGFP fusion of kAE1 (yeGFP-ykAE1) were constructed. The colocalization study of ykAE1^{HA} and yeGFP-ykAE1 variants with a plasma membrane marker Pma1p-mRFP further strengthened the hypothesis of plasma membrane targeting of kAE1 in yeast (Figure 3.11 and 3.12). Colocalization images suggested that a small pool of kAE1 is overlapping with Pma1p. These data align with a recently

published electron microscopy (EM) study, where a precise plasma membrane localization of full-length kAE1 is confirmed (Sarder *et al.*, 2020). In that study, two full-length kAE1 variants (HA-tagged ykAE1^{HA} and untagged ykAE1) were expressed in $\Delta end3$ mutant cells (defective in endocytosis) or $\Delta pep4$ mutant cells (defective in vacuolar degradation) and found at the cell surface to a small extent. A positive control, the truncated version of yeast codon-optimized kAE1 (ykAE1^{B3mem}, equivalent to AE1³⁶¹⁻⁹¹¹), was also detected at the plasma membrane of yeast cells to comparable quantities to the full-length kAE1. Besides, cell surface biotinylation of wild-type yeast cells (BY4742) expressing the untagged ykAE1 variant further indicates that a small fraction of full-length kAE1 is localized at the yeast plasma membrane (Figure 3.16).

Altogether, these data indicate—for the first time—that the full-length kAE1 variants are able to reach the plasma membrane of *S. cerevisiae*. Nevertheless, the plasma membrane localization of kAE1 is limited to a small fraction. The full-length versions of kAE1 are trafficked to the cell surface in a comparable amount to the previously reported AE1³⁶¹⁻⁹¹¹ variant. Notably, the kAE1 C-terminus interactions with carrier molecules in yeast are vital for the cell surface localization. Therefore, an unmodified C-terminus of kAE1 is the most critical factor for the plasma membrane targeting of kAE1 in *S. cerevisiae*.

Intracellular accumulation of kAE1 in *S. cerevisiae*

Former studies in yeast reported that kAE1 is highly prone to be trapped in different subcellular membrane structures (Bonar & Casey, 2010). The observation of spinning disk microscopy data suggested that a majority of the expressed kAE1 was intracellularly accumulated in protein-rich membrane-like structure (Figure 3.11). This finding was in agreement with the EM study of three different ykAE1 variants (ykAE1^{HA}, ykAE1 and ykAE1^{B3mem}) expressed in yeast cells. Furthermore, the EM results revealed that kAE1 was additionally found in multivesicular bodies (MVBs), indicating a partial targeting of kAE1 to the vacuole for subsequent degradation (Sarder *et al.*, 2020). MVBs usually form at late endosomes and are involved in the degradation of membrane proteins by fusing to the vacuole/lysosome. In yeast, proteins from the PM or trans-Golgi network are being sorted in MVBs and transported to the vacuole for degradation through endosomal sorting complexes for transport (ESCRT) pathways (Henne *et al.*, 2011; Piper & Katzmann, 2010). The presence of an increased amount of kAE1 protein in the vacuole compared to the plasma membrane in $\Delta end3$ cells suggests that the protein is more likely

transported from the Golgi network to the vacuole via the ESCRT-mediated pathway than the alternative route from the plasma membrane to the vacuole known as the endocytic pathway. An increased amount of kAE1 protein in the vacuole of vacuolar protease deficient $\Delta pep4$ cells further supports this hypothesis (Feyder *et al.*, 2015; Sarder *et al.*, 2020).

Since full-length kAE1 was severely aggregated in intracellular membranes, various parameters affecting protein synthesis and processing were tested for increasing the cell surface localization of the anion exchanger, such as inducer concentration, temperature, and UPR-activation. In this study, kAE1 was inducibly expressed by using a P_{GALI} promoter, which is a strong metabolic promoter. The reason for selecting a strong promoter was that transcription should not be the limiting factor of kAE1 synthesis. Therefore, it was tested whether robust expression of kAE1 is overwhelming for the cellular machinery of the host and leads to misfolded protein. It was found that the presence of 3% galactose in the selective medium (uracil d/o galactose) indeed produces a substantial amount of protein, which seems to be a burden for the protein processing machinery of *S. cerevisiae* resulting in aggregated protein (Figure 3.12). The reduction of the galactose amount from 3.0% to 1.0% showed less intracellular accumulation of yeGFP-kAE1 in wild-type BY4742. It is to be noted that the low amount of galactose overall decreases the kAE1 expression, but does not increase the plasma membrane localization of the protein. In addition, these results correspond with a previous work reporting that the production of bovine rhodopsin (an integral membrane protein) using a P_{GALI} promoter upon 2% galactose induction causes inactive partial/non-glycosylated protein due to overload on the secretory pathway (Mollaaghababa *et al.*, 1996). Nevertheless, a slight increase in peripheral kAE1 protein was detected in $\Delta end3$ mutant cells, which correspond to the impaired endocytosis processes in these cells (Figure 3.13). Therefore, it is conceivable that one of the reasons for the accumulation of kAE1 in the ER or ER-derived vesicles is due to the extreme rate of mRNA synthesis, which subsequently produces an abundant amount of kAE1 protein. The high amount of newly synthesized kAE1 protein is translocated into the ER and trapped there. However, first attempts for a singly copy integration of the kAE1 gene into the yeast genome to reduce potential cellular burdens were not successful (Xiaobing Li, unpublished data).

The next strategy considered to decrease the intracellular accumulation of kAE1 was a reduction of the culture temperature. During the heterologous protein expression, the sustainability of an expression vector imposes a significant metabolic burden on cells.

Reduction of culture temperature is often applied to decrease this burden. It has been previously reported that low culture temperature helps to improve protein folding by reducing the rate of protein synthesis followed by slowing down the cell growth rate (Vera *et al.*, 2007). To determine the effect of growth temperature on kAE1 synthesis, wild-type BY4742 and $\Delta end3$ cells co-expressing yeGFP-kAE1 and Pma1p-mRPF were cultivated at 20 °C. However, decreasing growth temperature from 30 °C to 20 °C did not reduce the intracellular accumulation of kAE1 in yeast. Fluorescence microscopy results showed that kAE1 was intracellularly accumulated in both wild-type and $\Delta end3$ yeast cells incubated at 20 °C (Figure 3.14). These results suggest that there is no significant influence of reduced culture temperature on kAE1 processing in wild-type BY4742 cells and $\Delta end3$ cells. Since low culture temperature also induces stress that influences major cellular processes including transcription, translation, protein folding rates and membrane composition (Barria *et al.*, 2013), a temperature lower than 20 °C was not considered for incubating cells.

Another way of improving proper protein folding is to alter the functional mechanism of the secretory pathway, in particular, the controlling of unfolded protein response (UPR). UPR is an adaptive cellular pathway that checks the folding state of a newly synthesized protein in the ER-lumen. During the membrane protein processing for subsequent migration in the secretory pathway, it regulates the level of luminal foldase and chaperones as required (Kaufman *et al.*, 2002; Spear & Ng, 2001). In this study, UPR was activated by additional overexpression of Hac1p, one of the main regulators of the UPR, in kAE1 expressing cells to determine whether activation of the UPR could enhance kAE1 processing in the secretory pathway as well as the subsequent targeting to the plasma membrane. The fluorescence microscopy images indicate that there was no significant reduction of intracellular accumulation of yeGFP-kAE1 as well as no noticeable increment of the cell surface localization (Figure 3.15). Previously, it was shown in many studies that manipulation of the stress response has a positive impact on membrane protein synthesis; however, the amplitude of the effect is only protein-specific (Breinig *et al.*, 2006; Griffith *et al.*, 2003; Lee *et al.*, 2012). These results indicate that merely overexpression of Hac1p could not significantly reduce intracellular retention and subsequent plasma membrane targeting of kAE1 in yeast.

In addition, an important element of membrane protein functionality is the adequate post-translational modification such as glycosylation. Improper glycosylation of membrane proteins

causes misfolding or aggregation that ultimately leads to dysfunctional proteins. For instance, glycosylation is critical for plasma membrane localization of nephrin, a transmembrane glycoprotein expressed in glomerular podocytes, and impairment of glycosylation results in a complete ER retention of the protein in HEK293 cells (Yan *et al.*, 2002). However, it has been reported that mammalian plasma membrane proteins typically display less maturation when expressed in yeast compared to their plant or fungi homologs (Groves *et al.*, 1999). Since full-length kAE1 lacks Asn⁶⁴² glycosylation (Figure 3.17), it is conceivable that the overexpression of this variant in *S. cerevisiae* causes folding defects which prevent its efficient trafficking through the secretory pathway. Nevertheless, unglycosylated full-length versions of kAE1 were able to reach the yeast plasma membrane, which is in agreement with mammalian studies reporting that the N-linked glycosylation is not essential for the kAE1 function and plasma membrane localization (Casey *et al.*, 1992; Groves & Tanner, 1994).

Taken together, optimization of the parameters including induction system, temperature and UPR regulation is necessary for maximizing the functional expression of multiple transmembrane proteins in yeast. However, the current undertaken approaches were not efficient enough to achieve an optimal plasma membrane expression of kAE1 protein in *S. cerevisiae*. Additionally, data represented in this study have not adequately addressed the basis of this massive accumulation of kAE1 in yeast. In the future, it would be interesting to examine the effects of overexpression of different proteins such as HSP10, PHB2 and/or ERV29 which are involved in the correct folding, secretion, or trafficking of synthesized proteins in the secretory pathway. In addition, previous yeast studies showed that co-expression of AE1³⁶¹⁻⁹¹¹ with glycophorin A substantially increased plasma membrane located functional protein (Groves *et al.*, 1999). As the electron microscopy images also demonstrate inefficient plasma membrane targeting of ykAE1^{B3^{mem}}, it can be assumed that a distinct interacting partner of kAE1 is absent in yeast, essential for the adequate trafficking of the protein to the plasma membrane. Thereby, it would also be interesting to verify the effect of other known interacting partners of kAE1 such as AP-1 mu1A, TMEM139, ILK (integral linked kinase) or glycophorin A on plasma membrane targeting by co-expressing them in yeast (Groves & Tanner, 1992; Keskanokwong *et al.*, 2007). Further experiments are needed to achieve an ideal condition for the cell surface localization of kAE1 in yeast.

Biological activity of full-length kAE1 in yeast

Once the expression of the full-length kAE1 was verified in yeast, the biological activity of the anion exchanger was determined. Initially, the activity was checked by performing a functional complementation assay of Bor1p and full-length kAE1. Bor1p is a borate transporter in yeast and shares structural homology with AE1/kAE1 (Thurtle-Schmidt & Stroud, 2016). Overexpression of ykAE1^{V5} variant could not compensate and rescue the growth of $\Delta bor1$ cells when challenged with boric acid (Figure 3.18 and 3.19). This result correlates with previous studies reported that the anion exchanger does not mediate borate transport (Jennings, 1976; Jennings & Adame, 1996), and likewise, could not recover cells from borate toxicity. Thus, this study did not support the hypothesis of the functional homology between kAE1 and Bor1p. Notably, both BY4742 and $\Delta bor1$ cells expressing ykAE1^{V5} exhibited an overall reduction of growth rate in the absence of boric acid, indicating that kAE1 expression likely induces cellular stress. It is known that heterologous expression of foreign proteins leads to cell growth defect which is often coupled with ER-stress (Kauffman *et al.*, 2002; Kintaka *et al.*, 2016). Since this finding was not within the scope of this study, no further experiments in that direction were carried out. However, it would be interesting to address kAE1 related growth defects in the future.

Next, the functionality of kAE1 was determined by intracellular pH measurements using the pH-sensitive dye SNARF-5F AM, and the results confirm the biological activity of the protein. Constitutive expression of untagged ykAE1 using a P_{PGK} promoter led to a significant drop in cytosolic pH compared to empty vector expression in wild-type BY4742 cells (Figure 3.21). To show that the decrease in cytosolic pH was mainly caused by kAE1, cytosolic pH of BY4742-GEV cells was further determined in which kAE1 expression was induced in a dose-dependent manner via β -estradiol addition. In BY4742-GEV cells, a clear correlation between kAE1 expression and the decline of cytosolic pH was observed (Figure 3.23). These data are consistent with previous research by Lashhab and colleagues, showing that the expression of wild-type kAE1 in mIMCD3 cells decreases the steady-state cytosolic pH level (Lashhab, *et al.*, 2019). Furthermore, it has been reported that AE1/kAE1 can perform non-bicarbonate transport such as transport of SO_4^{2-} ions instead of HCO_3^- ions in exchange for Cl^- ions (Jennings & Smith, 1992). This non-bicarbonate transport through kAE1 occurs when a proton (H^+) is transported with SO_4^{2-} ions in return for Cl^- ions as an electroneutral exchange. The

absence of HCO_3^- ions in the experimental setup likewise indicates the transportation of H^+ coupled with SO_4^{2-} ions than HCO_3^- ions in exchange with Cl^- ions via the yeast expressed kAE1. Figure 4.1 shows a hypothetical model of possible substrate exchange in a yeast model.

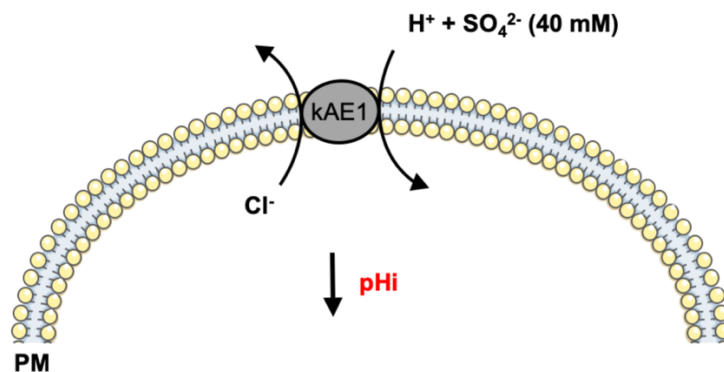


Figure 4.1: Hypothetical model for the observed cytosolic pH drop of *S. cerevisiae* expressing kAE1.

A small pool of kAE1 protein can reach the plasma membrane after being expressed in yeast cells and shows a biological activity of the protein. kAE1 is likely transporting intracellular Cl^- ions in exchange for $\text{H}^+ + \text{SO}_4^{2-}$ ions (alternative of HCO_3^- ions) due to the presence of 40 mM SO_4^{2-} in the growth medium and absence of HCO_3^- ions in the experimental setup. A previous study already mentioned that kAE1 could regulate the influx or efflux of SO_4^{2-} ions coupled with protons in yeast cells. The influx of excess H^+ ions then leads to the cytosolic pH drop in yeast cells. Figure is modified from Sarder *et al.*, 2020.

As illustrated in the aforementioned model, the presence of extracellular excess SO_4^{2-} ions in the culture medium (40 mM) would result in the influx of H^+ coupled with SO_4^{2-} and efflux of Cl^- ions in presence of kAE1. Therefore, this phenomenon led to an increased influx of H^+ inflow into the yeast cytosol that ultimately causes a reduction of cytosolic pH. In agreement with this theory, the gradual increment of kAE1 protein level resulted in a stepwise reduction of cytosolic pH, which was presumably caused by the increasing amount of functional kAE1 at the plasma membrane under higher expression level condition.

The biological activity of kAE1 in yeast was further demonstrated by measuring the Cl^- influx rate and intracellular Cl^- concentration of kAE1 expressing cells. Under hyperosmotic conditions (150 mM NaCl), there were neither SO_4^{2-} ions nor HCO_3^- ions present in the extracellular buffer solution. The results of anion-exchange chromatography showed a

significant difference between the influx rate of Cl^- and intracellular Cl^- concentration in cells expressing kAE1 than the empty vector expressing cells. Yeast cells expressing kAE1 exhibited a significant reduction of Cl^- ions influx rate compared to empty vector expressing cells (Figure 3.24). Nevertheless, it is still puzzling to explain why the kAE1 expression results in the efflux of Cl^- ions. In yeast, passive diffusion of Cl^- ions takes place under hyperosmotic conditions (Jennings & Cui, 2008). Based on the findings of this study, it could be possible that Cl^- ions, transgressing the yeast plasma membrane via passive diffusion, would constantly be exported from the cytosol by the activity of correctly localized and active kAE1. In contrast, cells expressing the empty vector could not conduct such outflow of Cl^- ions in a similar manner. The kAE1-mediated Cl^- efflux was additionally characterized by incubation of kAE1 expressing yeast cells with the supplementation of DIDS, a kAE1-specific inhibitor. As predicted, inactivation of kAE1 with DIDS leads to an impairment of kAE1-mediated Cl^- efflux causing a higher Cl^- influx rate than kAE1 expressing cells. This result indicates kAE1 function is necessary for the excessive efflux of Cl^- ions from the cytosol of yeast cells. However, these observations are opposite to a former study reporting an influx of Cl^- ions in yeast cells expressing truncated AE1³⁶¹⁻⁹¹¹ (Groves *et al.*, 1996). Notably, the results may not be suitable to be directly correlated to the results gained after the expression of a truncated AE1³⁶¹⁻⁹¹¹ version due to the entirely different experimental setups used in both studies. Moreover, a little is known about the Cl^- and cytosolic pH regulation of yeast cells impeding an extensive interpretation of the data obtained in this study. Figure 4.2 shows a hypothetical model of Cl^- efflux as a result of kAE1 expression in yeast cells.

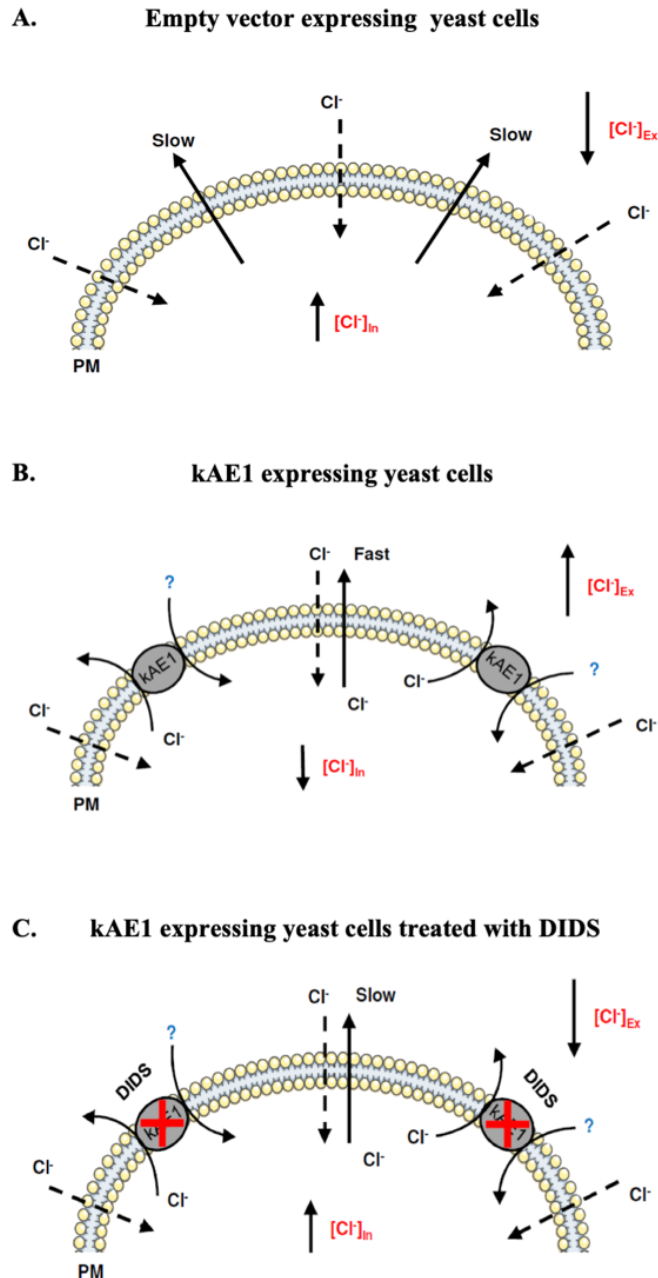


Figure 4.2: Hypothetical model for kAE1-mediated Cl⁻ efflux under hyperosmotic condition.

Under hyperosmotic conditions (150 mM NaCl), Cl⁻ passively diffuses into the cytosol of *S. cerevisiae* (dashed arrow). (A) Empty vector cells have less outflow of cytosolic Cl⁻ (solid arrow), which results in a rise of intracellular Cl⁻ ([Cl⁻]_{in}) and ultimately leading to a drop of extracellular Cl⁻ ([Cl⁻]_{ex}). (B). In case of kAE1 expressing yeast cells, it seems that the excess amount of cytosolic Cl⁻ is ejected by the activity of kAE1 which leads to the decrease of [Cl⁻]_{in}. Notably, it is still not clear which anion is exchanged for Cl⁻ (indicated as a question mark). Since SO₄²⁻ is absent in the extracellular buffer, it is most unlikely that the observed Cl⁻ efflux is achieved in exchange with SO₄²⁻ as previously observed in the pH measurement. (C) DIDS treatment of kAE1 expressing cells, which selectively blocks the activity of kAE1, again displays a rise of [Cl⁻]_{in} leading to a decrease of [Cl⁻]_{ex} comparable to empty vector expressing cells like phenotype. The model is modified from Sarder *et al.*, 2020.

In addition, wild-type BY4742 cells treated with DIDS displayed a little reduction of extracellular Cl^- concentration (data not shown). It might be possible that DIDS unspecifically binds/blocks some of the endogenous Cl^- transporters. In yeast, Gef1p is known as a voltage-gated Cl^- channel located in the Golgi membrane, endosomal compartments and plasma membrane. It plays a crucial role in ion homeostasis in yeast cells (Flis *et al.*, 2002; López-Rodríguez *et al.*, 2007). Additionally, Yh1008cp is another protein reported to be involved in the uptake of Cl^- (Jennings & Cui, 2008). Thus, Δgef1 or $\Delta\text{yh1008c}$ cells could be suitable candidates for a better understanding of the kAE1-mediated Cl^- efflux. Moreover, an increment of the NaCl concentration would be another approach to clarify the kAE1-mediated Cl^- transport. It was previously reported that high salt concentrations (≥ 0.6 M NaCl) have a negative impact on the growth of *S. cerevisiae* (André *et al.*, 1991; Prista *et al.*, 1997). Thus, it would be interesting to examine if the expression of kAE1 could improve/rescue the growth defects of *S. cerevisiae* in high salinity conditions. Indeed, further experiments are required for understanding the appropriate mechanism of kAE1 in yeast.

Expression and localization of kAE1 mutants in yeast

After the successful expression of different wild-typic kAE1 variants, attempts were taken to express kAE1 mutants in *S. cerevisiae* for further understanding of the kAE1 trafficking process. Interestingly, two kAE1 mutants were able to be expressed in *S. cerevisiae* in this study: the $\text{Cl}^-/\text{HCO}_3^-$ exchange impaired mutant kAE1 E681Q and the recessive mutant kAE1 G701D. The mutant proteins were expressed in BY4742-GEV cells upon 10 μM β -estradiol induction. The immunoblot results indicated that both kAE1 E681Q and G701D^{Flag} mutant protein levels are comparable to the wild-type kAE1 protein level (Figure 3.25). Hence, this data suggests that the expression of different kAE1 mutants is now possible in yeast at a high quantity. Furthermore, the indirect immunofluorescence results of the untagged E681Q showed a peripheral localization of the mutant protein (Figure 3.26), which is consistent with similar studies in mammalian cells. It was reported that E681Q mutant was predominantly localized at the plasma membrane of polarized and non-polarized mIMCD3 cells (Lashhab *et al.*, 2019) In contrast, the G701D^{Flag} mutant was retained in the ER in yeast cells that was similar to the results observed in MDCK cells (Cordat *et al.*, 2006). Altogether, localization of both E681Q and G701D in yeast was comparable to the results obtained in mammalian studies. These results suggest as a piece of first body evidence that it is possible to use *S. cerevisiae* for

characterization of kAE1 mutants to find their degradation pathway or interacting partners for the plasma membrane targeting. Thus, this study further highlights the potential of yeast as a model organism. Nevertheless, it was only the initial investigation of kAE1 mutant localization in yeast, and further analysis is needed by high-resolution microscopy or transmission electron microscopy to have a precise understanding of the intracellular localization of the kAE1 mutants.

Characterization of the novel dRTA mutants in mIMCD3 cells

In the second part of this study, three novel dRTA mutants, a recessive kAE1 R295H and two dominant kAE1 Y413H and S525F mutants, were characterized in a mouse inner medullary cell line (mIMCD3). It was mentioned in previous studies that the specific trafficking phenotypes of dRTA mutants could be influenced by the genetic background of the used host cells or organisms; however, it is also important to identify a suitable mammalian model system for analyzing the characteristics of dRTA mutants *in vitro*. Preliminary evidence in mIMCD3 cells supports that the kAE1 R589H mutant behaves similarly to the wild-type protein, which corresponds with the study in kAE1 R607H knock-in mice as well as biopsy data of dRTA patients (Mumtaz *et al.*, 2017; Vichot *et al.*, 2017). This observation highlights that mIMCD3 cells are an excellent mammalian cell model to mimic the *in vivo* dRTA situation. Therefore, the three new mutants were characterized in mIMCD3 cells by generating a stable cell line using the pLVX-TRE3G inducible expression system in which mutant proteins were expressed upon doxycycline induction. On the immunoblot, two distinct bands for wild-type protein and all the three mutants were seen, where the top band refers to protein carrying a complex-oligosaccharide and the bottom band refers to protein carrying a high-mannose oligosaccharide (Figure 3.27). The matured kAE1 protein resided at the plasma membrane naturally carries an N-linked complex-oligosaccharide (Drickamer, 1978). It is known that nascent membrane proteins are initially processed into the ER with the assist of an array of complex quality-control mechanisms for proper folding and subsequently sorting for targeting to the Golgi, trans-Golgi network (TGN) and plasma membrane (Chu *et al.*, 2013). Similarly, newly produced kAE1 protein is translocated into the ER where it co-translationally gains a high-mannose oligosaccharide at the position of Asn⁶⁴² (Li *et al.*, 2000; Quilty *et al.*, 2002). Furthermore, when kAE1 reaches the median Golgi compartment, its high-mannose glycosylation is modified to complex-oligosaccharide and sorted for its final destination from the TGN to the plasma

membrane (Toye *et al.*, 2004). Therefore, the location of kAE1 in the cell can be identified by its type of oligosaccharide processing. A careful observation of the immunoblot results points out that the two dominant kAE1 Y413H and S525F mutants produced a higher amount of high-mannose oligosaccharide protein compared to wild-type kAE1. This high-mannose protein indicates that a large amount of the protein resides in the ER and may have difficulties to move to the Golgi compartment. In contrast, the recessive mutant kAE1 R295H showed a comparable band pattern to wild-type kAE1 protein, suggesting that this mutant could escape from the ER and Golgi, and could be transported to the plasma membrane. In addition, all three mutants showed a significant reduction of half-life compared to the wild-type protein (Figure 3.28) which is due to the premature degradation of mutant proteins in mIMCD3 cells. It was also reported that ER accumulation of the misfolded proteins initiates the endoplasmic reticulum-associated degradation (ERAD) system for protein degradation (Bravo *et al.*, 2013). Therefore, it can be postulated that the mutant variants are recognized as misfolded proteins. In MDCK cells, dominant mutants kAE1 R589H and S613F were retained in the ER by chaperones and destined for the ERAD system (Toye *et al.*, 2004). However, plasma membrane-located misfolded proteins can be recognized by the peripheral quality control machinery, known as endosomal sorting complexes required for transport (ESCRT) system, and prematurely targeted for lysosomal degradation (Apaja *et al.*, 2010). For example, an investigation of the recessive mutant kAE1 G701D in MDCK cells showed that the mutant protein reached the plasma membrane but was prematurely endocytosed before it was targeted for lysosomal degradation using the ESCRT machinery (Chu *et al.*, 2014).

Previously, studies in kAE1 R607H knock-in mice revealed that there was a defect in the autophagy process, which was identified by the accumulations of p62 protein in α -intercalated cells (Mumtaz *et al.*, 2017). p62 is known as a regulator of autophagy and is usually found to be aggregated after defects in the autophagy process (Komatsu *et al.*, 2007). In this study, the overall level of p62 was found to be elevated in mIMCD3 cells expressing dRTA mutants compared to the cells expressing wild-type kAE1 (Figure 3.29). However, among the three dRTA mutants, only the dominant kAE1 Y413H mutant displayed a significant rise of p62 level. In addition, this mutant showed a more intense band of protein carrying high-mannose oligosaccharides compared to the other two dRTA mutants on the immunoblot. This result suggests that during the maturation process in mIMCD3, a large amount of kAE1 Y413H mutant is only connected to high-mannose oligosaccharides and consequently recognized as a

misfolded protein. Therefore, the accumulation of the misfolded mutant proteins in ER likely triggers the ERAD system followed by ubiquitination. The ubiquitinated protein aggregates are then recognized by p62 and destined for autophagy processes (Cohen-Kaplan *et al.*, 2016; Ichimura *et al.*, 2008). Previous studies reported that autophagy is activated when the proteasome can not adequately sequester the polyubiquitinated target protein (Liu *et al.*, 2016). Unfortunately, the data obtained in this study have not sufficiently addressed the reason for the increased level of p62 in mIMCD3 cells. Therefore, the elevated p62 level in mIMCD3 cells could be a result of either a high amount of protein marked for clearance via the autophagy process or an impairment in the proteasomal degradation pathway. Therefore, further experiments are needed for a detailed understanding of the effect on the autophagy process by the dRTA mutants in mIMCD3 cells. One possibility would be monitoring the degradation of p62 or analyzing the level of LC3-II (an autophagosome marker) in dRTA mutant expressing cells.

In addition, the effect of dRTA-causing mutants on the viability of mIMCD3 cells was investigated by a colorimetric assay (MTS assay). The basis of this analysis was that the number of α -intercalated cells found severely depleted in dRTA patients as well as in dominant dRTA knock-in mice (Mumtaz *et al.*, 2017; Vichot *et al.*, 2017). The dRTA mutants were expressed until 72 h to check their effect on cell viability. Expression of kAE1 R295H, Y413H and S525F mutants in mIMCD3 cells showed no adverse effect on mIMCD3 cell proliferation under normal or hyperosmotic conditions (Figure 3.30). This result suggests that these dRTA mutants are not toxic to mIMCD3 cells under the experimental conditions. It is conceivable that the cellular environment is different between mIMCD3 and α -intercalated cells. It was reported that wild-type kAE1 expression leads to the acidification of cytosolic pH in mIMCD3 cells due to the transport of bicarbonate into the growth medium (Lashhab *et al.*, 2019). Moreover, the *in vivo* study of kAE1 R607H knock-in mice proposed that the depletion of α -intercalated cells is based on the dysfunction of V-H⁺-ATPase coupled with defective autophagy processes (Mumtaz *et al.*, 2017). V-H⁺-ATPase was mistargeted in α -intercalated cells under dRTA condition, which likely results in impaired cellular pH homeostasis. Unfortunately, this is not possible in mIMCD3 cells due to the lack of expression of V-H⁺-ATPase (Madsen *et al.*, 1988). Therefore, it can be postulated that the expression of the kAE1 mutant may not alkalinize the cytosolic pH in mIMCD3 as observed *in vivo* dRTA conditions. Another possible reason might be the reduced osmotic pressure of *in vitro* culture condition of mIMCD3 cells. In distal

nephrons, α -intercalated cells are exposed to a hyperosmotic condition (up to 1200 mOsmol/kg H₂O) *in vivo* under normal physiological state (Gottschalk, 1960). The hyperosmotic medium used in this study (~500 mOsmol/kg H₂O) does not appear to be adequate to cause osmotic stress on mIMCD3 cells as the cells can adapt to osmotic pressure even higher (up to 910 mOsmol/kg H₂O). Therefore, a higher osmolarity of the culture medium would be interesting to analyze the effect of the mutant on mIMCD3 cells.

5. Outlook

The primary objective of this project was to establish *S. cerevisiae* as a cellular model system for a comprehensive analysis of kAE1 physiology and identifying the specific features of its disease-causing mutants. So far, the data presented in this study show the first insight of full-length kAE1 expression, localization, and functionality in yeast. However, only a minor amount of expressed protein was able to reach the yeast cell surface, which could hinder the understanding kAE1 activity and its trafficking mechanism(s) in yeast. To achieve a larger quantity of kAE1 at the cell surface, it is essential to identify the crucial interacting partners involved in the cell surface targeting of the anion exchanger in yeast. For this purpose, a single-gene overexpression screening, especially for the genes involved in protein transport, would permit for more understanding of the responsible genes in kAE1 trafficking. Moreover, a massive accumulation of the anion transporter was observed in intracellular membrane-like structures. The origin of the kAE1-aggregates would be possible to detect by using specific marker proteins for different intracellular organelles. A further knock-out screen of proteins responsible for the misfolded protein degradation in those particular compartments would be useful for attaining a more in-depth insight into kAE1 transport to the cell periphery. In addition, the data generated from those studies could then be translated to the situation of human cells for finding homologous genes. This would help to understand the premature degradation of the dRTA-causing mutants. However, baker's yeast also possesses few limitations likewise any other system for studying kAE1. Since it is a single cell organism and is not polarized, the cell-to-cell interaction study typically occurring in a complex organ like the kidney is not possible. Therefore, it might exclude the possibility to study more complex dRTA-causing conditions. Furthermore, investigation of the three novel dRTA mutants (kAE1 R295H, Y413H, and S525F) in mIMCD3 cells provided new information about the premature degradation of those mutants. Nevertheless, expression of the mutants did not affect the viability of mIMCD3 cells as it has been observed in the *in vivo* dRTA condition. In dRTA patients as well as in a dRTA knock-in mouse model, the trafficking defects of the V-H⁺-ATPase were found that likely result in cytotoxicity due to cellular acid-base imbalance. Since the *in vivo* dRTA condition is very complicated, the generation of a stable cell line of α -intercalated cells or three-dimensional cell culture of mIMCD3 cells mimicking the *in vivo* situation more closely would be interesting and could provide a better understanding of the molecular mechanism of dRTA in future.

6. Summary

Under physiological conditions, kAE1 plays a significant role in renal acid-base regulation. Mutations in the kAE1 encoding gene lead to a disease called dRTA. Until now, the underlying mechanism for disease progression is unknown. The detailed knowledge of kAE1 biogenesis, structural-functionality, and its interplay with other proteins is one of the fundamental ways to elucidate the complex process of dRTA progression. In this context, the present study highlighted the potential of *S. cerevisiae* as a “prototype” for investigating physiological aspects of kAE1 in a fast and affordable manner. To achieve that goal, several kAE1 variants were constructed. The data of this study confirm that different untagged and tagged full-length kAE1 variants can be expressed in yeast. Moreover, only the yeast codon-optimized kAE1 constructs were found to be expressed at a high level in *S. cerevisiae*. The subcellular localization of the protein was then determined by fluorescence-based and confocal microscopy. Tagging at the C-terminus of yeast codon-optimized kAE1 constructs inhibited the cell surface targeting of the anion exchanger in yeast. Additionally, the untagged full-length kAE1 variant was found at the plasma membrane of yeast—for the first time—though to a minor extent. The third exofacial loop HA tag did not alter plasma membrane targeting of kAE1 in yeast and was found at a comparable level on the cell surface to the untagged kAE1 variant. Notably, the results of cytosolic pH measurement and anion exchange chromatography represent a piece of primary evidence for the biological activity of kAE1 in yeast, although the complex molecular mechanistic of its activity remain unclear. Furthermore, three new dRTA mutants (kAE1 R295H, Y413H and S525F) were analyzed in mIMCD3 cells, and it was found that the mutants are degraded at a faster rate than the wild-type protein. However, expression of these mutants did not have any influence on the proliferation rate of mIMCD3 cells.

Overall, this work provided a first stepping stone to analyze the full-length functional kAE1 rapidly and inexpensively by utilizing yeast. Thus, the study facilitates a quick screening of the complete kAE1 sequence for mutants affecting transport activity. This will open the opportunity to map the global interactions of kAE1 with other proteins, which will further assist in identifying the crucial interacting partners and enlightening the complex dRTA mechanism in the future. Moreover, the investigations in mIMCD3 cells enable resolving the phenotype of dRTA mutants in an *in vivo* dRTA situation.

7. References

- Abbas, Y. M., Toye, A. M., Rubinstein, J. L., & Reithmeier, R. A. F. (2018). Band 3 function and dysfunction in a structural context. *Current Opinion in Hematology*, 25(3), 163–170. <https://doi.org/10.1097/MOH.0000000000000418>
- Alka, K., & Casey, J. R. (2014). Bicarbonate transport in health and disease. *IUBMB Life*, 66(9), 596–615. <https://doi.org/10.1002/iub.1315>
- Almomani, E., Kaur, S., Alexander, R., & Cordat, E. (2014). Intercalated Cells: More than pH Regulation. *Diseases*, 2(2), 71–92. <https://doi.org/10.3390/diseases2020071>
- Almomani, E. Y., Chu, C. Y. S., & Cordat, E. (2011). Mis-trafficking of bicarbonate transporters: Implications to human diseases. *Biochemistry and Cell Biology*, 89(2), 157–177. <https://doi.org/10.1139/O10-153>
- Almomani, E. Y., King, J. C., Netsawang, J., Yenchitsomanus, P., Malasit, P., Limjindaporn, T., Alexander, R. T., & Cordat, E. (2012). Adaptor protein 1 complexes regulate intracellular trafficking of the kidney anion exchanger 1 in epithelial cells. *American Journal of Physiology-Cell Physiology*, 303(5), C554–C566. <https://doi.org/10.1152/ajpcell.00124.2012>
- Alper, S. L., Natale, J., Gluck, S., Lodish, H. F., & Brown, D. (1989). Subtypes of intercalated cells in rat kidney collecting duct defined by antibodies against erythroid band 3 and renal vacuolar H⁺-ATPase. *Proceedings of the National Academy of Sciences*, 86(14), 5429–5433. <https://doi.org/10.1073/pnas.86.14.5429>
- Alper, S. L. (2002). Genetic diseases of acid-base transporters. *Annual Review of Physiology*, 64, 899–923. <https://doi.org/10.1146/annurev.physiol.64.092801.141759>
- Alper, S. L. (2006). Molecular physiology of SLC4 anion exchangers. *Experimental Physiology*, 91(1), 153–161. <https://doi.org/10.1113/expphysiol.2005.031765>
- Alper, S. L., Darman, R. B., Chernova, M. N., & Dahl, N. K. (2002). The AE gene family of Cl⁻/HCO₃⁻ exchangers. *Journal of Nephrology*, 15(Suppl 5), S41–S53.
- Alper, S. L., & Sharma, A. K. (2013). The SLC26 gene family of anion transporters and channels. *Molecular Aspects of Medicine*, 34(2–3), 494–515. <https://doi.org/10.1016/j.mam.2012.07.009>
- André, L., Hemming, A., & Adler, L. (1991). Osmoregulation in *Saccharomyces cerevisiae* Studies on the osmotic induction of glycerol production and glycerol 3-phosphate dehydrogenase (NAD⁺). *FEBS Letters*, 286(1–2), 13–17. [https://doi.org/10.1016/0014-5793\(91\)80930-2](https://doi.org/10.1016/0014-5793(91)80930-2)

- Apaja, P. M., Xu, H., & Lukacs, G. L. (2010). Quality control for unfolded proteins at the plasma membrane. *Journal of Cell Biology*, *191*(3), 553–570. <https://doi.org/10.1083/jcb.201006012>
- Arakawa, T., Kobayashi-Yurugi, T., Alguel, Y., Iwanari, H., Hatae, H., Iwata, M., Abe, Y., Hino, T., Ikeda-Suno, C., Kuma, H., Kang, D., Murata, T., Hamakubo, T., Cameron, A. D., Kobayashi, T., Hamasaki, N., & Iwata, S. (2015). Crystal structure of the anion exchanger domain of human erythrocyte band 3. *Science*, *350*(6261), 680–684. <https://doi.org/10.1126/science.aaa4335>
- Bai, J., Swartz, D. J., Protasevich, I. I., Brouillette, C. G., Harrell, P. M., Hildebrandt, E., Gasser, B., Mattanovich, D., Ward, A., Chang, G., & Urbatsch, I. L. (2011). A gene optimization strategy that enhances production of fully functional P-Glycoprotein in *Pichia pastoris*. *PLoS ONE*, *6*(8). <https://doi.org/10.1371/journal.pone.0022577>
- Baldwin, R. L. (1986). Temperature dependence of the hydrophobic interaction in protein folding. *Proceedings of the National Academy of Sciences of the United States of America*, *83*(21), 8069–8072. <https://doi.org/10.1073/pnas.83.21.8069>
- Barria, C., Malecki, M., & Arraiano, C. M. (2013). Bacterial adaptation to cold. *Microbiology*, *159*(12), 2437–2443. <https://doi.org/10.1099/mic.0.052209-0>
- Battle, D., Ghanekar, H., Jain, S., & Mitra, A. (2001). Hereditary Distal Renal Tubular Acidosis: New Understandings. *Annual Review of Medicine*, *52*(1), 471–484. <https://doi.org/10.1146/annurev.med.52.1.471>
- Battle, D., & Haque, S. K. (2012). Genetic causes and mechanisms of distal renal tubular acidosis. *Nephrology Dialysis Transplantation*, *27*(10), 3691–3704. <https://doi.org/10.1093/ndt/gfs442>
- Beane, W. S., Adams, D. S., Morokuma, J., & Levin, M. (2019). Live imaging of intracellular pH in planarians using the ratiometric fluorescent dye SNARF-5F-AM. *Biology Methods and Protocols*, *4*(1), 1–7. <https://doi.org/10.1093/biomethods/bpz005>
- Becker, B., Blum, A., Gießelmann, E., Dausend, J., Rammo, D., Müller, N. C., Tschacksch, E., Steimer, M., Spindler, J., Becherer, U., Rettig, J., Breinig, F., & Schmitt, M. J. (2016). H/KDEL receptors mediate host cell intoxication by a viral A/B toxin in yeast. *Scientific Reports*, *6*, 31105. <https://doi.org/10.1038/srep31105>
- Beckmann, R., Toyne, A. M., Smythe, J. S., Anstee, D. J., & Tanner, M. J. A. (2002). An N-terminal GFP tag does not alter the functional expression to the plasma membrane of red cell and kidney anion exchanger (AE1) in mammalian cells. *Molecular Membrane Biology*, *19*(3), 187–200. <https://doi.org/10.1080/09687680210141043>
- Benner, A., Patel, A. K., Singh, K., & Dua, A. (2018). *Physiology, Bohr Effect*. StatPearls.

- Bimboim, H. C., & Doly, J. (1979). A rapid alkaline extraction procedure for screening recombinant plasmid DNA. *Nucleic Acids Research*, 7(6), 1513–1523. <https://doi.org/10.1093/nar/7.6.1513>
- Bonar, P., & Casey, J. R. (2010). Purification of functional human Cl⁻/HCO₃⁻ exchanger, AE1, over-expressed in *Saccharomyces cerevisiae*. *Protein Expression and Purification*, 74(1), 106–115. <https://doi.org/10.1016/j.pep.2010.06.020>
- Bravo, R., Parra, V., Gatica, D., Rodriguez, A. E., Torrealba, N., Paredes, F., Wang, Z. V., Zorzano, A., Hill, J. A., Jaimovich, E., Quest, A. F. G., & Lavandero, S. (2013). Endoplasmic Reticulum and the Unfolded Protein Response. *International Review of Cell and Molecular Biology*, 301, 215–290. <https://doi.org/10.1016/B978-0-12-407704-1.00005-1>
- Breinig, F., Diehl, B., Rau, S., Zimmer, C., Schwab, H., & Schmitt, M. J. (2006). Cell surface expression of bacterial esterase A by *Saccharomyces cerevisiae* and its enhancement by constitutive activation of the cellular unfolded protein response. *Applied and Environmental Microbiology*, 72(11), 7140–7147. <https://doi.org/10.1128/AEM.00503-06>
- Bruce, L. J., Wrong, O., Toye, A. M., Young, M. T., Ogle, G., Ismail, Z., Sinha, A. K., McMaster, P., Hwaihwanje, I., Nash, G. B., Hart, S., Lavu, E., Palmer, R., Othman, A., Unwin, R. J., & Tanner, M. J. A. (2000). Band 3 mutations, renal tubular acidosis and South-East Asian ovalocytosis in Malaysia and Papua New Guinea: Loss of up to 95% band 3 transport in red cells. *Biochemical Journal*, 350(1), 41–51. <https://doi.org/10.1042/0264-6021:3500041>
- Bruce, L. J., Cope, D. L., Jones, G. K., Schofield, A. E., Burley, M., Povey, S., Unwin, R. J., Wrong, O., & Tanner, M. J. (1997). Familial distal renal tubular acidosis is associated with mutations in the red cell anion exchanger (Band 3, AE1) gene. *Journal of Clinical Investigation*, 100(7), 1693–1707. <https://doi.org/10.1172/JCI119694>
- Bruce, L. J., Pan, R. J., Cope, D. L., Uchikawa, M., Gunn, R. B., Cherry, R. J., & Tanner, M. J. A. (2004). Altered Structure and Anion Transport Properties of Band 3 (AE1, SLC4A1) in Human Red Cells Lacking Glycophorin A. *Journal of Biological Chemistry*, 279(4), 2414–2420. <https://doi.org/10.1074/jbc.M309826200>
- Buck, T. M., Kolb, A. R., Boyd, C. R., Kleyman, T. R., & Brodsky, J. L. (2010). The endoplasmic reticulum-associated degradation of the epithelial sodium channel requires a unique complement of molecular chaperones. *Molecular Biology of the Cell*, 21(6), 1047–1058. <https://doi.org/10.1091/mbc.E09-11-0944>
- Buckalew, V. M. (1989). Nephrolithiasis in Renal Tubular Acidosis. *Journal of Urology*, 141(3 Pt 2), 731–737. [https://doi.org/10.1016/S0022-5347\(17\)40997-9](https://doi.org/10.1016/S0022-5347(17)40997-9)
- Casey, J. R., Pirraglia, C. A., & Reithmeier, R. A. F. (1992). Enzymatic deglycosylation of

- human band 3, the anion transport protein of the erythrocyte membrane. Effect on protein structure and transport properties. *Journal of Biological Chemistry*, 267(17), 11940–11948.
- Chalfant, M., Barber, K. W., Borah, S., Thaller, D., & Lusk, C. P. (2019). Expression of TorsinA in a heterologous yeast system reveals interactions with luminal domains of LINC and nuclear pore complex components. *Molecular Biology of the Cell*, 30(5), 530–541. <https://doi.org/10.1091/mbc.E18-09-0585>
- Chernova, M. N., Stewart, A. K., Barry, P. N., Jennings, M. L., & Alper, S. L. (2008). Mouse AE1 E699Q mediates SO_4^{2-} / anion_o exchange with $[\text{SO}_4^{2-}]_i$ -dependent reversal of wild-type pH_o sensitivity. *American Journal of Physiology. Cell Physiology*, 295(2), 302–312. <https://doi.org/10.1152/ajpcell.00109.2008>
- Chu, C., Woods, N., Sawasdee, N., Guizouarn, H., Pellissier, B., Borgese, F., Yenchitsomanus, P., Gowrishankar, M., & Cordat, E. (2010). Band 3 Edmonton I, a novel mutant of the anion exchanger 1 causing spherocytosis and distal renal tubular acidosis. *Biochemical Journal*, 426(3), 379–388. <https://doi.org/10.1042/BJ20091525>
- Chu, C. Y., King, J., Berrini, M., Rumley, A. C., Apaja, P. M., Lukacs, G. L., Alexander, R. T., & Cordat, E. (2014a). Degradation mechanism of a Golgi-retained distal renal tubular acidosis mutant of the kidney anion exchanger 1 in renal cells. *American Journal of Physiology. Cell Physiology*, 307(3), 296–307. <https://doi.org/10.1152/ajpcell.00310.2013>
- Chu, C. Y., King, J., Berrini, M., Rumley, A. C., Apaja, P. M., Lukacs, G. L., Alexander, R. T., & Cordat, E. (2014b). Degradation mechanism of a Golgi-retained distal renal tubular acidosis mutant of the kidney anion exchanger 1 in renal cells. *American Journal of Physiology. Cell Physiology*, 307(3), C296–C307. <https://doi.org/10.1152/ajpcell.00310.2013>
- Chu, C. Y. S., King, J. C., Berrini, M., Alexander, R. T., & Cordat, E. (2013). Functional Rescue of a Kidney Anion Exchanger 1 Trafficking Mutant in Renal Epithelial Cells. *PLoS ONE*, 8(2), e57062. <https://doi.org/10.1371/journal.pone.0057062>
- Chu, D., & Von Der Haar, T. (2012). The architecture of eukaryotic translation. *Nucleic Acids Research*, 40(20), 10098–10106. <https://doi.org/10.1093/nar/gks825>
- Cohen-Kaplan, V., Livneh, I., Avni, N., Fabre, B., Ziv, T., Kwon, Y. T., & Ciechanover, A. (2016). p62- and ubiquitin-dependent stress-induced autophagy of the mammalian 26S proteasome. *Proceedings of the National Academy of Sciences of the United States of America*, 113(47), E7490–E7499. <https://doi.org/10.1073/pnas.1615455113>
- Cordat, E., & Casey, J. R. (2009). Bicarbonate transport in cell physiology and disease. *Biochemical Journal*, 417(2), 423–439. <https://doi.org/10.1042/BJ20081634>
- Cordat, E., Kittanakom, S., Yenchitsomanus, P., Li, J., Du, K., Lukacs, G. L., & Reithmeier, R.

- A. F. (2006). Dominant and recessive distal renal tubular acidosis mutations of kidney anion exchanger induce distinct trafficking defects in MDCK cells. *Traffic*, 7(2), 117–128. <https://doi.org/10.1111/j.1600-0854.2005.00366.x>
- Cordat, E., Li, J., & Reithmeier, R. A. F. (2003). Carboxyl-terminal truncations of human anion exchanger impair its trafficking to the plasma membrane. *Traffic*, 4(9), 642–651. <https://doi.org/10.1034/j.1600-0854.2003.00123.x>
- Cordat, E., & Reithmeier, R. A. F. (2014). Structure, function, and trafficking of SLC4 and SLC26 anion transporters. In *Current Topics in Membranes*, 73, 1–67. <https://doi.org/10.1016/B978-0-12-800223-0.00001-3>
- Cory, A. H., Owen, T. C., Barltrop, J. A., & Cory, J. G. (1991). Use of an aqueous soluble tetrazolium/formazan assay for cell growth assays in culture. *Cancer Communications*, 3(7), 207–212. <https://doi.org/10.3727/095535491820873191>
- Day, J. G., & McLellan, M. R. (1995). Cryopreservation and Freeze-Drying Protocols. *Methods in Molecular Biology (Clifton, N.J.)*, 38, 1–5. <https://doi.org/10.1385/0896032965>
- Devonald, M. A. J., Smith, A. N., Poon, J. P., Ihrke, G., & Karet, F. E. (2003). Non-polarized targeting of AE1 causes autosomal dominant distal renal tubular acidosis. *Nature Genetics*, 33(2), 125–127. <https://doi.org/10.1038/ng1082>
- Diakov, T. T., Tarsio, M., & Kane, P. M. (2013). Measurement of vacuolar and cytosolic pH *in vivo* in yeast cell suspensions. *Journal of Visualized Experiments*, 74, 1–7. <https://doi.org/10.3791/50261>
- Ding, Y., Caseyri, J. R., & Kopiton, R. R. (1994). The major kidney AE1 isoform does not bind ankyrin (Ank1) *in vitro*. An essential role for the 79 NH₂-terminal amino acid residues of band 3. *The Journal of biological chemistry*, 269(51), 32201–32208.
- Drenckhahn, D., Schlüter, K., Allen, D. P., & Bennett, V. (1985). Colocalization of band 3 with ankyrin and spectrin at the basal membrane of intercalated cells in the rat kidney. *Science*, 230(4731), 1287–1289. <https://doi.org/10.1126/science.2933809>
- Drickamer, L. K. (1978). Orientation of the band 3 polypeptide from human erythrocyte membranes. Identification of NH₂-terminal sequence and site of carbohydrate attachment. *Journal of Biological Chemistry*, 253(20), 7242–7248.
- Dubyak, G. R. (2004). Ion homeostasis, channels, and transporters: An update on cellular mechanisms. *Advances in Physiology Education*, 28(4), 143–154. <https://doi.org/10.1152/advan.00046.2004>
- Elegheert, J., Behiels, E., Bishop, B., Scott, S., Woolley, R. E., Griffiths, S. C., Byrne, E. F. X., Chang, V. T., Stuart, D. I., Jones, E. Y., Siebold, C., & Aricescu, A. R. (2018). Lentiviral

transduction of mammalian cells for fast, scalable and high-level production of soluble and membrane proteins. *Nature Protocols*, 13(12), 2991–3017. <https://doi.org/10.1038/s41596-018-0075-9>

Fairbanks, G., Steck, T. L., & Wallach, D. F. H. (1971). Electrophoretic analysis of the major polypeptides of the human erythrocyte membrane. *Biochemistry*, 10(13), 2606–2617. <https://doi.org/10.1021/bi00789a030>

Ferreira, T., Mason, A. B., & Slayman, C. W. (2001). The Yeast Pma1 Proton Pump: A Model for Understanding the Biogenesis of Plasma Membrane Proteins. *Journal of Biological Chemistry*, 276(32), 29613–29616. <https://doi.org/10.1074/jbc.R100022200>

Feyder, S., De Craene, J. O., Bär, S., Bertazzi, D. L., & Friant, S. (2015). Membrane trafficking in the yeast *Saccharomyces cerevisiae* model. *International Journal of Molecular Sciences*, 16(1), 1509–1525. <https://doi.org/10.3390/ijms16011509>

Finberg, K. E., Wagner, C. A., Bailey, M. A., Paunescu, T. G., Breton, S., Brown, D., Giebisch, G., Geibel, J. P., & Lifton, R. P. (2005). The B1-subunit of the H⁺ ATPase is required for maximal urinary acidification. *Proceedings of the National Academy of Sciences*, 102(38), 13616–13621. <https://doi.org/10.1073/pnas.0506769102>

Flis, K., Bednarczyk, P., Hordejuk, R., Szewczyk, A., Berest, V., Dolowy, K., Edelman, A., & Kurlandzka, A. (2002). The Gef1 protein of *Saccharomyces cerevisiae* is associated with chloride channel activity. *Biochemical and Biophysical Research Communications*, 294(5), 1140–1150. [https://doi.org/10.1016/S0006-291X\(02\)00610-1](https://doi.org/10.1016/S0006-291X(02)00610-1)

Fry, A. C., Su, Y., Yiu, V., Cuthbert, A. W., Trachtman, H., & Karet Frankl, F. E. (2012). Mutation conferring apical-targeting motif on AE1 exchanger causes autosomal dominant distal RTA. *Journal of the American Society of Nephrology*, 23(7), 1238–1249. <https://doi.org/10.1681/ASN.2012020112>

Gao, X., Eladari, D., Leviel, F., Tew, B. Y., Miro-Julia, C., Cheema, F. H., Miller, L., Nelson, R., Paunescu, T. G., McKee, M., Brown, D., & Al-Awqati, Q. (2010). Deletion of hensen/DMBT1 blocks conversion of β - to α - intercalated cells and induces distal renal tubular acidosis. *Proceedings of the National Academy of Sciences*, 107(50), 21872–21877. <https://doi.org/10.1073/pnas.1010364107>

Gautier, A., & Hinner, M. J. (2015). *Site-Specific Protein Labeling: Methods and Protocols*, Humana Press. <https://doi.org/10.1007/978-1-4939-2272-7>

Geertsma, E. R., Groeneveld, M., Slotboom, D. J., & Poolman, B. (2008). Quality control of overexpressed membrane proteins. *Proceedings of the National Academy of Sciences of the United States of America*, 105(15), 5722–5727. <https://doi.org/10.1073/pnas.0802190105>

Gekle, M., Wunsch, S., Oberleithner, H., & Silbernagl, S. (1994). Characterization of two

MDCK-cell subtypes as a model system to study principal cell and intercalated cell properties. *Pflügers Archiv: European Journal of Physiology*, 428(2), 157–162. <https://doi.org/10.1007/BF00374853>

Gibson, D. G., Benders, G. A., Axelrod, K. C., Zaveri, J., Algire, M. A., Moodie, M., Montague, M. G., Venter, J. C., Smith, H. O., & Hutchison, C. A. (2008). One-step assembly in yeast of 25 overlapping DNA fragments to form a complete synthetic *Mycoplasma genitalium* genome. *Proceedings of the National Academy of Sciences of the United States of America*, 105(51), 20404–20409. <https://doi.org/10.1073/pnas.0811011106>

Gietz, R. D., Schiestl, R. H., Willems, A. R., & Woods, R. A. (1995). Studies on the transformation of intact yeast cells by the LiAc/SS-DNA/PEG procedure. *Yeast*, 11(4), 355–360. <https://doi.org/10.1002/yea.320110408>

Goffeau, A., Barrell, B. G., Bussey, H., Davis, R. W., Dujon, B., Feldmann, H., Galibert, F., Hoheisel, J. D., Jacq, C., Johnston, M., Louis, E. J., Mewes, H. W., Murakami, Y., Philippsen, P., Tettelin, H., & Oliver, S. G. (1996). Life with 6000 Genes. *Science*, 274(5287), 546–567. <https://doi.org/10.1126/science.274.5287.546>

Gottschalk, C. W. (1960). Osmotic concentration and dilution in the mammalian nephron. *Circulation*, 21, 861–868. <https://doi.org/10.1161/01.CIR.21.5.861>

Griffith, D. A., Delipala, C., Leadsham, J., Jarvis, S. M., & Oesterhelt, D. (2003). A novel yeast expression system for the overproduction of quality-controlled membrane proteins. *FEBS Letters*, 553(1–2), 45–50. [https://doi.org/10.1016/S0014-5793\(03\)00952-9](https://doi.org/10.1016/S0014-5793(03)00952-9)

Groves, J. D., & Tanner, M. J. A. (1992). Glycophorin A facilitates the expression of human band 3-mediated anion transport in *Xenopus* oocytes. *Journal of Biological Chemistry*, 267(31), 22163–22170.

Groves, J. D., Falson, P., Le Maire, M., & Tanner, M. J. A. (1996). Functional cell surface expression of the anion transport domain of human red cell band 3 (AE1) in the yeast *Saccharomyces cerevisiae*. *Proceedings of the National Academy of Sciences of the United States of America*, 93(22), 12245–12250. <https://doi.org/10.1073/pnas.93.22.12245>

Groves, J. D., Parker, M. D., Askin, D., Falson, P., Le Maire, M., & Tanner, M. J. A. (1999). Heterologous expression of the red-cell anion exchanger (band 3; AE1). *Biochemical Society Transactions*, 27(6), 917–923. <https://doi.org/10.1042/bst0270917>

Groves, J. D., & Tanner, M. J. A. (1994). Role of n-glycosylation in the expression of human band 3-mediated anion transport. *Molecular Membrane Biology*, 11(1), 31–38. <https://doi.org/10.3109/09687689409161027>

Han, J., & Burgess, K. (2010). Fluorescent indicators for intracellular pH. *Chemical Reviews*, 110(5), 2709–2728. <https://doi.org/10.1021/cr900249z>

- Hassoun, H., Hanada, T., Lutchman, M., Sahr, K. E., Palek, J., Hanspal, M., & Chishti, A. H. (1998). Complete deficiency of glycophorin A in red blood cells from mice with targeted inactivation of the band 3 (AE1) gene. *Blood*, *91*(6), 2146–2151. <http://www.ncbi.nlm.nih.gov/pubmed/9490702>
- Henne, W. M., Buchkovich, N. J., & Emr, S. D. (2011). The ESCRT Pathway. *Developmental Cell*, *21*(1), 77–91. <https://doi.org/10.1016/j.devcel.2011.05.015>
- Hennings, J. C., Picard, N., Huebner, A. K., Stauber, T., Maier, H., Brown, D., Jentsch, T. J., Vargas-Poussou, R., Eladari, D., & Hübner, C. A. (2012). A mouse model for distal renal tubular acidosis reveals a previously unrecognized role of the V-ATPase a4 subunit in the proximal tubule. *EMBO Molecular Medicine*, *4*(10), 1057–1071. <https://doi.org/10.1002/emmm.201201527>
- Hutchison, C. A., Phillips, S., Edgell, M. H., Gillam, S., Jahnke, P., & Smith, M. (1978). Mutagenesis at a specific position in a DNA sequence. *Journal of Biological Chemistry*, *253*(18), 6551–6560.
- Ichimura, Y., Kumanomidou, T., Sou, Y. S., Mizushima, T., Ezaki, J., Ueno, T., Kominami, E., Yamane, T., Tanaka, K., & Komatsu, M. (2008). Structural basis for sorting mechanism of p62 in selective autophagy. *Journal of Biological Chemistry*, *283*(33), 22847–22857. <https://doi.org/10.1074/jbc.M802182200>
- Ito, H., Fukuda, Y., Murata, K., & Kimura, A. (1983). Transformation of intact yeast cells treated with alkali cations. *Journal of Bacteriology*, *153*(1), 163–168. <https://doi.org/10.1128/jb.153.1.163-168.1983>
- Jalimarada, S. S., Ogando, D. G., Vithana, E. N., & Bonanno, J. A. (2013). Ion Transport Function of SLC4A11 in Corneal Endothelium. *Investigative Ophthalmology & Visual Science*, *54*(6), 4330–4340. <https://doi.org/10.1167/iovs.13-11929>
- Jarolim, P., Shayakul, C., Prabakaran, D., Jiang, L., Stuart-Tilley, A., Rubin, H. L., Simova, S., Zavadil, J., Herrin, J. T., Brouillette, J., Somers, M. J. G., Seemanova, E., Brugnara, C., Guay-Woodford, L. M., & Alper, S. L. (1998). Autosomal dominant distal renal tubular acidosis is associated in three families with heterozygosity for the R589H mutation in the AE1 (Band 3) Cl⁻/HCO₃⁻ exchanger. *Journal of Biological Chemistry*, *273*(11), 6380–6388. <https://doi.org/10.1074/jbc.273.11.6380>
- Jennings, M. L., & Smith, J. S. (1992). Anion-proton cotransport through the human red blood cell band 3 protein. Role of glutamate 681. *Journal of Biological Chemistry*, *267*(20), 13964–13971.
- Jennings, M. L. (1976). Proton fluxes associated with erythrocyte membrane anion exchange. *The Journal of Membrane Biology*, *28*(1), 187–205. <https://doi.org/10.1007/BF01869697>
- Jennings, M. L. (2005). Evidence for a second binding/transport site for chloride in erythrocyte

- anion transporter AE1 modified at glutamate 681. *Biophysical Journal*, 88(4), 2681–2691. <https://doi.org/10.1529/biophysj.104.056812>
- Jennings, M. L., & Adame, M. F. (1996). Characterization of oxalate transport by the human erythrocyte band 3 protein. *Journal of General Physiology*, 107(1), 145–159. <https://doi.org/10.1085/jgp.107.1.145>
- Jennings, M. L., & Cui, J. (2008). Chloride homeostasis in *Saccharomyces cerevisiae*: High affinity influx, V-ATPase-dependent sequestration, and identification of a candidate Cl⁻ sensor. *Journal of General Physiology*, 131(4), 379–391. <https://doi.org/10.1085/jgp.200709905>
- Jennings, M. L., Howren, T. R., Cui, J., Winters, M., & Hannigan, R. (2007). Transport and regulatory characteristics of the yeast bicarbonate transporter homolog Bor1p. *American Journal of Physiology. Cell Physiology*, 293(1), C468–C476. <https://doi.org/10.1152/ajpcell.00286.2005>
- Jinks-Robertson, S., Michelitch, M., & Ramcharan, S. (1993). Substrate length requirements for efficient mitotic recombination in *Saccharomyces cerevisiae*. *Molecular and Cellular Biology*, 13(7), 3937–3950. <https://doi.org/10.1128/mcb.13.7.3937>
- Junge, F., Schneider, B., Reckel, S., Schwarz, D., Dötsch, V., & Bernhard, F. (2008). Large-scale production of functional membrane proteins. *Cellular and Molecular Life Sciences*, 65(11), 1729–1755. <https://doi.org/10.1007/s00018-008-8067-5>
- Junking, M., Sawasdee, N., Duangtum, N., Cheunsuchon, B., Limjindaporn, T., & Yenichitsomanus, P. (2014). Role of Adaptor Proteins and Clathrin in the Trafficking of Human Kidney Anion Exchanger 1 (kAE1) to the Cell Surface. *Traffic*, 15(7), 788–802. <https://doi.org/10.1111/tra.12172>
- Kang, Y. S., Kane, J., Kurjan, J., Stadel, J. M., & Tipper, D. J. (1990). Effects of expression of mammalian G alpha and hybrid mammalian-yeast G alpha proteins on the yeast pheromone response signal transduction pathway. *Molecular and Cellular Biology*, 10(6), 2582–2590. <https://doi.org/10.1128/mcb.10.6.2582>
- Kauffman, K. J., Pridgen, E. M., Doyle, F. J., Dhurjati, P. S., & Robinson, A. S. (2002). Decreased protein expression and intermittent recoveries in BiP levels result from cellular stress during heterologous protein expression in *Saccharomyces cerevisiae*. *Biotechnology Progress*, 18(5), 942–950. <https://doi.org/10.1021/bp025518g>
- Kaufman, R. J., Scheuner, D., Schröder, M., Shen, X., Lee, K., Liu, C. Y., & Arnold, S. M. (2002). The unfolded protein response in nutrient sensing and differentiation. *Nature Reviews Molecular Cell Biology*, 3(6), 411–421. <https://doi.org/10.1038/nrm829>
- Keskanokwong, T., Shandro, H. J., Johnson, D. E., Kittanakom, S., Vilas, G. L., Thorner, P., Reithmeier, R. A. F., Akkarapatumwong, V., Yenichitsomanus, P., & Casey, J. R. (2007).

Interaction of integrin-linked kinase with the kidney chloride/bicarbonate exchanger, kAE1. *Journal of Biological Chemistry*, 282(32), 23205–23218. <https://doi.org/10.1074/jbc.M702139200>

- Khositseth, S., Bruce, L. J., Walsh, S. B., Bawazir, W. M., Ogle, G. D., Unwin, R. J., Thong, M. K., Sinha, R., Choo, K. E., Chartapisak, W., Kingwatanakul, P., Sumboonnanonda, A., Vasuvattakul, S., Yenchitsomanus, P., & wrong, O. (2012). Tropical distal renal tubular acidosis: Clinical and epidemiological studies in 78 patients. *QJM: montly journal of the Association of Physicians*, 105(9), 861–877. <https://doi.org/10.1093/qjmed/hcs139>
- Kim, J., Kim, Y. H., Cha, J. H., Tisher, C. C., & Madsen, K. M. (1999). Intercalated cell subtypes in connecting tubule and cortical collecting duct of rat and mouse. *Journal of the American Society of Nephrology*, 10(1), 1–12.
- Kintaka, R., Makanae, K., & Moriya, H. (2016). Cellular growth defects triggered by an overload of protein localization processes. *Scientific Reports*, 6, 31774. <https://doi.org/10.1038/srep31774>
- Kittanakom, S., Cordat, E., Akkarapatumwong, V., Yenchitsomanus, P., & Reithmeier, R. A. F. (2004). Trafficking defects of a novel autosomal recessive distal renal tubular acidosis mutant (S773P) of the human kidney anion exchanger (kAE1). *Journal of Biological Chemistry*, 279(39), 40960–40971. <https://doi.org/10.1074/jbc.M405356200>
- Kloth, S., Aigner, J., Brandt, E., Moll, R., & Minuth, W. W. (1993). Histochemical markers reveal an unexpected heterogeneous composition of the renal embryonic collecting duct epithelium. *Kidney International*, 44(3), 527–536. <https://doi.org/10.1038/ki.1993.277>
- Koeppen, B. M. (2009). The kidney and acid-base regulation. *Advances in Physiology Education*, 33(4), 275–281. <https://doi.org/10.1152/advan.00054.2009>
- Koeppen, B. M., & Stanton, B. A. (2013). *Renal Physiology* (5th ed.). Elsevier. <https://doi.org/10.1016/B978-0-323-08691-2.00004-1>
- Kolb, A. R., Buck, T. M., & Brodsky, J. L. (2011). *Saccharomyces cerevisiae* as a model system for kidney disease: What can yeast tell us about renal function? *American Journal of Physiology. Renal Physiology*, 301(1), F1–F11. <https://doi.org/10.1152/ajprenal.00141.2011>
- Komatsu, M., Waguri, S., Koike, M., Sou, Y. shin, Ueno, T., Hara, T., Mizushima, N., Iwata, J., Ezaki, J., Murata, S., Hamazaki, J., Nishito, Y., Iemura, S., Natsume, T., Yanagawa, T., Uwayama, J., Warabi, E., Yoshida, H., Ishii, T., Kobayashi, A., Yamamoto, M., Yue, Z., Uchiyama, Y., Kominami, E., & Tanaka, K. (2007). Homeostatic Levels of p62 Control Cytoplasmic Inclusion Body Formation in Autophagy-Deficient Mice. *Cell*, 131(6), 1149–1163. <https://doi.org/10.1016/j.cell.2007.10.035>
- Kriz, W., Bankir, L., Bulger, R. E., Burg, M. B., Goncharevskaya, O. A., Imai, M., Kaissling,

- B., Maunsbach, A. B., Moffat, D. B., Morel, F., Morgan, T. O., Natochin, Y. V., Tisher, C. C., Venkatachalam, M. A., Whittembury, G., & Wright, F. S. (1988). A standard nomenclature for structures of the kidney. *Kidney International*, 33(1), 1–7. <https://doi.org/10.1038/ki.1988.1>
- Kriz, Wilhelm, & Kaissling, B. (2013). Structural Organization of the Mammalian Kidney. In R. J. Alperan & S. C. Hebert (Eds.), *Seldin and Giebisch's The Kidney* (4th ed., pp. 595–691). Elsevier. <https://doi.org/10.1016/B978-0-12-381462-3.00020-3>
- Laemmli, U. K. (1970). Cleavage of structural proteins during the assembly of the head of bacteriophage T4. *Nature*, 227(5259), 680–685. <https://doi.org/10.1038/227680a0>
- Lashhab, R., Rumley, A. C., Arutyunov, D., Rizvi, M., You, C., Dimke, H., Touret, N., Zimmermann, R., Jung, M., Chen, X. Z., Alexander, T., & Cordat, E. (2019). The kidney anion exchanger 1 affects tight junction properties via claudin-4. *Scientific Reports*, 9(1), 3099. <https://doi.org/10.1038/s41598-019-39430-9>
- Lashhab, R., Ullah, A. K. M. S., & Cordat, E. (2019). Renal collecting duct physiology and pathophysiology. *Biochemistry and Cell Biology*, 97(3), 234–242. <https://doi.org/10.1139/bcb-2018-0192>
- Lee, T. H., Bae, Y. H., Kim, M. D., & Seo, J. H. (2012). Overexpression of HAC1 gene increased levels of both intracellular and secreted human kringle fragment in *Saccharomyces cerevisiae*. *Process Biochemistry*, 47(12), 2300–2305. <https://doi.org/10.1016/j.procbio.2012.09.006>
- LeFurgey, A., & Tisher, C. C. (1979). Morphology of rabbit collecting duct. *American Journal of Anatomy*, 155(1), 111–123. <https://doi.org/10.1002/aja.1001550108>
- Lewis, S. E., Erickson, R. P., Barnett, L. B., Venta, P. J., & Tashian, R. E. (1988). N-ethyl-N-nitrosourea-induced null mutation at the mouse *Car-2* locus: an animal model for human carbonic anhydrase II deficiency syndrome. *Proceedings of the National Academy of Sciences*, 85(6), 1962–1966. <https://doi.org/10.1073/pnas.85.6.1962>
- Li, J., Quilty, J., Popov, M., & Reithmeier, R. A. F. (2000). Processing of N-linked oligosaccharide depends on its location in the anion exchanger, AE1, membrane glycoprotein. *Biochemical Journal*, 349(1), 51–57. <https://doi.org/10.1042/0264-6021:3490051>
- Liu, W. J., Ye, L., Huang, W. F., Guo, L. J., Xu, Z. G., Wu, H. L., Yang, C., & Liu, H. F. (2016). p62 Links the Autophagy Pathway and the Ubiquitin-Proteasome System Upon Ubiquitinated Protein Degradation. *Cellular and Molecular Biology Letters*, 21, 29. <https://doi.org/10.1186/s11658-016-0031-z>
- Liu, Z., Tyo, K. E. J., Martínez, J. L., Petranovic, D., & Nielsen, J. (2012). Different expression systems for production of recombinant proteins in *Saccharomyces cerevisiae*.

Biotechnology and Bioengineering, 109(5), 1259–1268. <https://doi.org/10.1002/bit.24409>

- Loew, R., Heinz, N., Hampf, M., Bujard, H., & Gossen, M. (2010). Improved Tet-responsive promoters with minimized background expression. *BMC Biotechnology*, 10, 81. <https://doi.org/10.1186/1472-6750-10-81>
- López-Rodríguez, A., Cárabez Trejo, A., Coyne, L., Halliwell, R. F., Miledi, R., & Martínez-Torres, A. (2007). The product of the gene *GEF1* of *Saccharomyces cerevisiae* transports Cl⁻ across the plasma membrane. *FEMS Yeast Research*, 7(8), 1218–1229. <https://doi.org/10.1111/j.1567-1364.2007.00279.x>
- Madsen, K. M., Clapp, W. L., & Verlander, J. W. (1988). Structure and function of the inner medullary collecting duct. *Kidney International*, 34(4), 441–454. <https://doi.org/10.1038/ki.1988.201>
- Malínská, K., Malínský, J., Opekarová, M., & Tanner, W. (2003). Visualization of Protein Compartmentation within the Plasma Membrane of Living Yeast Cells. *Molecular Biology of the Cell*, 14(11), 4427–4436. <https://doi.org/10.1091/mbc.E03-04-0221>
- Manivasakam, P., Weber, S. C., Mcelver, J., & Schiestl, R. H. (1995). Micro-homology mediated PCR targeting in *Saccharomyces cerevisiae*. *Nucleic Acids Research*, 23(14), 2799–2800. <https://doi.org/10.1093/nar/23.14.2799>
- Masuoka, J., Guthrie, L. N., & Hazen, K. C. (2002). Complications in cell-surface labelling by biotinylation of *Candida albicans* due to avidin conjugate binding to cell-wall proteins. *Microbiology*, 148(4), 1073–1079. <https://doi.org/10.1099/00221287-148-4-1073>
- Mattanovich, D., Gasser, B., Hohenblum, H., & Sauer, M. (2004). Stress in recombinant protein producing yeasts. *Journal of Biotechnology*, 113(1–3), 121–135. <https://doi.org/10.1016/j.jbiotec.2004.04.035>
- McIsaac, R. S., Silverman, S. J., McClean, M. N., Gibney, P. A., Macinskas, J., Hickman, M. J., Petti, A. A., & Botstein, D. (2011). Fast-acting and nearly gratuitous induction of gene expression and protein depletion in *Saccharomyces cerevisiae*. *Molecular Biology of the Cell*, 22(22), 4447–4459. <https://doi.org/10.1091/mbc.E11-05-0466>
- Mollaaghababa, R., Davidson, F. F., Kaiser, C., & Khorana, H. G. (1996). Structure and function in rhodopsin: Expression of functional mammalian opsin in *Saccharomyces cerevisiae*. *Proceedings of the National Academy of Sciences of the United States of America*, 93(21), 11482–11486. <https://doi.org/10.1073/pnas.93.21.11482>
- Mrsá, V., Seidl, T., Gentzsch, M., & Tanner, W. (1997). Specific labelling of cell wall proteins by biotinylation. Identification of four covalently linked O-mannosylated proteins of *Saccharomyces cerevisiae*. *Yeast*, 13(12), 1145–1154. [https://doi.org/10.1002/\(SICI\)1097-0061\(19970930\)13:12<1145::AID-YEA163>3.0.CO;2-Y](https://doi.org/10.1002/(SICI)1097-0061(19970930)13:12<1145::AID-YEA163>3.0.CO;2-Y)

- Mumtaz, R., Trepiccione, F., Hennings, J. C., Huebner, A. K., Serbin, B., Picard, N., Ullah, A. K. M. S., Paunescu, T. G., Capen, D. E., Lashhab, R. M., Mouro-Chanteloup, I., Alper, S. L., Wagner, C. A., Cordat, E., Brown, D., Eladari, D., & Hübner, C. A. (2017). Intercalated Cell Depletion and Vacuolar H⁺-ATPase Mistargeting in an AE1 R607H Knockin Model. *Journal of the American Society of Nephrology*, 28(5), 1507–1520. <https://doi.org/10.1681/ASN.2016020169>
- Naldini, L., Blömer, U., Gallay, P., Ory, D., Mulligan, R., Gage, F. H., Verma, I. M., & Trono, D. (1996). *In vivo* gene delivery and stable transduction of nondividing cells by a lentiviral vector. *Science*, 272(5259), 263–267. <https://doi.org/10.1126/science.272.5259.263>
- Norgett, E. E., Golder, Z. J., Lorente-Canovas, B., Ingham, N., Steel, K. P., & Karet Frankl, F. E. (2012). *Atp6v0a4* knockout mouse is a model of distal renal tubular acidosis with hearing loss, with additional extrarenal phenotype. *Proceedings of the National Academy of Sciences of the United States of America*, 109(34), 13775–13780. <https://doi.org/10.1073/pnas.1204257109>
- Nuiplot, N. O., Junking, M., Duangtum, N., Khunchai, S., Sawasdee, N., Yenchitsomanus, P. T., & Akkarapatumwong, V. (2015). Transmembrane protein 139 (TMEM139) interacts with human kidney isoform of anion exchanger 1 (kAE1). *Biochemical and Biophysical Research Communications*, 463(4), 706–711. <https://doi.org/10.1016/j.bbrc.2015.05.128>
- Ohana, E., Yang, D., Shcheynikov, N., & Muallem, S. (2009). Diverse transport modes by the solute carrier 26 family of anion transporters. *The Journal of Physiology*, 587(10), 2179–2185. <https://doi.org/10.1113/jphysiol.2008.164863>
- Park, M., Li, Q., Shcheynikov, N., Muallem, S., & Zeng, W. (2005). Borate Transport and Cell Growth and Proliferation: Not Only in Plants. *Cell Cycle*, 4(1), 24–26. <https://doi.org/10.4161/cc.4.1.1394>
- Parker, M. D., & Tanner, M. J. . (2004). The disruption of the third extracellular loop of the red cell anion exchanger AE1 does not affect electroneutral Cl⁻/HCO₃⁻ exchange activity. *Blood Cells, Molecules, and Diseases*, 32(3), 379–383. <https://doi.org/10.1016/J.BCMD.2004.01.010>
- Patterson, S. T., & Reithmeier, R. A. F. (2010). Cell surface rescue of kidney anion exchanger 1 mutants by disruption of chaperone interactions. *Journal of Biological Chemistry*, 285(43), 33423–33434. <https://doi.org/10.1074/jbc.M110.144261>
- Petranovic, D., & Nielsen, J. (2008). Can yeast systems biology contribute to the understanding of human disease? *Trends in Biotechnology*, 26(11), 584–590. <https://doi.org/10.1016/j.tibtech.2008.07.008>
- Piper, R. C., & Katzmann, D. J. (2010). Biogenesis and function of multivesicular bodies. *Annual Review of Cell and Developmental Biology*, 23, 519–547. <https://doi.org/10.1146/annurev.cellbio.23.090506.123319>. Biogenesis

- Plummer, T. H., Elder, J. H., Alexander, S., Phelan, A. W., & Tarentino, A. L. (1984). Demonstration of peptide:N-glycosidase F activity in endo- β -N-acetylglucosaminidase F preparations. *Journal of Biological Chemistry*, 259(17), 10700–10704.
- Prista, C., Almagro, A., Loureiro-Dias, M. C., & Ramos, J. (1997). Physiological basis for the high salt tolerance of *Debaryomyces hansenii*. *Applied and Environmental Microbiology*, 63(10), 4005–4009. <https://doi.org/10.1128/aem.63.10.4005-4009.1997>
- Quax, T. E. F., Claassens, N. J., Söll, D., & van der Oost, J. (2015). Codon Bias as a Means to Fine-Tune Gene Expression. *Molecular Cell*, 59(2), 149–161. <https://doi.org/10.1016/j.molcel.2015.05.035>
- Quilty, J. A., Cordat, E., & Reithmeier, R. A. F. (2002). Impaired trafficking of human kidney anion exchanger (kAE1) caused by hetero-oligomer formation with a truncated mutant associated with distal renal tubular acidosis. *Biochemical Journal*, 368(3), 895–903. <https://doi.org/10.1042/bj20020574>
- Quilty, J. A., Li, J., & Reithmeier, R. A. (2002). Impaired trafficking of distal renal tubular acidosis mutants of the human kidney anion exchanger kAE1. *American Journal of Physiology. Renal Physiology*, 282(5), 810–820. <https://doi.org/10.1152/ajprenal.00216.2001>
- Raths, S., Rohrer, J., Crausaz, F., & Reizman, H. (1993). *end3* and *end4*: two mutants defective in receptor-mediated and fluid-phase endocytosis in *Saccharomyces cerevisiae*. *Journal of Cell Biology*, 120(1), 55–65. <https://doi.org/10.1083/jcb.120.1.55>
- Rauchman, M. I., Nigam, S. K., Delpire, E., & Gullans, S. R. (1993). An osmotically tolerant inner medullary collecting duct cell line from an SV40 transgenic mouse. *American Journal of Physiology*, 265(3), 416–424. <https://doi.org/10.1152/ajprenal.1993.265.3.f416>
- Reithmeier, R. A. F. (2001). A membrane metabolon linking carbonic anhydrase with chloride/bicarbonate anion exchangers. *Blood Cells, Molecules, and Diseases*, 27(1), 85–89. <https://doi.org/10.1006/bcmd.2000.0353>
- Reithmeier, R. A. F., Casey, J. R., Kalli, A. C., Sansom, M. S. P., Alguel, Y., & Iwata, S. (2016). Band 3, the human red cell chloride/bicarbonate anion exchanger (AE1, SLC4A1), in a structural context. *Biochimica et Biophysica Acta - Biomembranes*, 1858(7), 1507–1532. <https://doi.org/10.1016/j.bbamem.2016.03.030>
- Robertson, A. D., & Murphy, K. P. (1997). Protein structure and the energetics of protein stability. *Chemical Reviews*, 97(5), 1251–1268. <https://doi.org/10.1021/cr960383c>
- Rodríguez Soriano, J. (2002). Renal tubular acidosis: The clinical entity. *Journal of the American Society of Nephrology*, 13(8), 2160–2170. <https://doi.org/10.1097/01.ASN.0000023430.92674.E5>

- Routledge, S. J., Mikaliunaite, L., Patel, A., Clare, M., Cartwright, S. P., Bawa, Z., Wilks, M. D. B., Low, F., Hardy, D., Rothnie, A. J., & Bill, R. M. (2016). The synthesis of recombinant membrane proteins in yeast for structural studies. *Methods*, *95*, 26–37. <https://doi.org/10.1016/j.ymeth.2015.09.027>
- Roy, A., Al-Bataineh, M. M., & Pastor-Soler, N. M. (2015). Collecting duct intercalated cell function and regulation. *Clinical Journal of the American Society of Nephrology*, *10*(2), 305–324. <https://doi.org/10.2215/CJN.08880914>
- Sahr, K. E., Taylor, W. M., Daniels, B. P., Rubin, H. L., & Jarolim, P. (1994). The Structure and Organization of the Human Erythroid Anion Exchanger (AE1) Gene. *Genomics*, *24*(3), 491–501. <https://doi.org/10.1006/geno.1994.1658>
- Sarder, H. A. M., Li, X., Funaya, C., Cordat, E., Schmitt, M. J., & Becker, B. (2020). *Saccharomyces cerevisiae* : First Steps to a Suitable Model System To Study the Function and Intracellular Transport of Human Kidney Anion Exchanger 1. *mSphere*, *5*(1), 16. <https://doi.org/10.1128/mSphere.00802-19>
- Sawasdee, N., Junking, M., Ngaojanlar, P., Sukomon, N., Ungsupravate, D., Limjindaporn, T., Akkarapatumwong, V., Noisakran, S., & Yenchitsomanus, P. T. (2010). Human kidney anion exchanger 1 interacts with adaptor-related protein complex 1 μ 1A (AP-1 μ 1A). *Biochemical and Biophysical Research Communications*, *401*(1), 85–91. <https://doi.org/10.1016/j.bbrc.2010.09.015>
- Schindelin, J., Arganda-Carreras, I., Frise, E., Kaynig, V., Longair, M., Pietzsch, T., Preibisch, S., Rueden, C., Saalfeld, S., Schmid, B., Tinevez, J. Y., White, D. J., Hartenstein, V., Eliceiri, K., Tomancak, P., & Cardona, A. (2012). Fiji: An open-source platform for biological-image analysis. *Nature Methods*, *9*(7), 676–682. <https://doi.org/10.1038/nmeth.2019>
- Schuster, V. L. (1993). Function and Regulation of Collecting Duct Intercalated Cells. *Annual Review of Physiology*, *55*(1), 267–288. <https://doi.org/10.1146/annurev.ph.55.030193.001411>
- Seddon, A. M., Curnow, P., & Booth, P. J. (2004). Membrane proteins, lipids and detergents: Not just a soap opera. *Biochimica et Biophysica Acta*, *1666*(1–2), 105–117. <https://doi.org/10.1016/j.bbamem.2004.04.011>
- Shapiro, A. L., Viñuela, E., & V. Maizel Jr., J. (1967). Molecular weight estimation of polypeptide chains by electrophoresis in SDS-polyacrylamide gels. *Biochemical and Biophysical Research Communications*, *28*(5), 815–820. [https://doi.org/10.1016/0006-291X\(67\)90391-9](https://doi.org/10.1016/0006-291X(67)90391-9)
- Sharma, A. P., Sharma, R. K., Kapoor, R., Kornecki, A., Sural, S., & Filler, G. (2007). Incomplete distal renal tubular acidosis affects growth in children. *Nephrology Dialysis Transplantation*, *22*(10), 2879–2885. <https://doi.org/10.1093/ndt/gfm307>

- Shayakul, C., & Alper, S. L. (2000). Inherited renal tubular acidosis. *Current Opinion in Nephrology and Hypertension*, 9(5), 541–546. <https://doi.org/10.1097/00041552-200009000-00014>
- Shcheynikov, N., Yang, D., Wang, Y., Zeng, W., Karniski, L. P., So, I., Wall, S. M., & Muallem, S. (2008). The SLC26A4 transporter functions as an electroneutral Cl⁻/I⁻/HCO₃⁻ exchanger: role of SLC26A4 and SLC26A6 in I⁻ and HCO₃⁻ secretion and in regulation of CFTR in the parotid duct. *The Journal of Physiology*, 586(16), 3813–3824. <https://doi.org/10.1113/jphysiol.2008.154468>
- Shi, X., Karkut, T., Chamankhah, M., Alting-Mees, M., Hemmingsen, S. M., & Hegedus, D. (2003). Optimal conditions for the expression of a single-chain antibody (scFv) gene in *Pichia pastoris*. *Protein Expression and Purification*, 28(2), 321–330. [https://doi.org/10.1016/S1046-5928\(02\)00706-4](https://doi.org/10.1016/S1046-5928(02)00706-4)
- Shnitsar, V., Li, J., Li, X., Calmettes, C., Basu, A., Casey, J. R., Moraes, T. F., & Reithmeier, R. A. F. (2013). A substrate access tunnel in the cytosolic domain is not an essential feature of the solute carrier 4 (SLC4) family of bicarbonate transporters. *Journal of Biological Chemistry*, 288(47), 33848–33860. <https://doi.org/10.1074/jbc.M113.511865>
- Sorrell, S. L., Golder, Z. J., Johnstone, D. B., & Karet Frankl, F. E. (2016). Renal peroxiredoxin 6 interacts with anion exchanger 1 and plays a novel role in pH homeostasis. *Kidney International*, 89(1), 105–112. <https://doi.org/10.1038/ki.2015.277>
- Spear, E., & Ng, D. T. W. (2001). The unfolded protein response: No longer just a special teams player. *Traffic*, 2(8), 515–523. <https://doi.org/10.1034/j.1600-0854.2001.20801.x>
- Stevens, T. H., & Forgac, M. (1997). Structure, function and regulation of the vacuolar (H⁺)-ATPase. *Annual Review of Cell and Developmental Biology*, 13(1), 779–808. <https://doi.org/10.1146/annurev.cellbio.13.1.779>
- Su, Y., Blake-Palmer, K. G., Fry, A. C., Best, A., Brown, A. C. N., Hiemstra, T. F., Horita, S., Zhou, A., Toye, A. M., & Karet, F. E. (2011). Glyceraldehyde 3-phosphate dehydrogenase is required for band 3 (anion exchanger 1) membrane residency in the mammalian kidney. *American Journal of Physiology. Renal Physiology*, 300(1), F157–F166. <https://doi.org/10.1152/ajprenal.00228.2010>
- Sun, X., Soleimani, M., & Petrovic, S. (2008). Decreased expression of SLC26A4 (pendrin) and SLC26A7 in the kidneys of carbonic anhydrase II-deficient mice. *Cellular physiology and biochemistry*, 21(1–3), 95–108. <https://doi.org/10.1159/000113751>
- Takano, J., Kobayashi, M., Noda, Y., & Fujiwara, T. (2007). *Saccharomyces cerevisiae* Bor1p is a boron exporter and a key determinant of boron tolerance. *FEMS Microbiology Letters*, 267(2), 230–235. <https://doi.org/10.1111/j.1574-6968.2006.00556.x>
- Tanner, M. J. A., Martin, P. G., & High, S. (1988). The complete amino acid sequence of the

- human erythrocyte membrane anion-transport protein deduced from the cDNA sequence. *Biochemical Journal*, 256(3), 703–712. <https://doi.org/10.1042/bj2560703>
- Tanphaichitr, V. S., Sumboonnanonda, A., Ideguchi, H., Shayakul, C., Brugnara, C., Takao, M., Veerakul, G., & Alper, S. L. (1998). Novel AE1 mutations in recessive distal renal tubular acidosis. Loss-of-function is rescued by glycophorin A. *Journal of Clinical Investigation*, 102(12), 2173–2179. <https://doi.org/10.1172/JCI4836>
- Tarradas, A., Selga, E., Riuró, H., Scornik, F., Brugada, R. and Vergés, M. (2013). Cell Surface Protein Biotinylation and Analysis. *Bio-protocol* 3(16): e857. <http://doi.org/10.21769/BioProtoc.857>
- Tate, C. G. (2001). Overexpression of mammalian integral membrane proteins for structural studies. *FEBS Letters*, 504(3), 94–98. [https://doi.org/10.1016/S0014-5793\(01\)02711-9](https://doi.org/10.1016/S0014-5793(01)02711-9)
- Teng-umnuay, P., Verlander, J. W., Yuan, W., Tisher, C. C., & Madsen, K. M. (1996). Identification of distinct subpopulations of intercalated cells in the mouse collecting duct. *Journal of the American Society of Nephrology*, 7(2), 260–274. <http://jasn.asnjournals.org/content/7/2/260.abstract>
- Thurtle-Schmidt, B. H., & Stroud, R. M. (2016). Structure of Bor1 supports an elevator transport mechanism for SLC4 anion exchangers. *Proceedings of the National Academy of Sciences of the United States of America*, 113(38), 10542–10546. <https://doi.org/10.1073/pnas.1612603113>
- Toei, M., Saum, R., & Forgac, M. (2010). Regulation and Isoform Function of the V-ATPases. *Biochemistry*, 49(23), 4715–4723. <https://doi.org/10.1021/bi100397s>
- Tortora, G. J., & Derrickson, B. (2014). *Principles of Anatomy & Physiology* (14th ed). Wiley.
- Towbin, H., Staehelin, T., & Gordon, J. (1979). Electrophoretic transfer of proteins from polyacrylamide gels to nitrocellulose sheets: Procedure and some applications. *Proceedings of the National Academy of Sciences of the United States of America*, 76(9), 4350–4354. <https://doi.org/10.1073/pnas.76.9.4350>
- Toye, A. M. (2005). Defective kidney anion-exchanger 1 (AE1, Band 3) trafficking in dominant distal renal tubular acidosis (dRTA). *Biochemical Society Symposia*, 72, 47–63. <https://doi.org/10.1042/bss0720047>
- Toye, A. M., Banting, G., & Tanner, M. J. A. (2004). Regions of human kidney anion exchanger 1 (kAE1) required for basolateral targeting of kAE1 in polarized kidney cells: Mis-targeting explains dominant renal tubular acidosis (dRTA). *Journal of Cell Science*, 117(8), 1399–1410. <https://doi.org/10.1242/jcs.00974>
- Trimble, R. B., Tarentino, A. L., Plummer, T. H., & Maley, F. (1978). Asparaginyl

glycopeptides with a low mannose content are hydrolyzed by endo-beta-N-acetylglucosaminidase H. *Journal of Biological Chemistry*, 253(13), 4508–4511.

- Vainsel, M., Fondu, P., Cardrenel, S., Rocmans, C., & Gepts, W. (1972). Osteopetrosis associated with proximal and distal tubular acidosis. *Acta Paediatrica*, 61(4), 429–434. <https://doi.org/10.1111/j.1651-2227.1972.tb15859.x>
- Valkonen, M., Mojzita, D., Penttilä, M., & Benčina, M. (2013). Noninvasive high-throughput single-cell analysis of the intracellular pH of *Saccharomyces cerevisiae* by ratiometric flow cytometry. *Applied and Environmental Microbiology*, 79(23), 7179–7187. <https://doi.org/10.1128/AEM.02515-13>
- Valkonen, M., Penttilä, M., & Saloheimo, M. (2003). Effects of inactivation and constitutive expression of the unfolded-protein response pathway on protein production in the yeast *Saccharomyces cerevisiae*. *Applied and Environmental Microbiology*, 69(4), 2065–2072. <https://doi.org/10.1128/AEM.69.4.2065-2072.2003>
- Valli, M., Sauer, M., Branduardi, P., Borth, N., Porro, D., & Mattanovich, D. (2005). Intracellular pH Distribution in. *Microbiology*, 71(3), 1515–1521. <https://doi.org/10.1128/AEM.71.3.1515>
- Vera, A., González-Montalbán, N., Aris, A., & Villaverde, A. (2007). The conformational quality of insoluble recombinant proteins is enhanced at low growth temperatures. *Biotechnology and Bioengineering*, 96(6), 1101–1106. <https://doi.org/10.1002/bit.21218>
- Vichot, A. A., Zsengellér, Z. K., Shmukler, B. E., Adams, N. D., Dahl, N. K., & Alper, S. L. (2017). Loss of kAE1 expression in collecting ducts of end-stage kidneys from a family with SLC4A1 G609R-associated distal renal tubular acidosis. *Clinical Kidney Journal*, 10(1), 135–140. <https://doi.org/10.1093/ckj/sfw074>
- Vilas, G. L., Loganathan, S. K., Liu, J., Riau, A. K., Young, J. D., Mehta, J. S., Vithana, E. N., & Casey, J. R. (2013). Transmembrane water-flux through SLC4A11: a route defective in genetic corneal diseases. *Human Molecular Genetics*, 22(22), 4579–4590. <https://doi.org/10.1093/hmg/ddt307>
- von der Haar, T. (2007). Optimized protein extraction for quantitative proteomics of yeasts. *PLoS ONE*, 2(10). <https://doi.org/10.1371/journal.pone.0001078>
- Wain, H. M. (2004). Genew: the Human Gene Nomenclature Database, 2004 updates. *Nucleic Acids Research*, 32(90001), D255–D257. <https://doi.org/10.1093/nar/gkh072>
- Weber, K., & Osborn, M. (1969). The reliability of molecular weight determinations by dodecyl sulfate-polyacrylamide gel electrophoresis. *Journal of Biological Chemistry*, 244(16), 4406–4412.

- West, M., Zurek, N., Hoenger, A., & Voeltz, G. K. (2011). A 3D analysis of yeast ER structure reveals how ER domains are organized by membrane curvature. *Journal of Cell Biology*, *193*(2), 333–346. <https://doi.org/10.1083/jcb.201011039>
- Wu, F., Saleem, M. A., Kampik, N. B., Satchwell, T. J., Williamson, R. C., Blattner, S. M., Ni, L., Toth, T., White, G., Young, M. T., Parker, M. D., Alper, S. L., Wagner, C. A., & Toyé, A. M. (2010). Anion exchanger 1 interacts with nephrin in podocytes. *Journal of the American Society of Nephrology*, *21*(9), 1456–1467. <https://doi.org/10.1681/ASN.2009090921>
- Yan, K., Khoshnoodi, J., Ruotsalainen, V., & Tryggvason, K. (2002). N-linked glycosylation is critical for the plasma membrane localization of nephrin. *Journal of the American Society of Nephrology*, *13*(5), 1385–1389. <https://doi.org/10.1097/01.ASN.0000013297.11876.5B>
- Yenchitsomanus, P., Kittanakom, S., & Rungroj, N. (2005). Molecular mechanisms of autosomal dominant and recessive distal renal tubular acidosis caused by SLC4A1 (AE1) mutations. *Journal of Molecular and Genetic Medicine*, *1*(2), 49–62. <https://doi.org/10.4172/1747-0862.1000013>
- Young, M. T., & Tanner, M. J. A. (2003). Distinct regions of human glycophorin A enhance human red cell anion exchanger (band 3; AE1) transport function and surface trafficking. *Journal of Biological Chemistry*, *278*(35), 32954–32961. <https://doi.org/10.1074/jbc.M302527200>
- Zhou, X., Vink, M., Klaver, B., Berkhout, B., & Das, A. T. (2006). Optimization of the Tet-On system for regulated gene expression through viral evolution. *Gene Therapy*, *13*(19), 1382–1390. <https://doi.org/10.1038/sj.gt.3302780>

Appendix

DNA sequences (5'–3' direction) purchased to generate various kAE1 expression plasmid for yeast are shown below. Restriction sites are displayed in lower-case letters, signal sequences are in **red** color, epitope-tag sequences are in **bold** and linker sequences are underlined. **(A)** V5-tagged human kAE1 sequence, **(B)** V5-tagged human kAE1 sequence with an additional Kar2p signal sequence at the N-terminus, **(C)** V5-tagged yeast codon-optimized kAE1 sequence, **(D)** yeast codon-optimized kAE1 sequence fused to a yeGFP sequence at the C-terminus, **(E)** yeast codon-optimized kAE1 sequence with an integrated HA tag in the third extracellular loop between amino acid 557 and 578 (according to AE1 sequence) and **(F)** the sequence of a N-terminal HA-tagged truncated yeast codon-optimized kAE1 version (361 to 911 aa).

(A) kAE1^{V5}

```
ctcgaggaattcATGGACGAAAAGAACCAGGAGCTGAGATGGATGGAGGCGGCGCTGGGTGCAACTG
GAGGAGAACCTGGGGGAGAATGGGGCCTGGGGCCGCCGCACCTCTCTCACCTCACCTTCTGGAGC
CTCCTAGAGCTGCGTAGAGTCTTCACCAAGGGTACTGTCCTCCTAGACCTGCAAGAGACCTCCCTG
GCTGGAGTGGCCAACCAACTGCTAGACAGGTTTATCTTTGAAGACCAGATCCGGCCTCAGGACCGA
GAGGAGCTGCTCCGGGCCCTGCTGCTTAAACACAGCCACGCTGGAGAGCTGGAGGCCCTGGGGGG
TGTGAAGCCTGCAGTCCTGACACGCTCTGGTGATCCTTCACAGCCTCTGCTCCCCAACACTCCTCA
CTGGAGACACAGCTCTTCTGTGAGCAGGGAGATGGGGGCACAGAAGGGCACTCACCATCTGGTAT
TCTGGAAAAGATTCCCCCGGATTCAGAGGCCACGTTGGTGCTAGTGGGCCGCGCCGACTTCCTGGA
GCAGCCGGTGCTGGGCTTCGTGAGGCTGCAGGAGGCAGCGGAGCTGGAGGCGGTGGAGCTGCCGG
TGCCTATACGCTTCCTCTTTGTGTTGCTGGGACCTGAGGCCCCCCACATCGATTACACCCAGCTTGG
CCGGGCTGCTGCCACCCTCATGTCAGAGAGGGTGTTCGCCATAGATGCCTACATGGCTCAGAGCCG
AGGGGAGCTGCTGCACTCCCTAGAGGGCTTCCTGGACTGCAGCCTAGTGCTGCCTCCCACCGATGC
CCCCTCCGAGCAGGCACTGCTCAGTCTGGTGCCTGTGCAGAGGGAGCTACTTCGAAGGCGCTATCA
GTCCAGCCCTGCCAAGCCAGACTCCAGCTTCTACAAGGGCCTAGACTTAAATGGGGGCCAGATGA
CCCTCTGCAGCAGACAGGCCAGCTCTTCGGGGGCCTGGTGCGTGATATCCGGCGCCGCTACCCCTA
TTACCTGAGTGACATCACAGATGCATTACAGCCCCAGGTCCTGGCTGCCGTCATCTTCATCTACTTT
GCTGCACTGTCACCCGCCATCACCTTCGGCGGCCTCCTGGGAGAAAAGACCCGGAACCAGATGGG
AGTGTCGGAGCTGCTGATCTCCACTGCAGTGCAGGGCATTCTCTTCGCCCTGCTGGGGGCTCAGCC
CCTGCTTGTGGTTCGGCTTCTCAGGACCCCTGCTGGTGTGTTGAGGAAGCCTTCTTCTCGTTCTGCGAG
ACCAACGGTCTAGAGTACATCGTGGGCCGCGTGTGGATCGGCTTCTGGCTCATCCTGCTGGTGGTG
TTGGTGGTGGCCTTCGAGGGTAGCTTCTGGTCCGCTTCATCTCCCGCTATAACCCAGGAGATCTTCT
CCTTCCTCATTTCCCTCATCTTCATCTATGAGACTTTCTCCAAGCTGATCAAGATCTTCCAGGACCAC
CCTACTACAGAAGACTTATAACTACAACGTGTTGATGGTGCCCAAACCTCAGGGCCCCCTGCCAAC
```

ACAGCCCTCCTCTCCCTTGTGCTCATGGCCGGTACCTTCTTCTTTGCCATGATGCTGCGCAAGTTCA
AGAACAGCTCCTATTTCCCTGGCAAGCTGCGTCGGGTATCGGGGACTTCGGGGTCCCCATCTCCA
TCCTGATCATGGTCCTGGTGGATTTCTTCATTCAGGATACCTACACCCAGAACTCTCGGTGCCTGA
TGGCTTCAAGGTGTCCAACCTCAGCCCGGGGCTGGGTATCCACCCACTGGGCTTGC GTTCCGA
GTTTCCCATCTGGATGATGTTTGCTCCGCCCTGCCCTGCTCTGCTGGTCTTCATCCTCATATTCTGG
AGTCTCAGATCACCACGCTGATTGTCAGCAAACCTGAGCGCAAGATGGTCAAGGGCTCCGGCTTCC
ACCTGGACCTGCTGCTGGTAGTAGGCATGGGTGGGGTGGCCGCCCTCTTTGGGATGCCCTGGCTCA
GTGCCACCACCGTTCGTTCCGTCACCCATGCCAACGCCCTCACTGTCATGGGCAAAGCCAGCACCC
CAGGGGCTGCAGCCAGATCCAGGAGGTCAAAGAGCAGCGGATCAGTGGACTCCTGGTCGCTGTG
CTTGTGGGCCTGTCCATCCTCATGGAGCCATCCTGTCCCGCATCCCCCTGGCTGTACTGTTTGCA
TCTTCCTCTACATGGGGGTACGTCGCTCAGCGGCATCCAGCTCTTTGACCGCATCTTGCTTCTGTT
CAAGCCACCAAGTATCACCCAGATGTGCCCTACGTCAAGCGGGTGAAGACCTGGCGCATGCACTT
ATTCACGGGCATCCAGATCATCTGCCTGGCAGTGTGTGGGTGGTGAAGTCCACGCCGGCCTCCCT
GGCCCTGCCCTTCGTCCTCATCCTCACTGTGCCGCTGCGGGCGCTCCTGCTGCCGCTCATCTCAGG
AACGTGGAGCTTCAGTGTCTGGATGCTGATGATGCCAAGGCAACCTTTGATGAGGAGGAAGGTGC
GGATGAATACGACGAAGTGGCCATGCCTGTGGGTAAGCCTATCCCTAACCCCTCTCCTCGGTCTC
GATTCTACGTGAggatccgtcgac

(B) Kar2^{SS}-kAE1^{V5}

ctcgaggaattcATGTTTTTCAACAGACTAAGCGCTGGCAAGCTGCTGGTACCACTCTCCGTGGTCTGTGA
CGCCCTTTTCGTGGTAATATTACCTTTACAGAATTCTTTCCACTCCTCCAATGTTTTAGTTAGAGGTG
CCGATGACGAAAAGAACCAGGAGCTGAGATGGATGGAGGCGGCGCTGGGTGCAACTGGAGGA
GAACCTGGGGGAGAATGGGGCCTGGGGCCCGCCGCACCTCTCTCACCTCACCTTCTGGAGCCTCCT
AGAGCTGCGTAGAGTCTTACCAAGGGTACTGTCTCCTAGACCTGCAAGAGACCTCCCTGGCTGG
AGTGGCCAACCAACTGCTAGACAGGTTTATCTTTGAAGACCAGATCCGGCCTCAGGACCGAGAGG
AGCTGCTCCGGGCCCTGCTGCTTAAACACAGCCACGCTGGAGAGCTGGAGGCCCTGGGGGGTGTG
AAGCCTGCAGTCTGACACGCTCTGGTGATCCTTACAGCCTCTGCTCCCCAACACTCCTCACTGG
AGACACAGCTCTTCTGTGAGCAGGGAGATGGGGGCACAGAAGGGCACTCACCATCTGGTATTCTG
GAAAAGATTCCCCCGGATTCAGAGGCCACGTTGGTGCTAGTGGGCGCGCCGACTTCCTGGAGCAG
CCGGTGTGGGCTTCGTGAGGCTGCAGGAGGCAGCGGAGCTGGAGGCGGTGGAGCTGCCGGTGCC
TATACGTTCTCTTTGTGTTGCTGGGACCTGAGGCCCCCACATCGATTACACCCAGCTTGCCGG
GCTGCTGCCACCCTCATGTCAGAGAGGGTGTCCGCATAGATGCCTACATGGCTCAGAGCCGAGGG
GAGCTGCTGCACTCCCTAGAGGGCTTCTGGACTGCAGCCTAGTGCTGCCTCCCACCGATGCCCCCT
CCGAGCAGGCACTGCTCAGTCTGGTGCCTGTGCAGAGGGAGCTACTTCGAAGGCGCTATCAGTCCA
GCCCTGCCAAGCCAGACTCCAGCTTCTACAAGGGCCTAGACTTAAATGGGGGCCAGATGACCCTC
TGCAGCAGACAGGCCAGCTCTTCGGGGGCCTGGTGCCTGATATCCGGCGCCGCTACCCCTATTACC
TGAGTGACATCACAGATGCATTCAGCCCCAGGTCCTGGCTGCCGTCATCTTCATCTACTTTGCTGC
ACTGTCACCCGCCATCACCTTCGGCGGCCTCCTGGGAGAAAAGACCCGGAACCAGATGGGAGTGTG

GGAGCTGCTGATCTCCACTGCAGTGCAGGGCATTCTCTTCGCCCTGCTGGGGGCTCAGCCCCTGCTT
GTGGTCGGCTTCTCAGGACCCCTGCTGGTGTGTTGAGGAAGCCTTCTTCTCGTTCTGCGAGACCAACG
GTCTAGAGTACATCGTGGGCCGCGTGTGGATCGGCTTCTGGCTCATCCTGCTGGTGGTGTGGTGGT
GGCCTTCGAGGGTAGCTTCCTGGTCCGCTTCATCTCCCGCTATACCCAGGAGATCTTCTCCTTCCTC
ATTTCCCTCATCTTCATCTATGAGACTTTCTCCAAGCTGATCAAGATCTTCCAGGACCACCCACTAC
AGAAGACTTATAACTACAACGTGTTGATGGTGCCCAAACCTCAGGGCCCCCTGCCAACACAGCCC
TCCTCTCCCTTGTGCTCATGGCCGGTACCTTCTTCTTTGCCATGATGCTGCGCAAGTTCAAGAACAG
CTCCTATTTCCCTGGCAAGCTGCGTCGGGTATCGGGGACTTCGGGGTCCCCATCTCCATCCTGATC
ATGGTCTGGTGGATTTCTTCATTACAGGATACCTACACCCAGAACTCTCGGTGCCTGATGGCTTCA
AGGTGTCCAACCTCCTCAGCCCCGGGGTGGGTATCCACCCACTGGGCTTTCGTTCCGAGTTTCCCAT
CTGGATGATGTTTGCCTCCGCCCTGCCTGCTCTGCTGGTCTTCATCCTCATATTCCTGGAGTCTCAGA
TCACCACGCTGATTGTCAGCAAACCTGAGCGCAAGATGGTCAAGGGCTCCGGCTTCCACCTGGACC
TGCTGCTGGTAGTAGGCATGGGTGGGGTGGCCGCCCTCTTTGGGATGCCCTGGCTCAGTGCCACCA
CCGTGCGTTCCGTCACCCATGCCAACGCCCTCACTGTCATGGGCAAAGCCAGCACCCCAGGGGGCTG
CAGCCCAGATCCAGGAGGTCAAAGAGCAGCGGATCAGTGGACTCCTGGTCGCTGTGCTTGTGGGCC
TGTCATCCTCATGGAGCCCATCCTGTCCCGCATCCCCCTGGCTGTACTGTTTGGCATCTTCCTCTAC
ATGGGGGTACGTCGCTCAGCGGCATCCAGCTCTTTGACCGCATCTTGCTTCTGTTCAAGCCACCCA
AGTATCACCCAGATGTGCCCTACGTCAAGCGGGTGAAGACCTGGCGCATGCACTTATTCACGGGCA
TCCAGATCATCTGCCTGGCAGTGCTGTGGGTGGTGAAGTCCACGCCGGCCTCCCTGGCCCTGCCCTT
CGTCTCATCCTCACTGTGCCGCTGCGGGCGCTCCTGCTGCCGCTCATCTTCAGGAACGTGGAGCTT
CAGTGTCTGGATGCTGATGATGCCAAGGCAACCTTTGATGAGGAGGAAGGTTCGGGATGAATACGA
CGAAGTGGCCATGCCTGTGGGTAAGCCTATCCCTAACCTCTCCTCGGTCTCGATTCTACGTGA
ggatccgtcgac

(C) ykAE1^{V5}

ctcgaggaattcATGGACGAAAAGAATCAAGAATTGAGATGGATGGAAGCTGCTAGATGGGTTCAATTGG
AAGAAAATTTGGGTGAAAATGGTGCTTGGGGTAGACCACATTTGTCTCATTGACTTTTTGGTCCTT
GTTGGAATTGAGAAGAGTTTTCACTAAGGGTACTGTCTTGTGGACTTGCAAGAACTTCTTTGGCT
GGTGTGGCCAATCAATTATTGGACAGATTCATTTTCGAAGATCAAATCAGACCACAAGATAGAGAA
GAATTATTGAGAGCCTTGTGTTGAAGCACTCTCATGCTGGTGAATTGGAAGCTTTAGGTGGTGTTA
AGCCAGCTGTTTTGACTAGATCTGGTGATCCATCACAACCATTATTGCCACAACATTCTTCATTGGA
AACCCAAATTATTCTGCGAACAAGGTGATGGTGGTACTGAAGGTCATTCTCCATCTGGTATTTTGGAA
AAAGATTCCACCAGATTCTGAAGCCACTTTGGTTTTGGTTGGTAGAGCTGATTTTTTGGAAACAACCA
GTTTTGGGTTTTCGTTAGATTGCAAGAAGCTGCTGAATTAGAAGCAGTTGAATTGCCAGTTCCAATC
AGATTCTTGTTCGTTTTGTTGGGTCCAGAAGCTCCACATATTGATTATACTCAATTGGGTAGAGCCG
CTGCTACTTTGATGTCTGAAAGAGTTTTTTAGAATCGACGCTTACATGGCTCAATCCAGAGGTGAATT
ATTGCATTCTTTGGAAGGTTTTCTTGGACTGCTCTTTAGTTTTGCCACCAACTGATGCTCCATCTGAAC
AAGCTTTGTTGTCTTTGGTTCAGTTCAAAGAGAATTATTGAGAAGAAGATACCAATCCTCTCCAGC

TAAACCAGACTCTTCATTTTACAAGGGTTTGGATTTGAATGGTGGTCCAGATGATCCATTGCAACA
AACTGGTCAATTATTCGGTGGTTTGGTTAGAGACATCAGAAGAAGATATCCTTACTACTTGTCCGAT
ATCACCGATGCTTTTTCCACCACAAGTTTTGGCTGCTGTTATCTTCATCTATTTTCGCTGCTTTGTCACC
AGCTATTACTTTTGGTGGTTTATTAGGTGAAAAGACCAGAAATCAAATGGGTGTTTCCGAATTATTG
ATCTCCACTGCTGTTCAAGGTATTTTGTGTTGCTTTGTTAGGTGCCCAACCTTTGTTGGTTGTTGGTTT
TTCTGGTCCATTATTGGTCTTTGAAGAAGCTTTCTTCTCCTTCTGTGAAACTAACGGTTTGAATATA
TCGTCGGTAGAGTTTGGATTGGTTTCTGGTTAATTTGTTGGTCGTTTTGGTCGTCGCTTTTGAAGGT
TCATTTTTGGTAAGATTCATCTCCAGATACACCCAAGAAATCTTTTTCTTCTTGATCTCCTTGATTTT
CATCTACGAAACCTTCTCCAAGTTGATCAAGATCTTCCAAGATCACCCATTGCAAAAGACCTACAA
CTACAACGTTTTGATGGTTCCAAAACCACAAGGTCCATTGCCAAATACTGCTTTATTATCCTTGGTT
TTAATGGCCGGTACTTTCTTCTTTGCCATGATGTTGAGAAAGTTCAAGAACTCCTCTTACTTCCCAG
GTAAGTTGAGAAGAGTCATTGGTGATTTTGGTGTCCCAATCTCCATTTGATTATGGTCTTGGTTGA
CTTCTTCATCCAAGATACTTACACCCAAAAGTTGTCTGTTCCAGATGGTTTCAAGGTCAGTAATTCT
TCAGCTAGAGGTTGGGTTATTCATCCATTGGGTTTGGATCCGAATTTCCAATTTGGATGATGTTCCG
CTTCTGCTTTGCCAGCTTTATTGGTTTTTATCTTGATATTCTTGGAAATCCCAAATCACACCTTGATC
GTTTCTAAACCTGAAAGAAAGATGGTCAAGGGTCTGGTTTTCACTTGGATTTGTTGTTAGTTGTCG
GTATGGGTGGTGTTCAGCTTTGTTTGGTATGCCATGGTTGTCTGCTACTACTGTTAGATCTGTTACT
CATGCTAACGCTTTGACTGTTATGGGTAAAGCTTCTACTCCAGGTGCTGCTGCTCAAATTCAGAAG
TAAAAGAACAAGAATTTCCGGTTTGTGGTAGCCGTTTTAGTTGGTTTGTCAATCTTGATGGAACC
TATCTGTCTAGAATCCCATTTGGCTGTTTTGTTTCGGTATTTTCTTGTACATGGGTGTCACATCCTTGT
CCGGTATCCAATTTTATGATAGAATCTTGTGTTATTCAAGCCACCAAAGTACCATCCAGATGTTCC
TTATGTTAAGAGAGTCAAGACTTGGAGAATGCATTTGTTTACCAGGTTTCAAATTTATCTGCTTGGCA
GTTTTGTGGGTTGTTAAGTCAACTCCAGCTTCTTTAGCATTGCCATTCGTTTTGATTTTGACCGTCCC
ATTAAGAAGAGTCTTGTGCCATTGATATTCAGAAACGTCGAATTGCAATGTTTGGATGCTGATGA
TGCTAAGGCTACTTTTGACGAAGAAGAAGGTAGAGACGAATACGATGAAGTTGCTATGCCAGTTG
GTAAGCCAATTCCAAATCCATTATTAGGTTTGGACTCCACTTA

Aggatccgtagac

(D) ykAE1-yeGFP

ctcaggaattcATGGACGAAAAGAATCAAGAATTGAGATGGATGGAAGCTGCTAGATGGGTTCAATTGG
AAGAAAATTTGGGTGAAAATGGTGCTTGGGGTAGACCACATTTGTCTCATTGACTTTTTGGTCCTT
GTTGGAATTGAGAAGAGTTTTACTAAGGGTACTGTCTTGTGGACTTGCAAGAACTTCTTTGGCT
GGTGTGCCAATCAATTATTGGACAGATTCATTTTCGAAGATCAAATCAGACCACAAGATAGAGAA
GAATTATTGAGAGCCTTGTGTTGAAGCACTCTCATGCTGGTGAATTGGAAGCTTTAGGTGGTGTTA
AGCCAGCTGTTTTGACTAGATCTGGTGATCCATCACAACCATTATTGCCACAACATTCTTCATTGGA
AACCAATTATTCTGCGAACAAGGTGATGGTGGTACTGAAGGTCATTCTCCATCTGGTATTTTGGAA
AAAGATTCCACCAGATTCTGAAGCCACTTTGGTTTTGGTTGGTAGAGCTGATTTTTTGGAAACAACCA
GTTTTGGGTTTCGTTAGATTGCAAGAAGCTGCTGAATTAGAAGCAGTTGAATTGCCAGTTCCAATC
AGATTCTTGTTCGTTTTGTTGGGTCCAGAAGCTCCACATATTGATTATACTCAATTGGGTAGAGCCG

CTGCTACTTTGATGTCTGAAAGAGTTTTTAGAATCGACGCTTACATGGCTCAATCCAGAGGTGAATT
ATTGCATTCTTTGGAAGGTTTCTTGGACTGCTCTTTAGTTTTGCCACCAACTGATGCTCCATCTGAAC
AAGCTTTGTTGTCTTTGGTTCCAGTTCAAAGAGAATTATTGAGAAGAAGATACCAATCCTCTCCAGC
TAAACCAGACTCTTCATTTACAAGGGTTTGGATTTGAATGGTGGTCCAGATGATCCATTGCAACA
AACTGGTCAATTATTCGGTGGTTTGGTTAGAGACATCAGAAGAAGATATCCTTACTACTTGTCCGAT
ATCACCGATGCTTTTTACCACAAGTTTTGGCTGCTGTTATCTTCATCTATTTTCGCTGCTTTGTCACC
AGCTATTACTTTTGGTGGTTTATTAGGTGAAAAGACCAGAAATCAAATGGGTGTTTCCGAATTATTG
ATCTCCACTGCTGTTCAAGGTATTTTGGTTGCTTTGTTAGGTGCCAACCTTTGTTGGTTGTTGGTTT
TTCTGGTCCATTATTGGTCTTTGAAGAAGCTTTCTTCTCCTTCTGTGAAACTAACGGTTTGAATATA
TCGTCGGTAGAGTTTGGATTGGTTTCTGGTTAATTTGTTGGTCGTTTTGGTCGTCGCTTTTGAAGGT
TCATTTTTGGTAAGATTCATCTCCAGATACACCCAAGAAATCTTTTCTTTCTTGATCTCCTTGATTTT
CATCTACGAAACCTTCTCCAAGTTGATCAAGATCTTCCAAGATCACCCATTGCAAAGACCTACAA
CTACAACGTTTTGATGGTTCCAAAACCACAAGGTCCATTGCCAAATACTGCTTTATTATCCTTGGTT
TTAATGGCCGGTACTTTCTTCTTTGCCATGATGTTGAGAAAGTTCAAGAACTCCTCTTACTTCCCAG
GTAAGTTGAGAAGAGTCATTGGTGATTTTGGTGTCCCAATCTCCATTTTGATTATGGTCTTGGTTGA
CTTCTTCATCCAAGATACTTACACCCAAAAGTTGTCTGTTCCAGATGGTTTCAAGGTCAGTAATTCT
TCAGCTAGAGGTTGGGTTATTCATCCATTGGGTTTGGATCCGAATTTCCAATTTGGATGATGTTCCG
CTTCTGCTTTGCCAGCTTTATTGGTTTTTATCTTGATATTCTTGGAATCCCAAATCACACCTTGATC
GTTTCTAAACCTGAAAGAAAGATGGTCAAGGGTCTGGTTTTCACTTGGATTGTTGTTAGTTGTCTG
GTATGGGTGGTGTTCAGCTTTGTTGGTATGCCATGGTTGTCTGCTACTACTGTTAGATCTGTTACT
CATGCTAACGCTTTGACTGTTATGGGTAAAGCTTCTACTCCAGGTGCTGCTGCTCAAATTCAGAAG
TAAAGAACAAGAATTTCCGGTTTGGTGGTAGCCGTTTTAGTTGGTTTGTCAATCTTGATGGAACC
TATCTTGTCTAGAATCCCATGGCTGTTTTGTTCCGGTATTTTCTTGTACATGGGTGTCACATCCTTGT
CCGGTATCCAATTTTATGATAGAATCTTGTGTTATTCAAGCCACCAAAGTACCATCCAGATGTTCC
TTATGTTAAGAGAGTCAAGACTTGGAGAATGCATTTGTTACCGGTATTCAAATTATCTGCTTGGCA
GTTTTGTGGTTGTTAAGTCAACTCCAGCTTCTTTAGCATTGCCATTGTTTTGATTTTGACCGTCCC
ATTAAGAAGAGTCTTGTGCCATTGATATTCAGAAACGTGCAATTGCAATGTTTGGATGCTGATGA
TGCTAAGGCTACTTTTGACGAAGAAGAAGGTAGAGACGAATACGATGAAGTTGCTATGCCAGTTT
TAAAGGTGAAGAATTATTCACTGGTGTGTGCCAATTTTGGTTGAATTAGATGGTGATGTTAA
TGGTCACAAATTTTCTGTCTCCGGTGAAGGTGAAGGTGATGCTACTTACGGTAAATTGACCTT
AAAATTTATTTGTACTACTGGTAAATTGCCAGTTCCATGGCCAACCTTAGTCACTACTTTCCG
TTATGGTGTTCATGTTTTGCTAGATACCAGATCATATGAAACAACATGACTTTTTCAAGTC
TGCCATGCCAGAAGGTTATGTTCAAGAAAGAACTATTTTTTTCAAAGATGACGGTAACTACAA
GACCAGAGCTGAAGTCAAGTTTGAAGGTGATACCTTAGTTAATAGAATCGAATTAAGGTA
TTGATTTTAAAGAAGATGGTAACATTTTAGGTACAAATTGGAATACAACATAACTCTCACAA
ATGTTTACATCATGGCTGACAAACAAAAGAATGGTATCAAAGTTAACTTCAAATTAGACACA
ACATTGAAGATGGTTCTGTTCAATTAGCTGACCATTATCAACAAAATACTCCAATTGGTGATG
GTCCAGTCTTGTACCAGACAACCATTACTTATCCACTCAATCTGCCTTATCCAAAGATCCAA

ACGAAAAGAGAGACCACATGGTCTTGTTAGAATTTGTTACTGCTGCTGGTATTACCCATGGTA
TGGATGAATTGTACAAATAA_{Aggatccgctcgac}

(E) ykAE1^{HA}

ctcgagATGGACGAAAAGAATCAAGAATTGAGATGGATGGAAGCTGCTAGATGGGTTCAATTGGAAG
AAAATTTGGGTGAAAATGGTGCTTGGGGTAGACCACATTTGTCTCATTTGACTTTTTGGTCTTGT
GGAATTGAGAAGAGTTTTCACTAAGGGTACTGTCTTGTGGACTTGCAAGAACTTCTTTGGCTGGT
GTTGCCAATCAATTATTGGACAGATTCATTTTCGAAGATCAAATCAGACCACAAGATAGAGAAGAA
TTATTGAGAGCCTTGTGTGAAGCACTCTCATGCTGGTGAATTGGAAGCTTTAGGTGGTGTAAAGC
CAGCTGTTTTGACTAGATCTGGTGATCCATCACAACCATTATTGCCACAACATTCTTCATTGGAAAC
CCAATTATTCTGCGAACAAGGTGATGGTGGTACTGAAGGTCATTCTCCATCTGGTATTTTGGAAAA
GATTCCACCAGATTCTGAAGCCACTTTGGTTTTGGTTGGTAGAGCTGATTTTTTGGAAACAACCAGTT
TTGGGTTTTCGTTAGATTGCAAGAAGCTGCTGAATTAGAAGCAGTTGAATTGCCAGTTCCAATCAGA
TTCTTGTTCGTTTTGTTGGGTCCAGAAGCTCCACATATTGATTATACTCAATTGGGTAGAGCCGCTG
CTACTTTGATGTCTGAAAGAGTTTTTAGAATCGACGCTTACATGGCTCAATCCAGAGGTGAATTATT
GCATTCTTTGGAAGGTTTCTTGGACTGCTCTTTAGTTTTGCCACCAACTGATGCTCCATCTGAACAA
GCTTTGTTGTCTTTGGTTCAGTTCAAAGAGAATTATTGAGAAGAAGATACCAATCCTCTCCAGCTA
AACCAGACTCTTCATTTTACAAGGGTTTTGGATTTGAATGGTGGTCCAGATGATCCATTGCAACAAA
CTGGTCAATTATTCGGTGGTTTTGGTTAGAGACATCAGAAGAAGATATCCTTACTACTTGTCCGATAT
CACCGATGCTTTTTACCACAAGTTTTGGCTGCTGTTATCTTCATCTATTTTCGCTGCTTTGTCACCAG
CTATTACTTTTTGGTGGTTTTATTAGGTGAAAAGACCAGAAATCAAATGGGTGTTTTCCGAATTATTGAT
CTCCACTGCTGTTCAAGGTATTTTGTGTTTTGTTAGGTGCCAACCTTTGTTGGTTGTTGGTTTTT
CTGGTCCATTATTGGTCTTTGAAGAAGCTTTCTTCTCCTTCTGTGAAACTAACGGTTTTGGAATATAT
CGTCGGTAGAGTTTTGGATTGGTTTCTGGTTAATTTGTTGGTTCGTTTTGGTTCGTCGCTTTCGAAGGTT
CATTTTTGGTAAGATTCATCTCCAGATACACCCAAGAAATCTTTCTTTCTTGATCTCCTTGATTTTC
ATCTACGAAACCTTCTCCAAGTTGATCAAGATCTTCCAAGATCACCCATTGCAAAAGACCTACAAC
TACAAC**TACCCATACGATGTTCCAGATTACGCTGTTTTGATGGTTCCAAAACCACAAGGTCCATT**
GCCAAATACTGCTTTATTATCCTTGGTTTTAATGGCCGGTACTTTCTTCTTTGCCATGATGTTGAGAA
AGTTCAAGAACTCCTTACTTCCCAGGTAAGTTGAGAAGAGTCATTGGTGATTTTGGTGTCCCAAT
CTCCATTTTGATTATGGTCTTGGTTGACTTCTTCATCCAAGATACTTACACCCAAAAGTTGTCTGTTC
CAGATGGTTTCAAGGTCAGTAATTCTTCAGCTAGAGGTTGGGTTATTCATCCATTGGGTTTGAGATC
CGAATTTCCAATTTGGATGATGTTTCGCTTCTGCTTTGCCAGCTTTATTGGTTTTTATCTTGATATTCT
TGGAATCCCAAATCACCACTTGATCGTTTTCTAAACCTGAAAGAAAGATGGTCAAGGGTTCTGGTT
TTCCTTGGATTTGTTGTTAGTTGTCGGTATGGGTGGTGTTCAGCTTTGTTGGTATGCCATGGTTG
TCTGCTACTACTGTTAGATCTGTTACTCATGCTAACGCTTTGACTGTTATGGGTAAAGCTTCTACTCC
AGGTGCTGCTGCTCAAATTCAGAAGTAAAAGAACAAAGAATTTCCGGTTTTGTTGGTAGCCGTTTT
AGTTGGTTTTGTCAATCTTGATGGAACCTATCTTGTCTAGAATCCCATTGGCTGTTTTGTTCCGGTATTT
TCTTGACATGGGTGTCACATCCTTGTCCGGTATCCAATTATTGATAGAATCTTGTGTTATTCAAG

CCACCAAAGTACCATCCAGATGTTCCCTTATGTAAAGAGAGTCAAGACTTGGAGAATGCATTTGTTCC
ACCGGTATTCAAATTATCTGCTTGGCAGTTTTGTGGGTTGTAAAGTCAACTCCAGCTTCTTTAGCAT
TGCCATTCGTTTTGATTTTGACCGTCCCATTAAGAAGAGTCTTGTTGCCATTGATATTCAGAAACGT
CGAATTGCAATGTTTGGATGCTGATGATGCTAAGGCTACTTTTGACGAAGAAGAAGGTAGAGACGA
ATACGATGAAGTTGCTATGCCAGTTTAAggtatcc

(F) ykAE1^{B3mem} (361 to 911 aa)

gtcgacggattcctcgagATGTACCCATACGATGTTCCAGATTACGCTggtggtggtgtagtGGTTTGGATTTGAA
TGGTGGTCCAGATGATCCATTGCAACAACTGGTCAATTATTCGGTGGTTTGGTTAGAGACATCAG
AAGAAGATATCCTTACTACTTGTCCGATATCACCGATGCTTTTCCACCACAAGTTTTGGCTGCTGTT
ATCTTCATCTATTCGCTGCTTTGTCCAGCTATTACTTTTGGTGGTTTATTAGGTGAAAAGACCA
GAAATCAAATGGGTGTTTCCGAATTATTGATCTCCACTGCTGTTCAAGGTATTTTGTGTTGCTTTGTTA
GGTGCCCAACCTTTGTGGTTGTTGGTTTTTCTGGTCCATTATTGGTCTTTGAAGAAGCTTTCTTCTC
CTTCTGTGAAACTAACGGTTTGAATATATCGTCGGTAGAGTTTGGATTGGTTTCTGGTTAATTTG
TTGGTCGTTTTGGTCGTCGCTTTCGAAGGTTCATTTTTGGTAAGATTCATCTCCAGATACACCCAAG
AAATCTTTTCTTTCTTGATCTCCTTGATTTTTCATCTACGAAACCTTCTCCAAGTTGATCAAGATCTC
CAAGATCACCCATTGCAAAAGACCTACAACCTACAACGTTTTGATGGTTCCAAAACCACAAGGTCCA
TTGCCAAATACTGCTTTATTATCCTTGGTTTTAATGGCCGGTACTTTCTTCTTTGCCATGATGTTGAG
AAAGTTCAAGAACTCCTCTTACTTCCCAGGTAAGTTGAGAAGAGTCATTGGTGATTTTGGTGTCCCA
ATCTCCATTTTGATTATGGTCTTGGTTGACTTCTTCATCCAAGATACTTACACCCAAAAGTTGTCTGT
TCCAGATGGTTTCAAGGTCAGTAATTCTTCAGCTAGAGGTTGGGTTATTCATCCATTGGGTTTGA
TCCGAATTTCCAATTTGGATGATGTTTCGCTTCTGCTTTGCCAGCTTTATTGGTTTTTATCTTGATATT
CTTGGAATCCCAAATCACACCTTGATCGTTTCTAAACCTGAAAGAAAGATGGTCAAGGGTTCTGG
TTTTCACTTGGATTTGTTGTTAGTTGTCGGTATGGGTGGTGTTCAGCTTTGTTTGGTATGCCATGGT
TGTCTGCTACTACTGTTAGATCTGTTACTCATGCTAACGCTTTGACTGTTATGGGTAAAGCTTCTACT
CCAGGTGCTGCTGCTCAAATTCAAGAAGTAAAAGAACAAGAATTTCCGGTTTGTGGTAGCCGTT
TTAGTTGGTTTTGTCAATCTTGATGGAACCTATCTTGTCTAGAATCCATTGGCTGTTTTGTTCGGTAT
TTTCTTGTACATGGGTGTCACATCCTTGTCCGGTATCCAATTATTTGATAGAATCTTGTGTTATTCA
AGCCACCAAAGTACCATCCAGATGTTCCCTTATGTAAAGAGAGTCAAGACTTGGAGAATGCATTTGT
TCACCGGTATTCAAATTATCTGCTTGGCAGTTTTGTGGGTTGTAAAGTCAACTCCAGCTTCTTTAGC
ATTGCCATTCGTTTTGATTTTGACCGTCCCATTAAGAAGAGTCTTGTTGCCATTGATATTCAGAAAC
GTCGAATTGCAATGTTTGGATGCTGATGATGCTAAGGCTACTTTTGACGAAGAAGAAGGTAGAGAC
GAATACGATGAAGTTGCTATGCCAGTTTAAggtatccgagctc

Acknowledgements

First of all, I would like to thank my “Doktorvater” (principal supervisor), Prof. Dr. Manfred J. Schmitt, for allowing me to achieve a doctoral degree under his supervision. Throughout the program, his endless support, suggestions, and encouragement guide me to overcome challenges that came across in my research project. Moreover, he gave me the freedom to endeavor on new concepts that eventually help me to resolve research questions. His patience and immense knowledge facilitate my research work as well as writing this thesis.

I sincerely thank Prof. Dr. Ekkehard Neuhaus to agree for becoming my second supervisor in this thesis, and for his suggestions and comments on my projects. A special thanks to Prof. Dr. Emmanuelle Cordat for sharing her idea, motivation, and recommendation during my whole doctoral period as well as allowing me to spend six months in her lab as an IRTG exchange student. Furthermore, I would like to share my heartfelt gratitude to all members of the jury for agreeing to participate in the defense of this thesis.

I am truly thankful to all my lab members and technical staff for their tremendous help in the lab and for providing an excellent environment for research. In particular, I want to share my sincere gratitude to Dr. Björn Becker, who not only helped me to learn new techniques but also assisted me in publishing research articles, reviewing posters, presentations, and this thesis. I am also very grateful to Dr. Stefanie Gier for reviewing my doctoral thesis and providing critical suggestions for its improvement, as well as to Achim Bauer and Matthias Lehmen for their useful comments on thesis writing. Many thanks go to Nicole Jundel and Dr. Gabriele Amoroso for their substantial assistance with the organizational questions and issues, which made my life easy. In addition, I would like to thank the members of the IRTG 1830 for making an informative and friendly atmosphere at the corresponding seminars and conferences.

I want to share my heartfelt thanks to my family, particularly my parents and my wife. My parents, Sarder Abdul Hafeez and Nazma Khatun, always gave me their support, advises, and good wishes. My wife, Elizabeth Razzaque, has stood by me throughout this entire process and has made countless sacrifices to help me get to this point. Without her contribution, it would be tremendously difficult for me to come here and continue the research work. I want to share my deep appreciation for her for loving, caring, and always staying on my side in the hard times.

Many thanks go to my little son, Hamin Ehan Sarder, for his calmness and decent sleep at night. Additionally, I want to thank my younger brother, S M Haris, for continually cheering for me. Their reinforcement gave me the mental strength to enduring the difficulties during the time of my doctoral thesis.

Lastly, I like to thank all of my friends and well-wisher, especially Dr. Aditya Chandru, Shahid Ullah, Santanu Basu, Dr. Sina Noor and Dr. Ibrahim Khalil, for their kind words and motivation for boosting me up during the period of doctoral study.

Declaration of originality

I, hereby, confirmed that this doctoral thesis entitled “**Analysis of intracellular transport and functionality of human kidney anion exchanger 1 (kAE1) in yeast and mammalian cells**” was pursued by me for obtaining the degree of Doctor rerum naturalium (Dr. rer. nat.). This work has not been submitted in this or any other similar formate to any university before.

Saarbrücken, 2020

S M A Hasib

Curriculum vitae

S M A Hasib

Personal information

Date of birth : 15.01.1990
Place of birth : Khulna, Bangladesh
Nationality : Bangladeshi

Education

06/2015 – Present : Doctoral candidate
Department of Molecular and Cell Biology
Saarland University, Germany
Supervisor: Prof. Dr. Manfred J. Schmitt
Thesis title: “Analysis of intracellular transport and functionality of human anion exchanger 1 (kAE1) in yeast and mammalian cells.”

09/2011 – 10/2012 : M. Sc. in Pharmacology and Biotechnology
Sheffield Hallam University, United Kingdom
Thesis title: “Parkinson’s disease: effect of phosphorylation of alpha-synuclein on aggregate formation in the presence of metals.”

09/2006 – 10/2010 : B. Sc. in Pharmacy (Honours)
University of Asia Pacific, Bangladesh

06/2004 – 07/2006 : Higher Secondary Certificate
Group: Science
Government Shahid Bulbul College, Bangladesh

Employment:

03/2013 – 05/2015 : Quality Control Officer
Biotechnology Unit
Healthcare Pharmaceuticals Limited, Bangladesh

06/2013 – 05/2015 : Virology Laboratory Collaborator
International Center for Diarrheal Disease Research, Bangladesh